KANUMAS MET/ICE/OCEAN Overview Report 2011 - East Greenland

Toudal Pedersen, Leif; Tonboe, Rasmus T.; Brandt Jensen, Matilde; Dybkjær, Gorm; Nissen, Martin; Rasmussen, Jesper; Olsen, Steffen M.; Skourup, Henriette; Saldo, Roberto; Forsberg, René

Publication date:
2011

Document Version
Publisher's PDF, also known as Version of record

KANUMAS MET/ICE/OCEAN Overview Report 2011

East Greenland

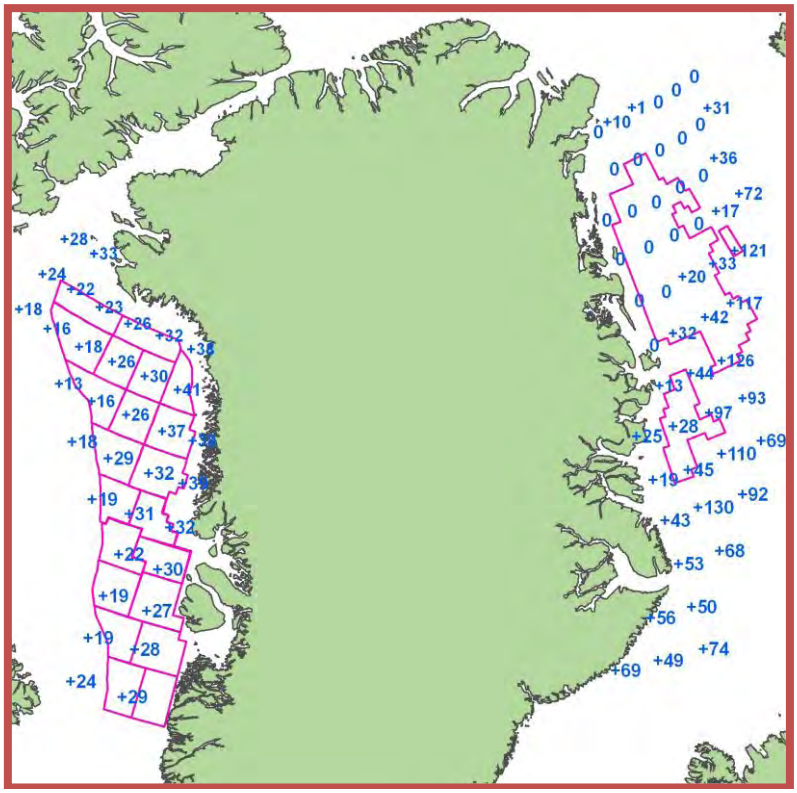

Produced for BMP by

Leif Toudal Pedersen
Rasmus T. Tonboe
Matilde Brandt Jensen
Gorm Dybkjær
Martin Nissen
Jesper Rasmussen
Steffen M. Olsen
Danish Meteorological Institute

Henriette Skourup
Roberto Saldo
Rene Forsberg
DTU-Space

This page is intentionally left blank

Table of Contents

This page is intentionally left blank

1. Introduction

This report is a deliverable from a project carried out for the Greenland Bureau of Minerals and Petroleum (BMP) by the Danish Meteorological Institute (DMI) and the Technical University of Denmark (DTU-Space).

The objective is to present an updated overview of physical environmental conditions, especially ice conditions, observed in recent or near future licence areas off the north-east and north-west coasts of Greenland.

Most chapters contain information updated with data until mid 2011.

The report is in 2 volumes with some duplication in order to present a unified overview of the north-east and north-west areas respectively. In particular the "**Overview of Weather, Ice and Oceanographic conditions around Greenland and the Arctic Ocean**" presented in chapter 2 is the same in both reports.

A similar report was produced in 2008, and is available from the BMP. However, the old report did not include weather and ocean conditions.

It is noted that many dataseries are not as long as could be desired, and that it is therefore difficult to evaluate the relative importance of natural variability and systematic climate change. The reader is therefore warned not to over-interprete the changes in recent years even though there seem to be a clear trend towards longer ice free periods.

Especially it is noted that a number of years with very northerly retreat of the ice on the east coast during summer in the early 2000s has been followed by years with substantially more difficult ice conditions.

Chapter 2 provides an overview of the weather, ice and ocean conditions in the Arctic and recent developments.

The following chapters provide details on ice distribution, drift and thickness in the area off north east Greenland.

Chapter 3 use a recently published dataset from EUMETSAT's Ocean and Sea Ice Satellite Aplication Facility (OSISAF) to provide information about the length of the ice free season. The satelllite passive microwave dataset is excellent for this purpose due to it's daily resolution. However, the data do not always corerespond to icecharts, so a comparative study has been included.

Chapter 4 deals with overall ice thickness distribution. Very little data exist, and we have combined measurements of freeboard heights from ICESAT with ice type measurements using radar backscatter to provide a picture of the seasonal and interannual variability.

In chapter 5 we look at ice drift. We use data from 2 different sources and discuss the relationship between wind and ice drift.

Chapter 6 provides an overview of the meteorological and oceanographical conditions of the area.

In chapter 7 we present in more detail the airborne ice freeboard measurements carried out

specifically for this project, and relate them to satellite measurements.

Chapters 8 and 9 provide more details on the ice free periods and the ice drift data.

Finally chapter 10 provides a list of references used.

2. Overview of Weather, Ice and Oceanographic conditions around Greenland and the Arctic Ocean

2.1. Oceanography

The Arctic Ocean is encircled by land and shallow straits to all sides except the passage to the Greenland Sea and the North Atlantic through the Fram Strait. In spite of its Mediterranean nature the Arctic Ocean is thus a part of the Atlantic Ocean (Rudels, 1998). The Eurasian and Canadian basins (depth>2000m) in the central Arctic Ocean are divided by the narrow Lomonosov Ridge (~1000m).

The Euasian Arctic Ocean i.e. the Barents Sea, Kara Sea, Laptev Sea, East Siberian Sea, and Chukchi Sea, are characterised by very broad shelves (~600km) and shallow waters (<100m) (Wadhams, 2000). The upper ~200m of the Arctic Ocean water column is called the polar surface water. It is characterised by relatively low salinity (30-32ppt) and temperature near the freezing point (-1.8˚C). The low salinity of this layer is caused by the influx of fresh water from the rivers entering the Arctic (total annual discharge about 3300km^3/yr), in particular Yenisey (603km^3/yr), Ob (530km^3/yr), Lena (520km^3/yr), Mackenzie (340km^3/yr) and other smaller rivers (1224km^3/yr) (Aagaard & Carmack, 1989). At mid depths (200-900m) below the surface water, is the Atlantic water. This layer is characterised by relatively high salinity (35ppt) and temperature (3˚C). As the name indicates this water has entered the Arctic Ocean by advection from the North Atlantic through the Fram Strait and the Barents Sea at mid depths. The North Atlantic Current that enters the Arctic Ocean through the Barents Sea and west of Spitsbergen also converges with the East Greenland Current where it underlies the polar surface water flowing south through the Fram Strait. The strong halocline between the fresher polar surface waters and the warmer but more saline Atlantic waters creates a stable stratification. The stability limits the flux of heat from the Atlantic waters to the surface and is together with the cooling atmosphere and negative radiation budget conditioning the Arctic Ocean ice cover (Aagaard & Carmack, 1989; Dickson, 1999). The Arctic Ocean deep waters are below the two upper layers at depths below 900m. The deep waters are colder than the Atlantic waters (-1-0˚C) but has about the same salinity (Wadhams, 2000). The deep waters of the Arctic Ocean originate from sinking waters in the central Greenland Sea (Rudels, 1998). Only at the Siberian shelves where the entire water column is cooled to the freezing point and in polynyas is it possible for brine enriched plumes to sink to the shelf floor and eventually continue into the Arctic Basin where it mixes with waters at the same density (Rudels, 1998; Haarpaintner et al., 2001a; Haarpaintner et al., 2001b). The circulation of the deep water is very slow (Wadhams, 2000). Two major surface current systems characterise the circulation of the surface waters: 1) the anti-cyclonic Beaufort Gyre centred on about 150˚W, 80˚N, and 2) the transpolar drift from the Siberian shelves across the pole and through the Fram Strait (Wadhams, 2000).

The density difference between surface waters and the underlying waters in the Greenland Sea is small in winter due to the atmospheric cooling of the Atlantic waters as they enter the region (Rudels, 1998). Due to atmospheric cooling Atlantic surface waters in the Greenland Sea can become denser than the underlying warmer but slightly more saline water and convection is initiated. Distillation of the surface waters due to new-ice formation may together with cooling contribute to convection. Convection and the ventilation of the deep waters is a significant process in the north Atlantic circulation system (Aagaard & Carmack, 1989; Broecker, 1997). Convective regions in the North Atlantic i.e. the Greenland Sea, Iceland Sea and the Labrador Sea are in the proximity of the East Greenland Current and the Labrador Current which transport sea ice and relatively low saline waters out of the Arctic Ocean and Baffin Bay respectively. The occasional influx of low saline surface waters into the convective regions („fresh' water capping) effectively

prevents convection (Aagaard & Carmack, 1989). The East Greenland Current continue south through the Denmark Strait where it meets the warm Irminger current south of Iceland, a branch of the North Atlantic Current. The East Greenland Current rounds Cape Farewell and become the West Greenland Current along the west coast. The general surface circulation and ice drift in Baffin Bay is cyclonic i.e. the West Greenland Current is northbound along the West Greenland Coast up to about 65˚-66˚N where a branch of it is diverged west and merge with the Baffin Current. The West Greenland Current continues north to Melville Bay where it merges with the Baffin Current. The Baffin Current is southbound along Baffin Island Coast. The Baffin Current becomes the Labrador Current south of Hudson Strait (60˚N) where it is also mixed with Arctic waters from the Canadian archipelago. With the exception of the North Water polynya, convection in the Baffin Bay is limited to the upper 200m or so. The surface waters are of Atlantic origin while the bottom waters are of Arctic Ocean origin (Rudels, 1998).

2.2. Meteorology

Greenland is due to its size and height (Summit about 3200m) significantly affecting the atmospheric flow of the lower troposphere and the air exchange between North and South (Cappelen et al., 2001). In winter, northern winds dominate along the coasts. A surface high pressure due to cold dense air is a depression in the 500hPa isobar height. The track of the cyclones around Greenland is related to the atmospheric circulation at 500hPa and the deepening of the 500hPa depression (Thompson & Wallace, 1998). Such a high pressure and corresponding 500hPA depression, called the polar vortex, is normally situated over Baffin Island in winter (Cappelen et al., 2001). Surface low pressure systems are formed as waves on the polar front east of USA and Canada at the Gulf Stream margin between cold and warm ocean waters (Cappelen et al., 2001). The low pressure systems normally follow the 500hPa height contours south of Greenland across or south of Iceland and towards Europe. The depth of the polar vortex is coupled to the North Atlantic Oscillation (NAO) index (Thompson & Wallace, 1998). When the index is positive i.e. when the Icelandic low is deep and the polar vortex is weak the cyclone track is south of Greenland and cold dry polar air is in return advected south through Baffin Bay and Davis Strait (Hurell, 1995). Further, during positive NAO index cyclones travel into the Barents Sea and the Siberian Arctic Ocean at increased frequency (Maslanik et al., 1996; Maslowski et al., 2001; Hurrell et al., 2003). Positive NAO events are also correlated to a negative air temperature anomaly (about -3˚C), increased extent and thickness of the sea ice in Baffin Bay (Wang et al., 1994). When the NAO index is negative, i.e. weak Icelandic low and a deep polar vortex extending east, cyclones are travelling through Davis Strait and into the Baffin Bay at higher frequency and the Greenland West Coast experience mild and humid winters (Cappelen et al., 2001; Hurrell et al., 2003).

Major cyclones entering the Arctic Ocean in winter (December – February) are concentrated in a triangle between the Greenland Sea, eastern Kara Sea and the North Pole. Maximal occurrence of about 3 systems is concentrated on Spitsbergen, northern Novaya Zemlya and the North Pole. The cyclone systems enter from the Barents and Greenland Seas or across Greenland from Baffin Bay during winter (Serreze & Barry, 1988).

Cyclones approaching the Greenland coast may entrain local weather phenomena's on land such as katabatic winds (Cappelen et al., 2000). Katabatic winds can blow with almost unaltered speed 200km off the coast in east Greenland (Tonboe, 2001). Low pressures travelling directly towards Cape Farewell tend to split into two centres and continue north along the Greenland West and East Coasts (Cappelen et al., 2001).
Polar lows, similar in principle to tropical cyclones, are relatively short lived (1-3 days) cyclone systems formed when cold arctic air is advected over a relatively warm body of water, e.g. in the Davis Strait and Greenland Sea (Barry & Chorley, 1992). Polar lows are more common in Greenland when the polar vortex is extending over Baffin Bay and Greenland.

The large scale changes in the atmospheric flow pattern reflected in NAO is coupled to climatologically large scale sea ice extent and variability (Kwok & Rothrock, 1999; Deser et al., 2000).

2.3. The Arctic Ocean energy balance

The Atmospheric energy budget of the Arctic Ocean is roughly divided into 3 terms (Overland, 1998): 1) long-wave radiation to space -157W/m^2, lateral atmospheric heat influx 108W/m^2, and surface heat flux from the ocean to the atmosphere 48W/m^2. The heat budget of the arctic atmosphere is very sensitive to the lateral influx of heat across 70˚N (Overland, 1998). Using a simple model Thorndike (1992) show that if the lateral heat flux to the Arctic is increased by about 30W/m^2, the Arctic Ocean ice cover would become completely ice free even in winter. On the other hand if the lateral heat flux to the Arctic is reduced by about 20W/m^2 the ice cover would reach an equilibrium ice thickness of >12m and not even reach the melting point in summer. The Thorndike (1992) model may be simple. However, it is with clarity illustrating the sensitivity and feedback of the ice cover to changes in the global energy balance. More sophisticated models largely confirm Thorndike's (1992) results and further identify the ice thickness distribution, the albedo and ocean mixed layer thickness as important (Björk & Söderkvist, 2002). The response-time to small heat flux perturbations ($<\pm$5W/m^2) is in the order of 6 years while the ice cover adjust to larger (10W/m^2) positive perturbations in about 20years (Björk & Söderkvist, 2002).

In response to changes in the large scale atmospheric circulation in the North Atlantic; cyclone activity in magnitude, duration and frequency, has increased during the 1990'ies in the Greenland-Norwegian Arctic (Barents Sea, Greenland Sea and Atlantic sector of the Arctic Ocean) (Maslowski et al., 2001) and the eastern Arctic Ocean north of Severnya Zemlya (Maslanik et al., 1996). The increase in cyclone activity in these regions is related to the positive NAO index during the 1990'ies. The cyclones are advecting heat to the Arctic Ocean and the increased heat flux is further linked to the observed reduction of the perennial ice cover in the east Siberian Arctic Ocean (Maslanik et al., 1996). The atmospheric pressure situation reflected in a positive NAO index is also capable of driving warmer and fresher waters from the North Atlantic Current into the Arctic Ocean at higher rate. Together with an observed thinning of the Polar surface waters in the Eurasian Arctic Ocean this has had a profound effect on the increased sea ice heat and reduced mass balance during the 1990'ies (Dickson, 1999). The positive NAO index is thus driving both an atmospheric and oceanographic heat flux into the Arctic Ocean. The net result is an observed reduction in the perennial Arctic ice cover (e.g. Cavalieri et al., 1997; Vinje, 2001).

2.4. The sea ice in the waters around Greenland

The Arctic sea ice cover varies between an annual minimum of about 8.5 x 10^6 km^2 in September to a maximum of about 15.0 x 10^6 km^2 in March (Parkinson & Cavalieri, 1989). The sea ice cover around Greenland also shows a significant seasonal variation even though the area north of Greenland is permanently covered by ice. The sea ice types covering these waters can roughly be divided into multi-year and first-year ice. However, due to advection multi-year ice is also found in the seasonal ice cover and *vise-versa* for first year ice. As a rule of thumb the free ice drift speed is about 2% of the surface wind speed (Thorndike & Colony, 1982). For wind speeds of 10m/s the ice drift rate is about 17km/day. Numerical models simulating ice variability are using both thermodynamic and advective terms (e.g. Hibler, 1979). The advection of ice is determined by water and air shear stress, ice floe interaction and other terms such as ice mass, Coriolis parameter, ice acceleration etc. (Hibler, 1979; Thorndike & Colony, 1982). The thermodynamic formation, growth or melt of sea ice is determined by the surface heat and mass balance (Maykut, 1986). The

radiation budget includes long-wave radiation emitted by the atmosphere and the ice itself, short wave radiation during the summer months and optical properties of the ice i.e. albedo and penetration depth. Sensible heat exchange due to wind turbulence, air temperature, evaporation, sublimation and condensation is dictated by: the wind speed, the surface roughness and temperature, and the air temperature and water vapour gradients. Thermal properties of the ice are determining the conductive heat flux and the Oceanic heat flux is determined by e.g. water temperature and ice cover concentration (Maykut, 1986). It should be noted that the optical albedo is significantly affected by the presence of a snow layer, liquid water in the snow and melt water ponds on the ice surface (Perovich, 1998), and the conductive heat flux is almost an order of magnitude less in snow (about $0.3W/m^2$) than ice (about $2.1W/m^2$).
In addition to daily and seasonal variability, evidence suggests that the ice cover in the North Atlantic Arctic (Greenland, Iceland, Norwegian, Barents, and Western Kara Seas) has been reduced by about 33% during the last 135 years (Vinje, 2001).

2.4.1. Baffin Bay

The ice cover in Baffin Bay and Davis Strait is part of the seasonal ice zone, i.e. the zone varying annually between open water and ice covered. The annual maximum in February – March is 1.4 x $10^6 km^2$ and the minimum in September is about 0.2 x $10^6 km^2$ (Parkinson & Cavalieri, 1989). The first-year ice cover is isolated from influx of ice from other waters, except 1) small amounts of multi-year ice from the Arctic Ocean through Narres Strait, 2) and occasional advection of Arctic ice south of Greenland, and 3) first and occasional multi-year ice through Lancaster Sound and Hudson Strait (Wadhams, 1986). Certain regions in Baffin Bay are covered by significant concentrations of glacier ice, in fjords and along the Greenland West Coast with glacier outlets, e.g. Disko Bay, Uummannaq, Melville Bay and Cape York. Most fjords along the Greenland West Coast are further covered by fast ice in winter (December – April). The ice in the Davis Strait is exported south from the Baffin Bay along the Baffin Island east coast with the Baffin and Labrador Currents, at a rate of about 16km/day (Wadhams, 1986). The ice thickness in Davis Strait in February (1967) has been measured by submarine along the margin to 0.25-0.51m and the interior 0.77-1.66m (Wadhams, 1986). The average maximum ice thickness is about 1.75m in the north-western part of the bay gradually thinning towards south-west and the Greenland Coast to about 0.7m.

2.4.2. The Lincoln Sea

The Arctic Ocean in vicinity of North Greenland i.e. Lincoln Sea, is all year round covered by multi-year ice. The mean ice draft of a line section north of Greenland from mid between Nordostrundingen and Svalbard in the Fram Strait to a point 180km north of Ellesmere Island was measured by submarine sonar (*H. M. S. Sovereign*, October 1976) to between 5.07 - 7.49m (Wadhams, 1981). The most compact and thickest ice was found north of Greenland at the second half of the section. The ice in the entire section was characterised as heavily deformed with ridge keel drafts of up to 30-40m.

2.4.3. Fram Strait & East Coast

The Fram Strait is the only deep passage between the Arctic Ocean and the Atlantic Ocean. Nearly all ice exported from the Arctic Ocean is advected trough the Fram Strait (90%, Rudels, 1998). The sea ice drifting in the East Greenland Current along the Greenland East Coast consist in general of multi-year ice from the Central Arctic, first-year ice formed along the Siberian coast and in leads, icebergs from the East Greenland glaciers and new-ice formed in polynyas and along the ice edge (Wadhams, 1986). Wadhams (1981) reviews earlier estimates of mean ice drift rates in the East Greenland Current. The southbound drift is mainly driven by winds between the atmospheric high

pressure over the Arctic Ocean and the Icelandic low pressure. The mean drift; typically 5-35cm/s, is largest over the shelf break and increase from Nordostrundingen to around Scoresby Sound. The mean ice thickness in the Fram Strait has a seasonal variation from 2.25m in September to 3.25m in April-May (Vinje et al., 1998). This measure includes open water measurements (ice thickness = 0). However excluding open water measurements, the mean ice thickness of 3.27m corresponds to earlier submarine sonar measurements (Vinje et al., 1998). The seasonal variation of the ice cover from the Fram Strait to Cape Farewell is between the seasonal maximum in February: 1.1 x 10^6km^2 and the minimum in August: 0.5 x 10^6km^2 (Parkinson & Cavalieri, 1989).

The East Greenland Current has two branches pointing east between Fram and Denmark Straits i.e. the Jan Mayen Current (~73˚N) forming the Greenland Sea Gyre and the East Icelandic Current (~67˚N) (Wadhams, 1981). New-ice formation along the ice edge in and around the Jan Mayen Current is common in winter and spring (Wadhams & Comiso, 1999). This new-ice cover is often appended to the older ice drifting in the East Greenland Current as an ice peninsula is called the Odden and the bay of open water north of the peninsula is called Nordbukta (Wadhams, 1981).

All ice advected south through Fram Strait melts on its journey to southern Greenland. The melt adds significant amounts of low-saline water to the East Greenland Current. Aagaard & Carmack (1989) compare the equivalent fresh water flux (2800km^3/yr) to the largest rivers of the world and it is indeed comparable to the total fresh water influx from the rivers entering the Arctic Ocean (3300km^3/yr). As mentioned above, ice flux trough the Fram Strait varies both seasonally and annually (Vinje et al., 1998).

2.5. The Arctic Ocean climate change and consequences for sea ice conditions in Greenland waters

Greenland is situated at the exchange pathway between the Arctic Ocean and the North Atlantic. The Arctic Ocean sea ice has changed recently in particular over the last 10 years i.e. the summer sea ice extent has decreased, a large fraction of area covered thick old ice in winter has been replaced by thinner winter ice, the ice drift speed and deformation rate have increased in response to the thinning etc. This means that the ice originating from the Arctic Ocean and drifting south along the east Greenland coast is changing. On the one hand the ice in the Greenland Sea may have become thinner and it contains a larger fraction winter ice relative to old ice. On the other hand there may be a greater occurrence of deformation features, i.e. pressure ridges. The ice in the east Greenland current is a mixture of old ice from north of Greenland, winter ice from north of Spitsbergen and ice formed *in situ*. Even though the old ice is disappearing from the Beaufort Sea and large areas in the central and eastern parts of the Arctic Ocean the old ice still remains north of Greenland. Therefore there is still a supply of old ice being exported through Fram Strait to the Greenland Sea. It is unclear how long there this situation will be maintained. However, the consequences of thinner ice being exported through Fram Strait is more rapid melt in summer in particular at lower latitudes and more open water in the Greenland Sea in summer. It is unclear if the balance between ice drift and melt between the Greenland Sea and the Cape Farewell can be maintained in summer and if there will be sea ice in the Cape Farewell region during summer also in the future.

Except for some old ice drifting south through the Nares Strait from the Lincoln Sea the Baffin Bay is dominated entirely by winter ice. The winter ice thickness thickens in response to the winter severity and the export rate towards Davis Strait and eventual melt at lower latitudes. The Baffin Bay winter climate is controlled primarily by atmospheric circulation patterns correlated to e.g. the NAO index. It is unclear how the NAO index responds to climate change. The consequences of altered sea ice conditions in the Arctic Ocean in Baffin Bay are minor unless the atmospheric circulation in general is changed because of changing sea ice conditions in the Arctic Ocean.

However the Baffin Bay sea ice changes in response to the Arctic warming: 1) the freeze up is delayed due to increased summer warming of the surface waters, 2) the ice break-up comes earlier due to earlier melt onset, 3) warming of the Atlantic water entering the Baffin Bay affects not only the outlet glaciers along the Greenland west coast but also the sea ice formation in the eastern part of the Baffin Bay.

2.6. Ice Type and ice thickness maps for the Arctic

The following figures show mapped satellite sensor measurements of sea ice freeboard heights (**figure 2.1**) and backscatter data (**figure 2.2-4**) for the Arctic Ocean over the last decade. There is a clear spatial correlation between the distribution of MYI and FYI in the freeboard maps and the QuikSCAT backscatter maps, where large sea ice freeboard heights (> 38 cm) are correlated with high backscatter values (> -12.5 dB) from thick multiyear sea ice. A detailed description of freeboard heights and backscatter data in the license areas is given in **chapter 4**.

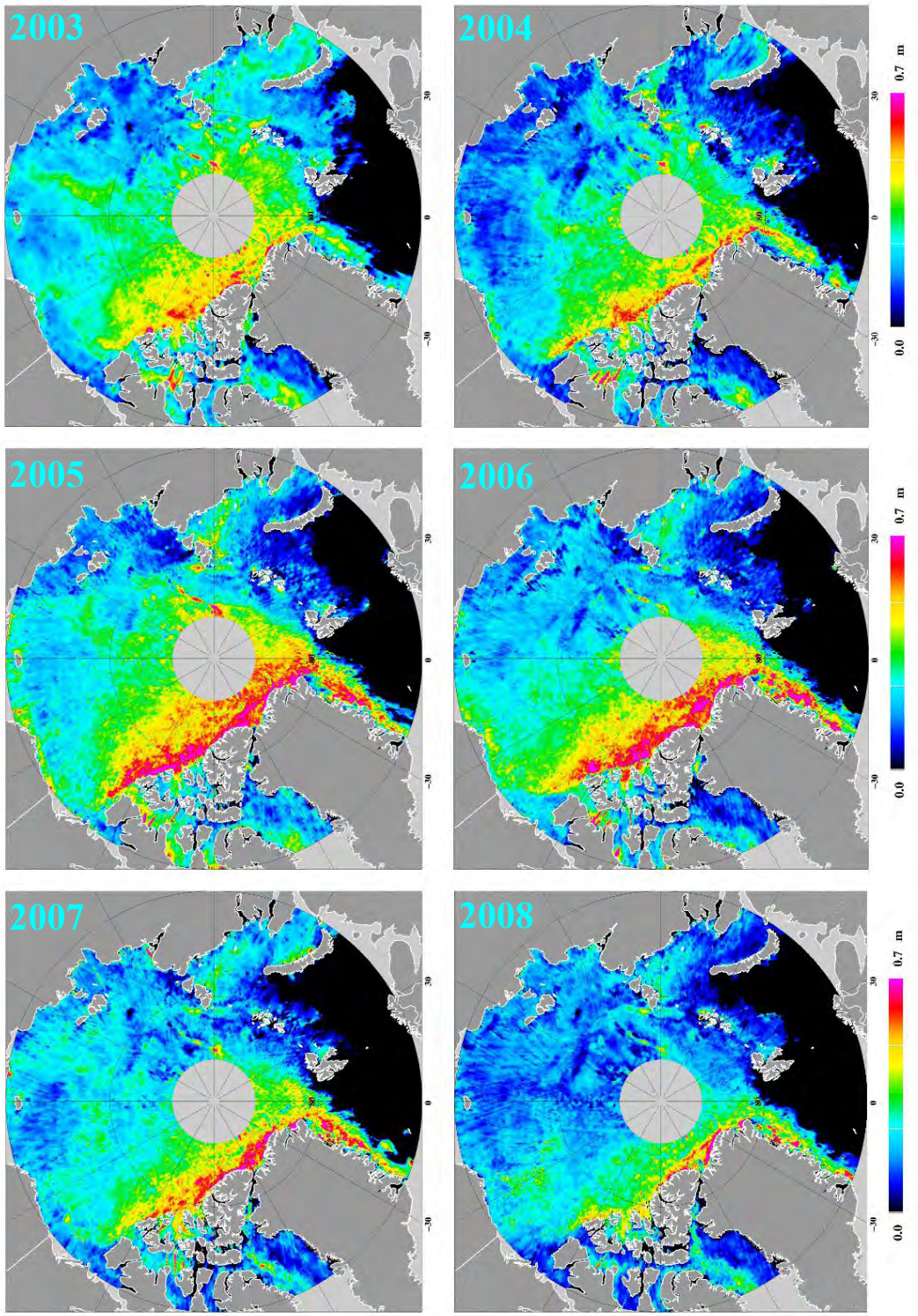

Figure 2.1: Estimated sea ice freeboard heights over the Arctic Ocean from ICEsat data, for early spring period (February-April) 2003-2008.

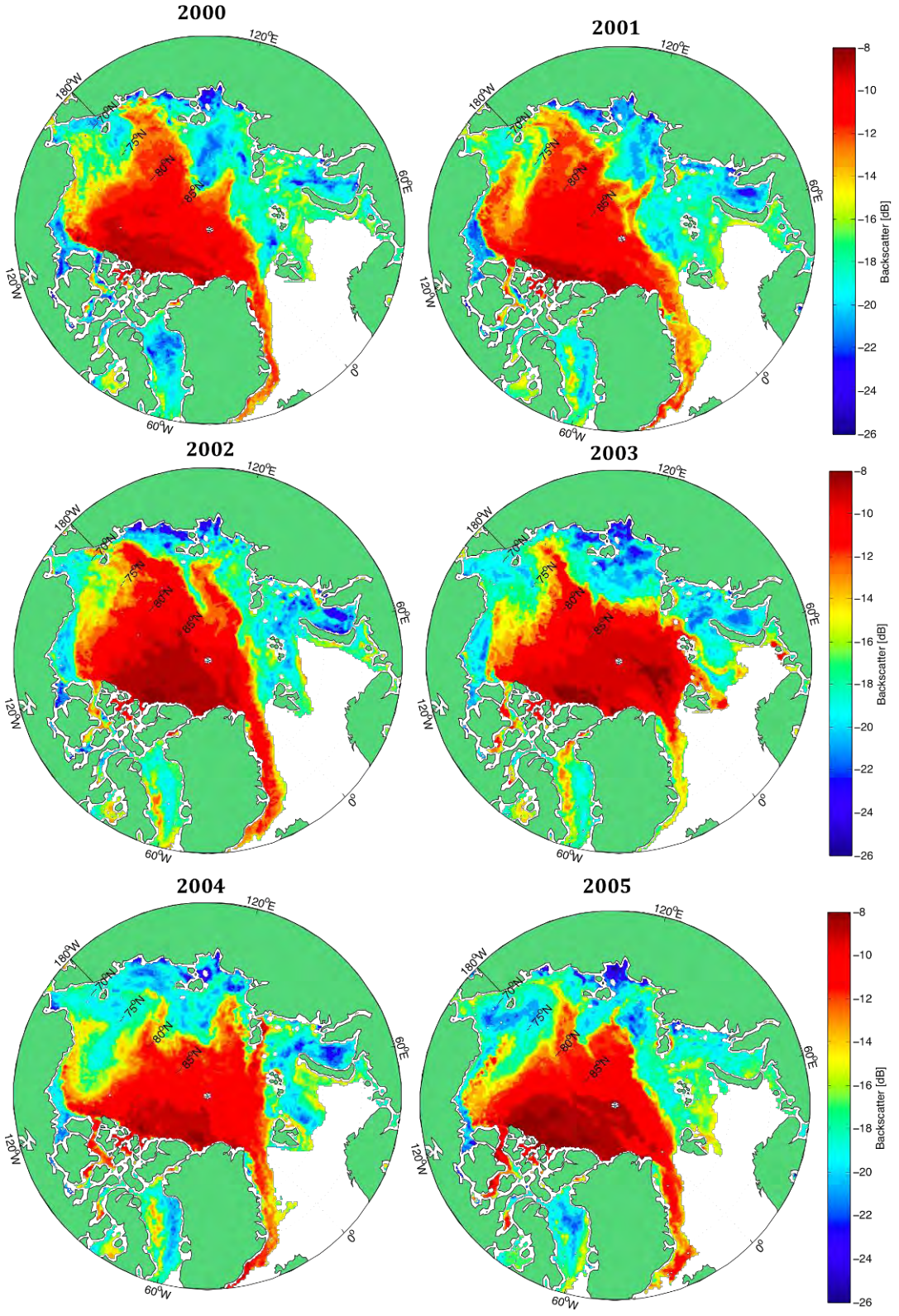

Figure 2.2: Sea ice backscatter maps from Quikscat data Ultimo February 2000-2005. The backscatter threshold value used for deliniating MYI zone (area of all partial concentrations of MYI) from FYI zone (area with all ice being FYI) is ~-12.5 dB.

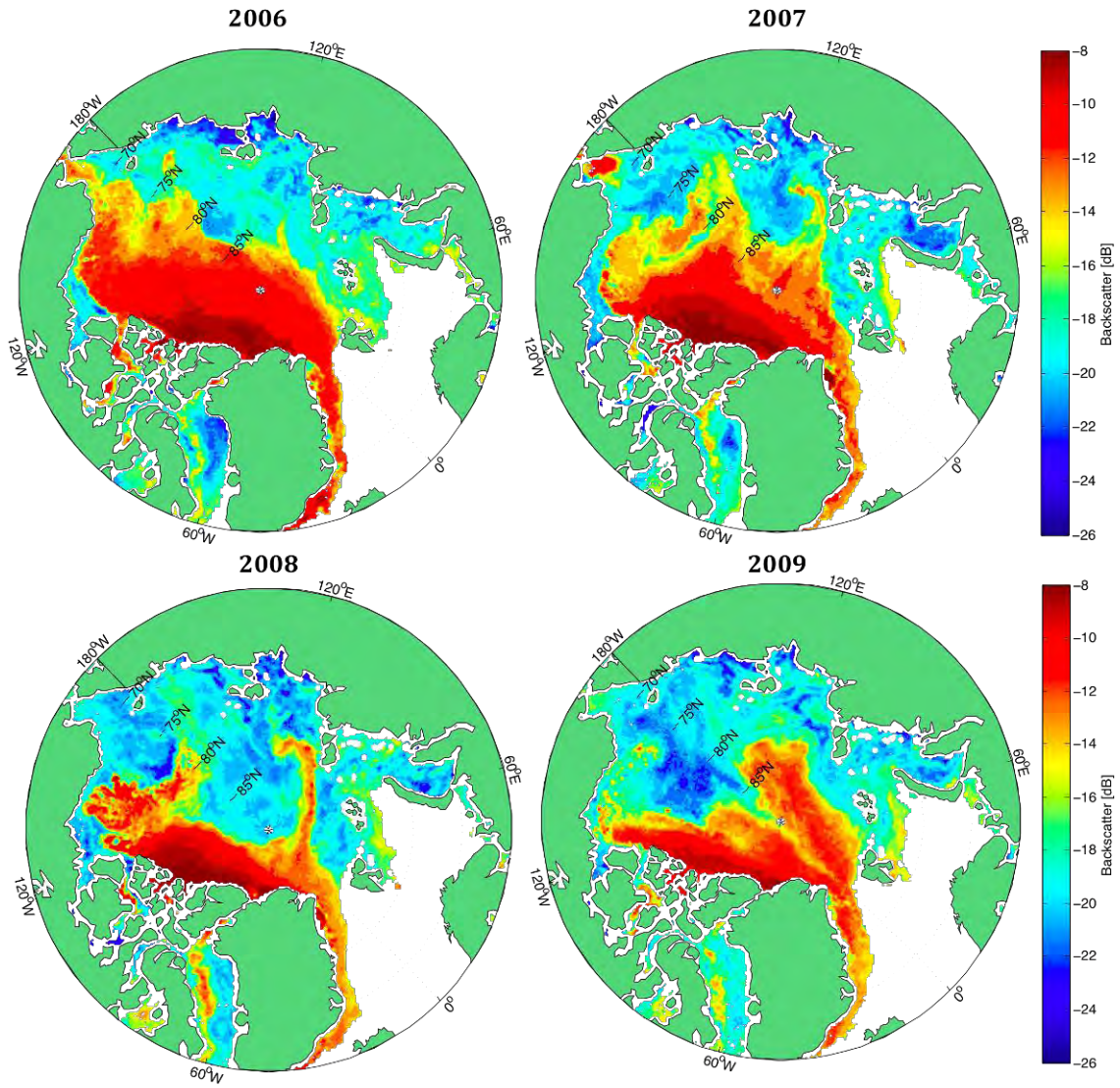

Figure 2.3: Sea ice backscatter maps from Quikscat data Ultimo February 2006-2009. The backscatter threshold value used for deliniating MYI zone (area of all partial concentrations of MYI) from FYI zone (area with all ice being FYI) is ~-12.5 dB.

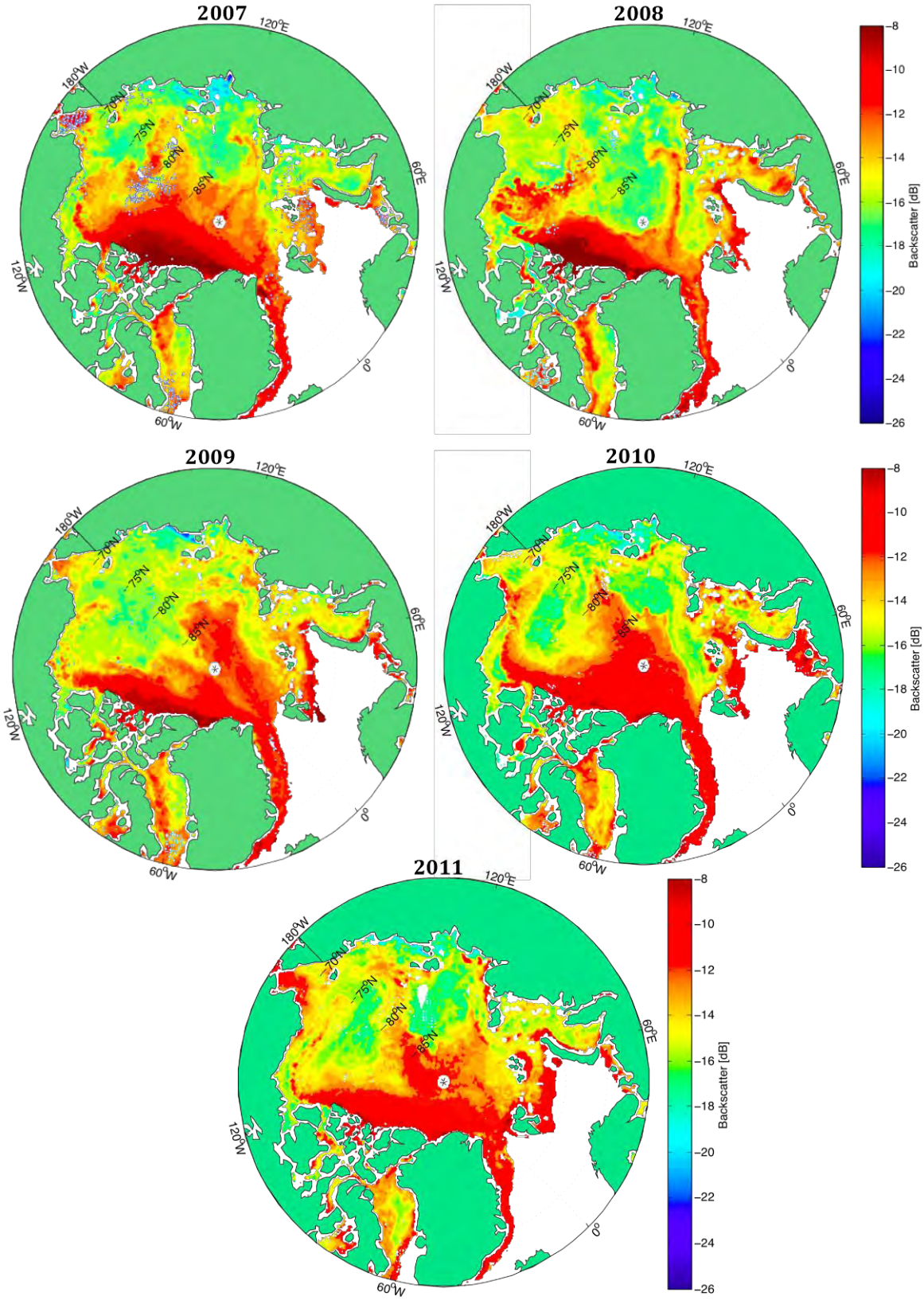

Figure 2.4: Sea ice backscatter maps from Ascat data 2007-2011. The estimated backscatter threshold value used for deliniating MYI zone (area of all partial concentrations of MYI) from FYI zone (area with all ice being FYI) is ~-10.5 dB.

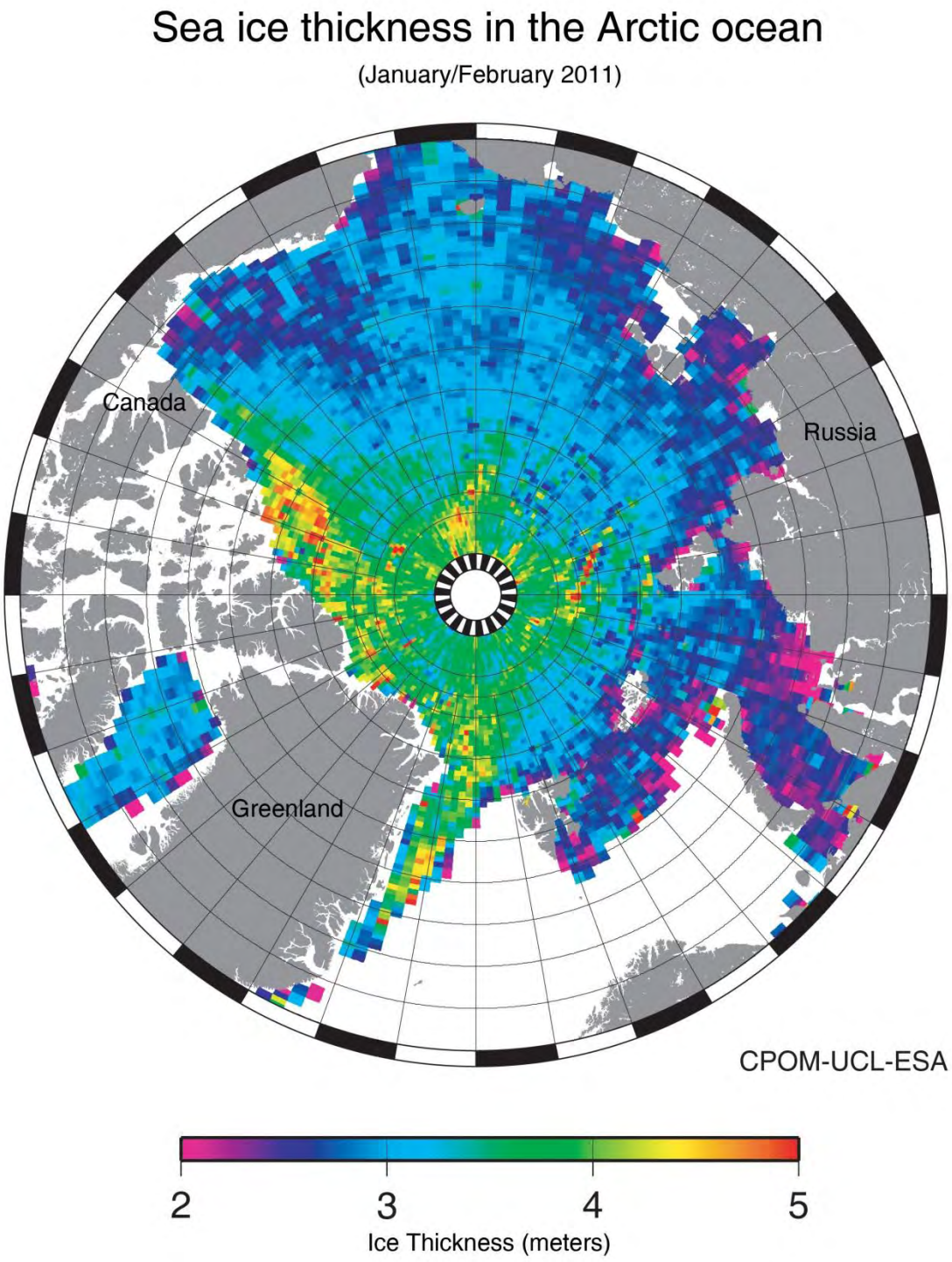

Figure 2.5. Very preliminary first sea ice thickness chart of the Arctic from ESA's Cryosat. Relative differences are clear, but absolute thicknesses of the ice still needs calibration in some areas. By courtesy: European Space Agency in collaboration with Centre for Polar Observation and Modelling, University College London

3. Ice extent off north east Greenland

3.1. Ice free season from passive microwave data

The use of satellite passive microwave radiometry for mapping of sea ice concentration, extent and area is perhaps the most successful application of satellite remote sensing for sea ice monitoring. Summer month sea ice concentrations from passive microwave data are subject to some uncertainty (up to several % in ice concentration) due to ice surface melting. Uncertainties are much less under freezing conditions in the winter months.
Data from several satellite passive microwave sensors are combined in the newly reprocessed sea ice concentration data set of the EUMETSAT OSISAF (Ocean and Sea Ice Satellite Application Facilities) extending from 1979-2009. The sea ice concentration data are given as daily 12.5x12.5 km grid cell maps (bi-daily in the period 1979-1987, due to the satellite sensor only operating every second day). This data set is used in this study to calculate the total number of days in each year with ice cover (ice concentration) less than 30%, 40% and 60% respectively in each of the regular latitude-longitude-boxes shown in **figure 3.1**, covering the East Greenland license areas. The data period is extended to the year 2010 by the use of the operational OSISAF sea ice concentration data set, given as daily 10x10 km grid cell maps.
In the first part of the data set, where data is only given for every second day, the calculated total number of days (with ice cover less than 30%, 40% and 60%) is doubled, to compensate for the missing data. Some shorter periods with lack of data (due to sensor faults) are not included in the calculations, which may lead to a reduced estimated length of the „ice free' season.

The minimum number of days with ice cover less than 30% in the Northeast Greenland waters is shown in **figure 3.1** for the period 1979-2010 and in **figure 3.2** for the period 2001-2010 . All calculated numbers of days are given in the table in **chapter 8.**.
The numbers are lowest over most of the Northeast Greenland continental shelf, in the mean drift area of the Northeast Greenland Current. Even during the rather week ice seasons of the 2000s, there are still years with ice in almost the entire continental shelf area during summers, cf. **figure 3.2**. From comparing the two periods in **figure 3.1 and 3.2** it is seen, that the average length of the ice free season has increased in Northeast Greenland waters. This is especially evident in the central eastern part, south of the KANUMAS area.
It is also evident from **figure 3.2**, that the ice free season in the area of the Northeast Polynia (east of the northeasternmost tip of Greenland) have become longer in the last decade.
Additional statistics on the data is given in **chapter 8**.
Figure 3.3 shows the difference between number of ice free days during 2001-2010 and 1979-2010.

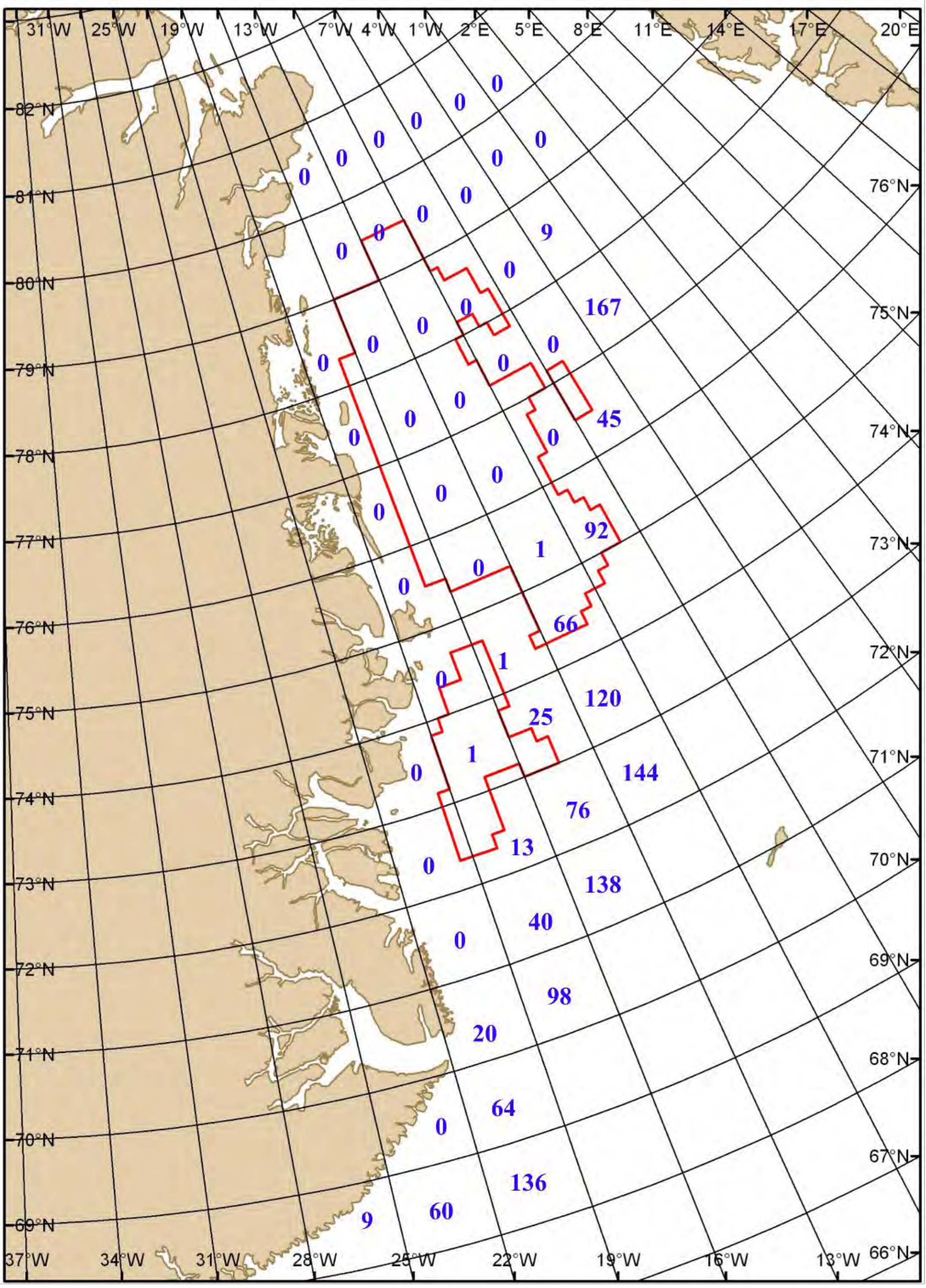

Figure 3.1: Minimum number of ice free days for the period 1979-2010 defined as number of days with passive microwave ice concentration below 30% in each box.

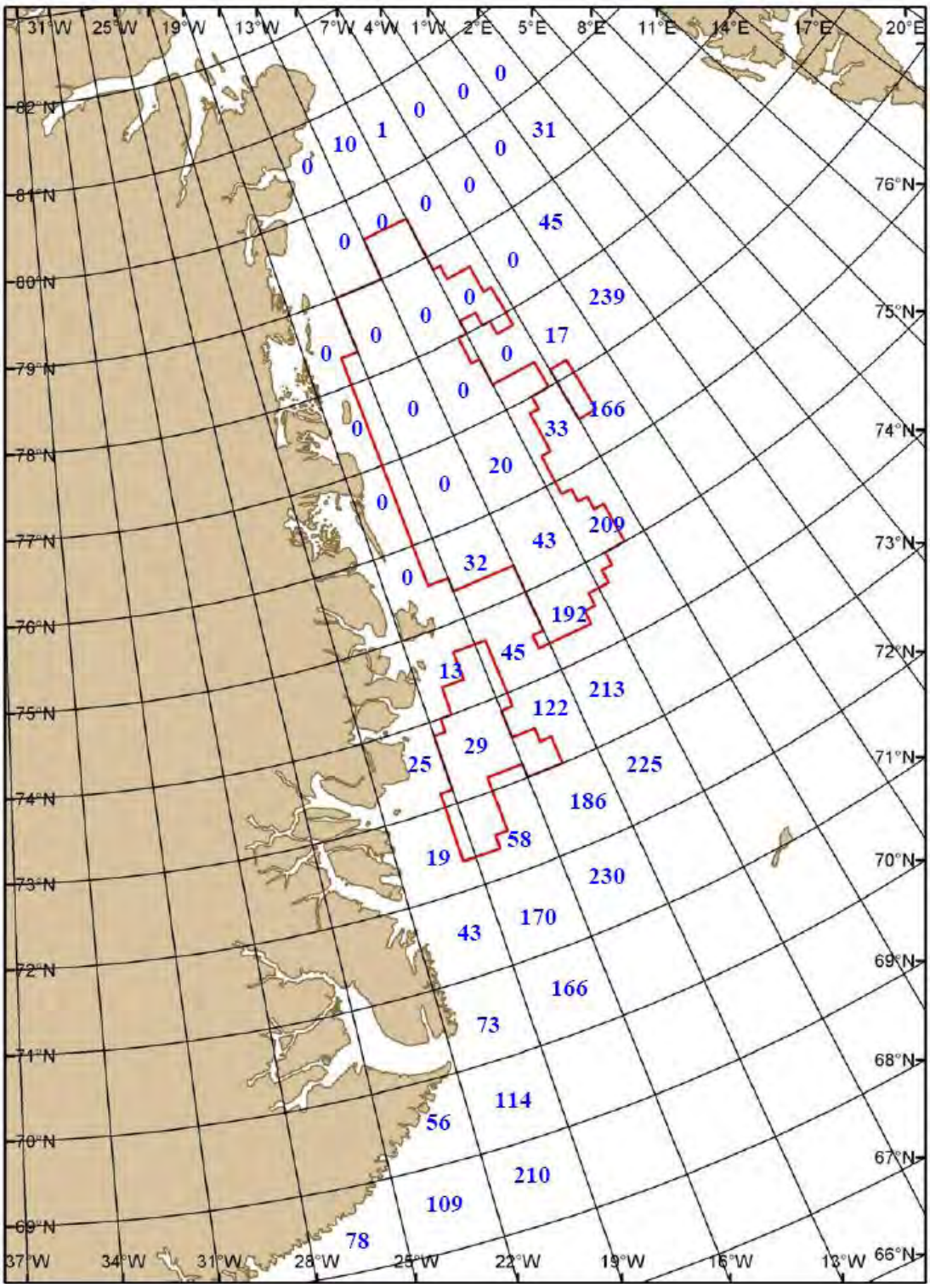

Figure 3.2: Minimum number of ice free days for the period 2001-2010 defined as number of days with passive microwave ice concentration below 30% in each box.

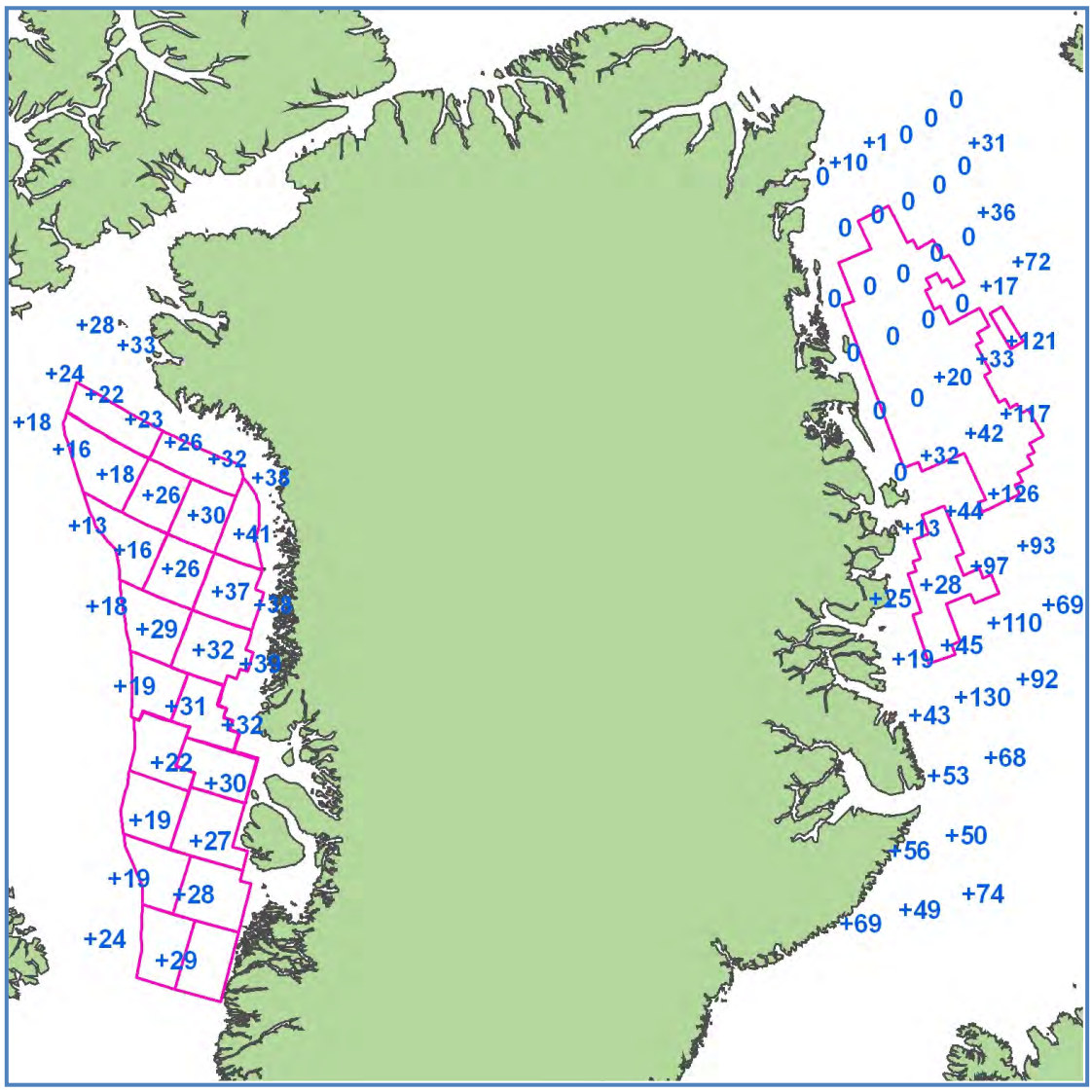

Figure 3.3. Difference in number of ice free days between the 2000-2010 period and the 1979-2010 period. In most areas off north-east Greenland the length of the minimum ice free period is still 0 days. More details in chapter 8. Note that the west-coast numbers are average number of ice free days whereas the east coast numbers are minimum numbers.

3.2. OSI SAF sea ice concentration data comparison to sea ice charts

In Greenland waters the OSISAF sea ice concentration data are compared to navigational ice charts from the Danish Meteorological Institute (DMI) and the Norwegian Meteorological Institute (Met.no). These ice charts are an independent source of sea ice data . The charts are the result of the manual interpretation of Synthetic Aperture Radar (SAR) and MODIS images as the primary data sources.

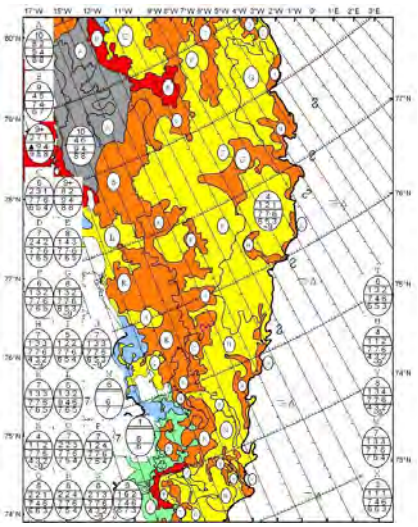

DMI ice chart

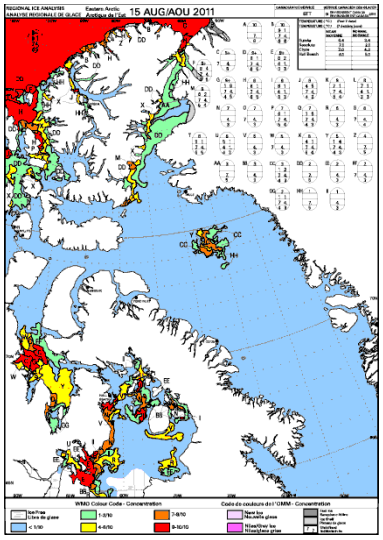

CIS ice chart

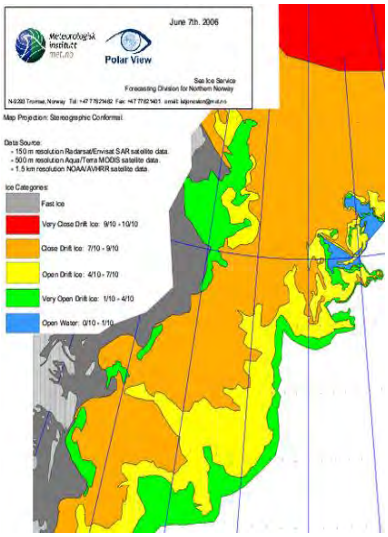

Met.no ice chart

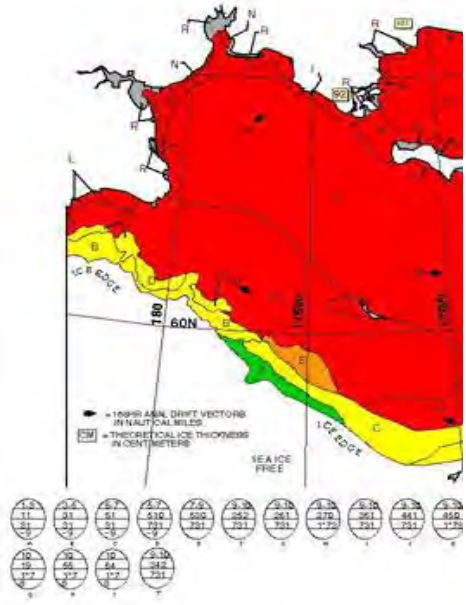

NIC ice chart

Figure 3.4 The figure show examples of ice charts from the four national ice services: DMI, CIS, met.no, and NIC (see the abbreviations explaned below).
The DMI and Met.no ice charts are used for comparison to OSI SAF sea ice concentration data while CIS, NIC and DMI data are used in the present report to estimate the open water period (operation season length).

DMI - Danish Meteorological Institute
Met.no - Norwegian Meteorological Institute
CIS - Canadian Ice Service
NIC - National Ice Service, US

3.2.1. Annual variation and accuracy of OSISAF grid data

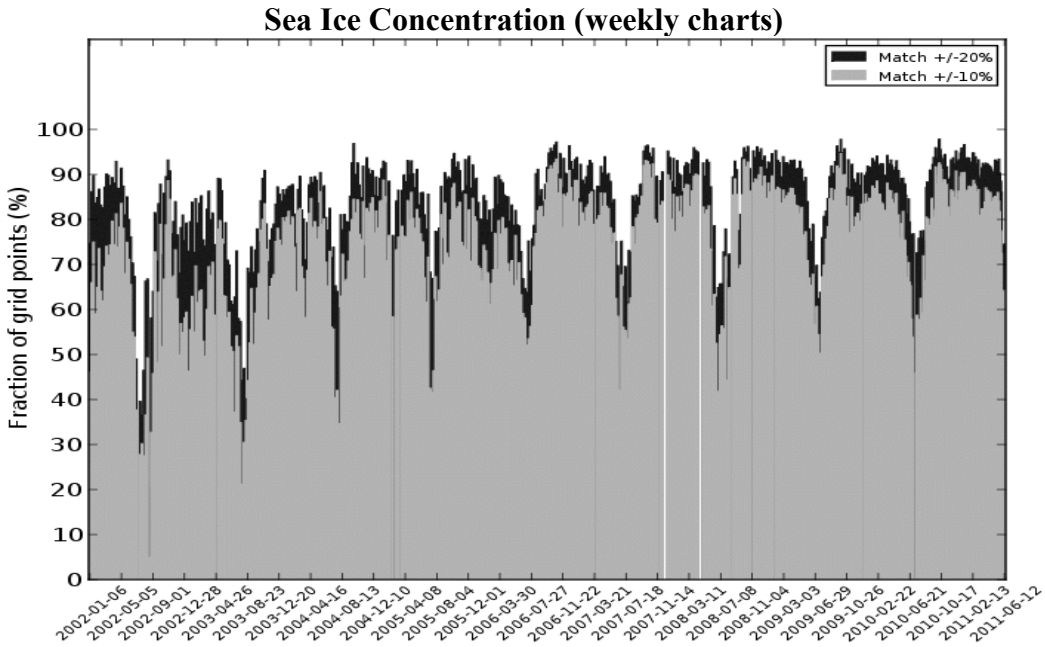

Figure 3.5 Sea ice concentration comparison of OSISAF against DMI and Met.no ice charts. The comparison is carried out as a weekly comparison by means of automatic comparison of OSISAF grid with navigational ice charts for ice concentration. Only grid points based on Radarsat high resolution data are used. Courtesy of the Norwegian Meteorological Institute. The analysis area is all of Greenland and Svalbard waters.

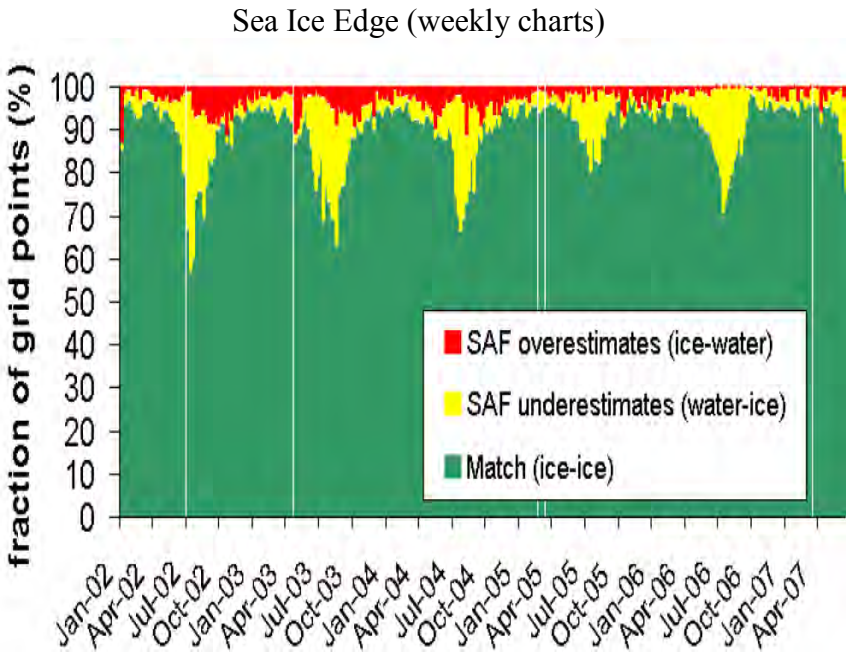

Figure 3.6 Sea ice edge comparison of OSI SAF with DMI Weekly Ice Charts. The figure shows that the largest differences occur during the summer/autumn sea ice minimum (the melt season) where OSISAF has a tendency to underestimate compared to sea ice charts. It is also noted that ice edge precision increased during the period 2002-2007. Courtesy of the Norwegian Meteorological Institute. As seen in figure 2 the largest difference occur during the summer/autumn months thus coinciding with the potential operational season for extractive industry (open water period). The analysis area is all of Greenland and Svalbard waters.

3.2.2. Point analysis validation of OSISAF against CIS and DMI ice charts

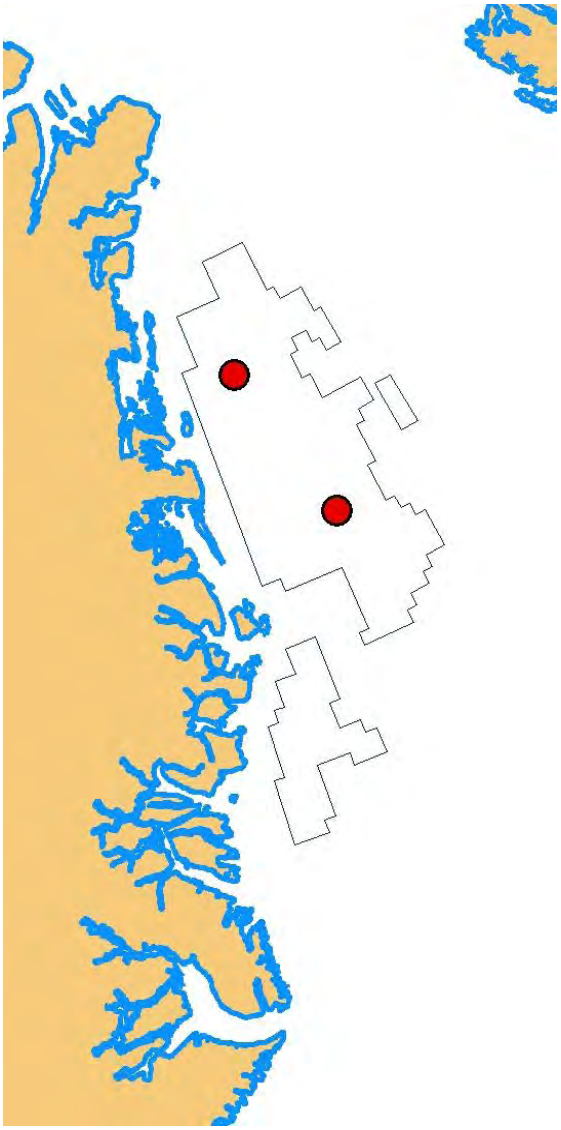

	KANUMAS EAST	
Validation points	76.00N 12.00W	78.30N 14.30W
Open water days based on DMI ice charts	Mean 24 Median 21	Mean 10 Median 0
Open water days based on NIC ice charts	Mean 32 Median 42	Mean 9 Median 0
Open water days based on OSISAF	Mean 83 Median 79	Mean 18 Median 0

The OSISAF data are in the following compared with ice charts at two selected locations in KAMUMAS East.
The open water analyses are done using ice charts from Danish Meteorological Institute and the US National Ice Center. Data are based on weekly and regional ice charts from DMI and weekly and bi-weekly charts from NIC during the period 2000-2010.

Figure 3.7. Position of the validation points used to compare the open water period in OSISAF data with operational ice charts from Danish Meteorological Institute and National Ice Center.

From the comparison of open water (OW) days in OSISAF data with the ice chart open water days it is seen that there is a substantisl difference in the estimated mean number of days between OSISAF and the DMI and NIC ice charts, especially for the northern validation point in the KANUMAS area.

The reason for the OSISAF OW length being longer than those from the ice charts, could be due to the fact that OW in OSISAF data is defined as an ice concentration below 30%. This threshold is chosen as a result of the relatively coarser resolution in the data. Longer periods with ice less than 30% will lead to a longer 'ice free' period in the OSISAF data. In the icechart analysis the open water period is defined as the period where ice concentration is less than 0 which means a shorter period.

For both data points, the number of OW days calculated from OSISAF data is longer compared to the OW period found in the DMI and NIC ice charts. This may be due to the validation points

experiencing lower ice concentrations in the summer months, as evident from the sea ice concentration tables below. OSISAF data may successfully capture the high ice concentrations in the main drift of the East Greenland Current in winter time, but estimating the length of the open water season in areas of extended periods of low concentrations should be used with caution. This is especially true for the south-eastern validation point (76.00N, 12.00W) being closest to the ice edge.

3.2.3. Analysis point KANUMAS East 76.12N 12.00W (2000-2009)

Summer of	Season start	Season End	Max Season Length (dys)	Max Season less Intrups	Intrups (days)	Winter of	Duration days
2000	27-Sep-00	27-Sep-00	0	0	0	2000/01	343
2001	06-Sep-01	27-Sep-01	21	21	0	2001/02	315
2002	09-Aug-02	27-Sep-02	49	49	0	2002/03	322
2003	16-Aug-03	27-Sep-03	42	42	0	2003/04	336
2004	30-Aug-04	04-Oct-04	35	35	0	2004/05	343
2005	13-Sep-05	27-Sep-05	14	14	0	2005/06	350
2006	13-Sep-06	27-Sep-06	14	14	0	2006/07	322
2007	16-Aug-07	27-Sep-07	42	28	14	2007/08	322
2008	16-Aug-08	04-Oct-08	49	42	7	2008/09	301
2009	02-Aug-09	27-Sep-09	56	49	7	2009/10	*****
Mean	23-Aug	27-Sep	32	29	3		328
Median	30-Aug	27-Sep	42	35	0		336
Number of years with no season =			1	out of	10	years, or 1 in	10
When there are seasons, the mean values are:							
Actual Seasons	23-Aug	27-Sep	36	33			

Season Start and End dates, and summer and winter season durations.
Latitude 76* 12'N and Longitude 12* 00'W
Season Starts when All Ice is <= 1/10 in spring and Ends when All Ice is > 1/10 in fall.

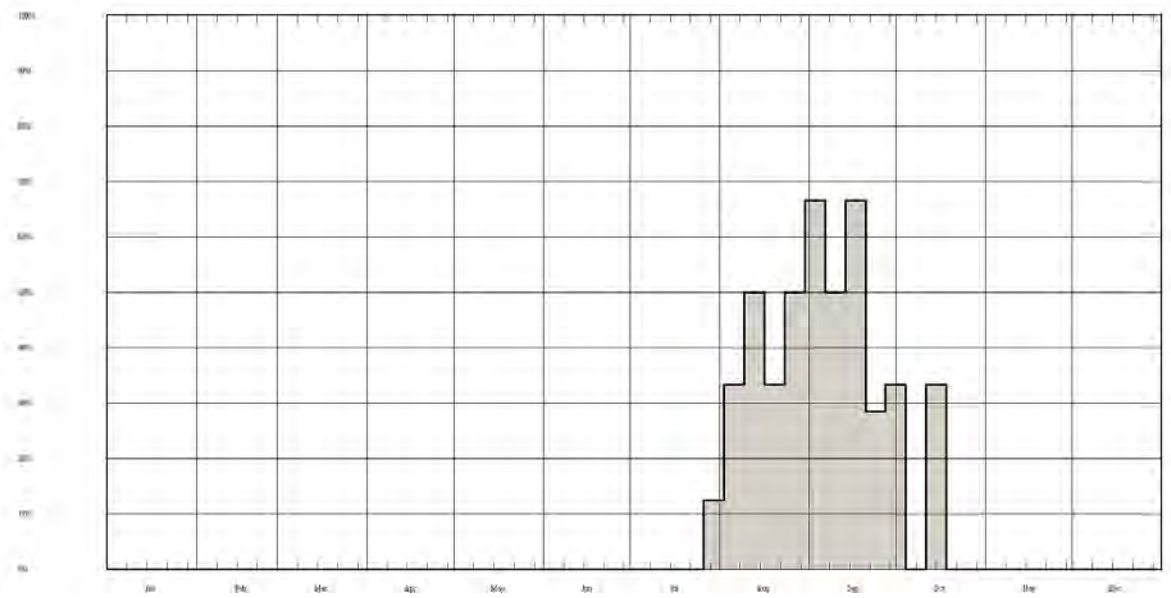

Figure 3.8, Average length of ice free season at the southern location (76.12N, 12W) according to NIC icecharts.

3.2.4. Analysis point KANUMAS East 78.30N 14.30W (2000-2009)

Summer of	Season start	Season End	Max Season Length (dys)	Max Season less Intrups	Intrups (days)	Winter of	Duration days
2000	27-Sep-00	27-Sep-00	0	0	0	2000/01	364
2001	27-Sep-01	27-Sep-01	0	0	0	2001/02	343
2002	06-Sep-02	27-Sep-02	21	21	0	2002/03	294
2003	19-Jul-03	27-Sep-03	70	70	0	2003/04	364
2004	27-Sep-04	27-Sep-04	0	0	0	2004/05	364
2005	27-Sep-05	27-Sep-05	0	0	0	2005/06	364
2006	27-Sep-06	27-Sep-06	0	0	0	2006/07	364
2007	27-Sep-07	27-Sep-07	0	0	0	2007/08	364
2008	27-Sep-08	27-Sep-08	0	0	0	2008/09	364
2009	27-Sep-09	27-Sep-09	0	0	0	2009/10	*****
Mean	13-Sep	27-Sep	9	9	0		353
Median	27-Sep	27-Sep	0	0	0		364
Number of years with no season =			8	out of	10	years, or 1 in	1
When there are seasons, the mean values are:							
Actual Seasons	09-Aug	27-Sep	46	46			

Season Start and End dates, and summer and winter season durations.
Latitude 78* 30'N and Longitude 14* 30'W
Season Starts when All Ice is <= 1/10 in spring and Ends when All Ice is > 1/10 in fall.

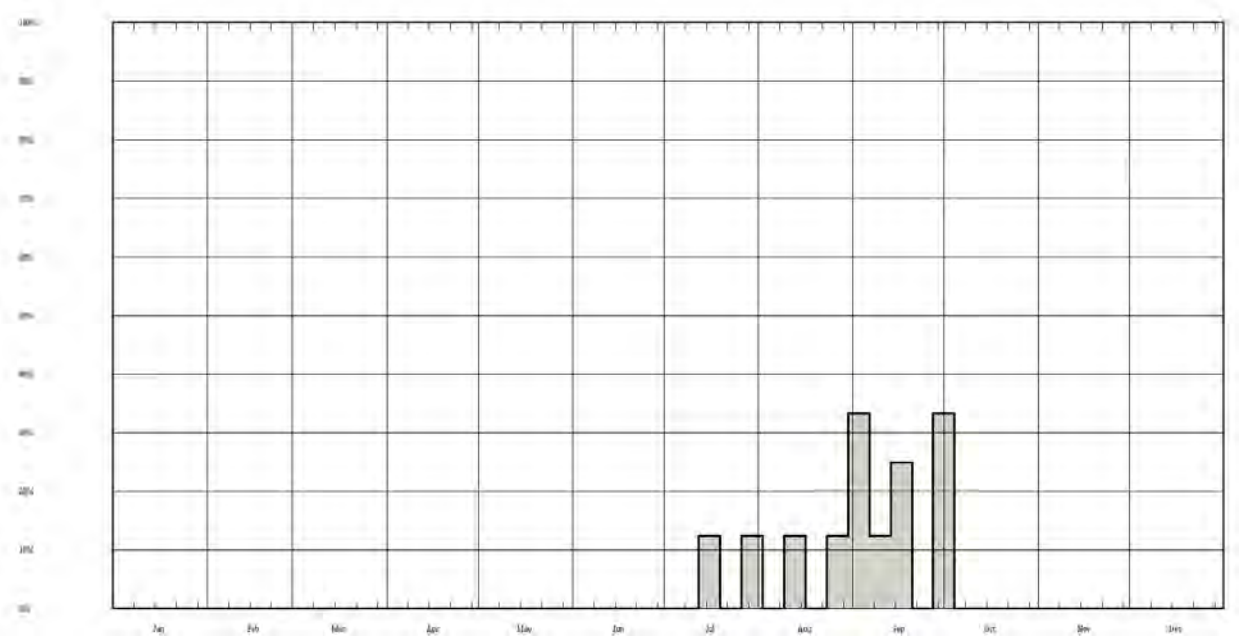

Figure 3.9, Average length of ice free season at northern location according to NIC ice charts.

3.2.5. KANUMAS East analysis points

Figure 3.10 shows a graphical representation of ice concentrations extracted from DMI weekly icecharts from the last 10 years at the 2 locations. The figure illustrates the interannual variability of the ice cover. This will be further illustrated in **chapter 3.3**.

	KANUMAS EAST 76.00N 12.00 W											KANUMAS EAST 78.30N 14.30W										
Week of	2000	2001	2002	2003	2004	2005	2006	2007	2008	2009	2010	2000	2001	2002	2003	2004	2005	2006	2007	2008	2009	2010
Jan 01	9+	9+	9	9	9+	9	9	9	9	9	9	9+	9+	9	9	9+	9	10	9	9	9	9
Jan 08	9+	9+	9+	9	9+	9	9	8	9	9	9	9+	9+	9+	9	9+	9	9	9+	9	9	9
Jan 15	9+	9+	9+	9	9+	9	9	9+	9	9	9	9+	9+	9+	9	9+	9	9	9+	9	9	9
Jan 22	9+	9+	9+	9	9+	8	9	9+	9	9	9	9+	9+	9+	9	9+	9	9	9+	9	9	9
Jan 29	9+	9+	9+	9	9+	8	9	9	9	9	9	9+	9+	9+	9	9+	9	9	9	9	9	9
Feb 05	9+	9	9	9	9+	9	9	8	9	9	9	9+	9	9	9	9+	9	9	9	9	9	9
Feb 12	9+	9	9+	9	9+	9	9	9	9	9	9	9+	9	9+	9	9+	9	9	9	9	9	9
Feb 19	9+	9	9+	9	9+	9	8	9	9	9	9	9+	9	9+	9	9+	9	8	9	9	9	9
Feb 26	0	9	9+	9	8	9	8	9	9	9	9	9+	9	9+	9	9	9	9	9	9	9	9
March 05	9+	9	9+	9	9	9	9	9+	9	9	9	9+	9	9+	9	9	9	9	9+	9	9	9
March 12	9+	9	9+	9	9	9	9	9+	9	9	9	9+	9	9+	9	9	9	9	9+	9	9	9
March 19	9+	9	9+	9	9+	9	9	9	9	9	9	9+	9	9+	9	10	9	9	9	9	9	9
March 26	9+	8	9+	9	9	9	9	9	9	9	9	9+	8	9+	9	10	9	9	9	9	9	9+
April 02	9+	9	9+	9	9	9	9	9	9	9	9	9+	9	9+	9	9	9	9	9	9	9	9+
April 09	9+	9	9+	9	9	9	9	9	9	9	9	9+	9	9+	9	9	9	9	9	9	9	9+
April 16	9+	9	9+	9	9	8	9	9	9+	9	9	9+	9	9+	9	9	8	9	9	9+	9	9
April 23	9+	9	9+	9	9	9	8	9	8	9	9	9+	9	9+	9	9	9	9	9	9	9	9
April 30	9	9	9+	9	9	9	9	9	9	9	9	9	9	9+	9	9	9	9	9	9	9	9
May 07	9+	9	9+	9	8	9	9	9	9	9	9	9+	9	9+	9	8	9	9	9	10	9	9
May 14	9+	9	9+	9	0	8	5	9	9	9	9	9+	9	9+	9	8	9	9	9	9	9	9
May 21	9+	9	9+	9	9	8	6	9	9	8	9	9+	9	9+	9	9	9	9	9	9	8	9
May 28	9+	9+	9	8	9		7	9	9	8	9	9+	9+	9	8	9	6	9	9	9	8	9
June 04	9+	8	9	8		9	0	8	9	7	9	9+	8	9	8		9	9	8	9	7	9
June 11	9+	8	8	8	9	9	4	9	8	7	9	9+	8	8	8	9	9	8	9	8	7	9
June 18	9	7	8	8	9	8	7	9	8	8	8	9	9	8	8	9	9	9	9	8	8	9
June 25	9	9	6	8	8	8	7	8	8	8	9	8	9	8	2	8	8	9	9	8	8	9
July 02	8	5	8	8	8	8	9	8	6	7	9	8	9	8	8	8	8	9	8	8	9	9
July 09	8	8	6	8	7	4	9	8	9	9	9	8	8	8	2	8	8	9	8	9	9	9
July 16	8	8	6	6	7	7	4	7	6	7	8	8	8	6	6	7	8	9	8	8	7	9
July 23	8	8	6	8	4	9	8	5	6	3	8	8	8	6	8	7	8	9	8	6	8	8
July 30	8	8	6	6	7	9	3	7	5	3	8	7	8	2	0	7	8	7	8	6	9	8
Aug 06	8	8	3	6	6	8	7	0	6	8	8	7	8	4	0	6	9	7	9	6	9	9
Aug 13	8	6	3	5	10	8	3	0	2	0	7	7	7	3	0	10	8	7	10	9	8	9
Aug 20	6	6	3	4	8	6	2	6	0	0	7	6	6	3	0	6	7	7	10	5	9	8
Aug 27	7	5	0	1	0	6	2	4	0	0	6	7	6	0	1	6	7	9+	7	2	8	7
Sep 03	6	0	0	0	0	0	5	5	6	6	5	6	5	4	1	2	4	8	5	0	7	8
Sep 10	6	0	0	0	0	2	1	5	0	4	6	6	5	0	1	6	5	5	5	0	9	8
Sep 17	7	0	0	0	0		0	8	0	7	0	4	2	0	0	2		9	9	0	9	6
Sep 24	7	0	0	0	0	5	2	8	0	8	3	7	5	0	0	0	8	8	7	0	9	6
Oct 01	6	0	0	2	0	9	4	8	0	6	5	9+		0	6	7	9	8	9	0	9	8
Oct 08	8	6	0	8		9	8	8	6	9	7	8	3	0	8		9	9	8	7	9	9
Oct 15	8	2	0	8	5	9	9	8	7	8	9	8	6	0	8	8	9	9	8	7	9	9
Oct 22	8	8	0	8	5	9	9	8	7	9	9	9	8	8	8	8	9	9	8	9	9	9
Oct 29	9+	8	8	8	9	9	8	7	8	9	9	9+	8	8	8	9+	9	8	8	9	9	9
Nov 05	9+	8	8	9	8	9	8	7	9	9	9	9+	8	8	9	8	9	8	8	9	9	9
Nov 12	9+	9	9	9	5	9	8	9	9	9	9	9+	9	9	9	8	9	8	9	9	9	9
Nov 19	9+	9	9	9	8	9	8	9	9	9	9	9+	9	9	9	9	9	9+	9	9	9	9+
Nov 26	9+	9	9	9	8	9	9+	9+	9	9	9	9+	9	9	9	9	9	9+	9+	9	9	9
Dec 03	9+	9	9	9	9+	9	9+	9	9	9	9	9+	9	9	9	9+	9	9+	9	9	9	9
Dec 10	9+	9	9	8	9	9	9+	9+	9	9	9	9+	9	9	9	9	9	9+	9+	9	9	9
Dec 17	9+	9	9	9+	9	9	9	9	9	9	9	9+	9	9	9+	9	9	9	9	9	9	9
Dec 24	9+	9+	9	9+	9	9	9+	9	9	9	9	9+	9+	9	9+	9	9	9+	9	9	9	9

Figure 3.10. The numbers represent sea ice concentration. Blue 0 are open water. White blocks are weeks when no ice charts are available. Note a tendency over the last 10 years to shorter ice free periods.

3.3. Overview images from AMSR-E microwave radiometer for the entry and exit of the ice free season

The images below are extracted from http://www.seaice.dk which is operated by DTU-Space and provides a wealth of daily satellite images from the last almost 10 years.

The images are acquired by NASA's microwave radiometer on-board the AQUA satellite.

The purpose of the images is to illustrate interannual variability. Especially during summer some atmospheric features such as heavy clouds may be misinterpreted as ice so please always use images from several days or refer to icecharts when operational support is needed.

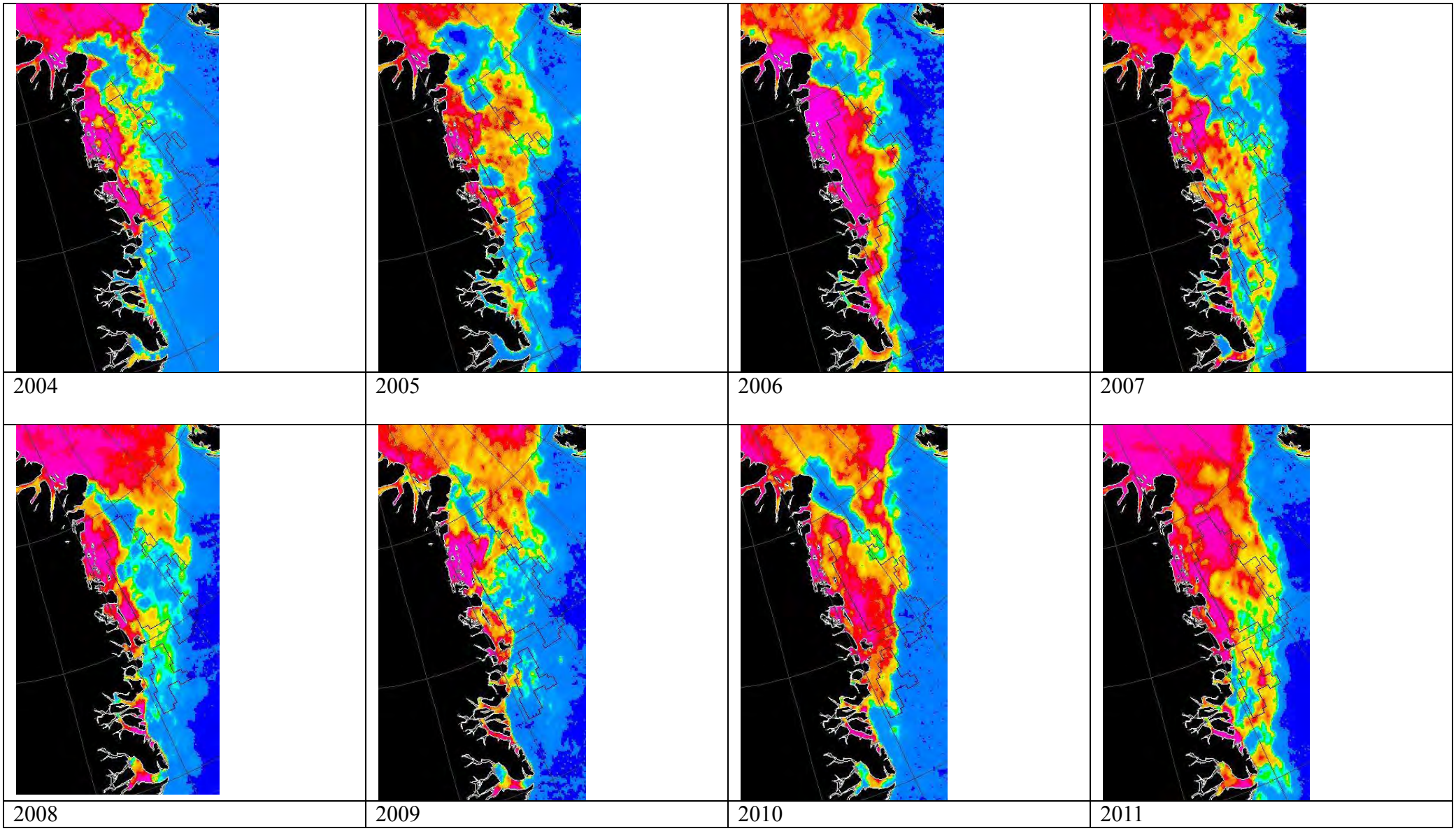

Figure 3.10. Ice conditions July 11 from AMSR-E data

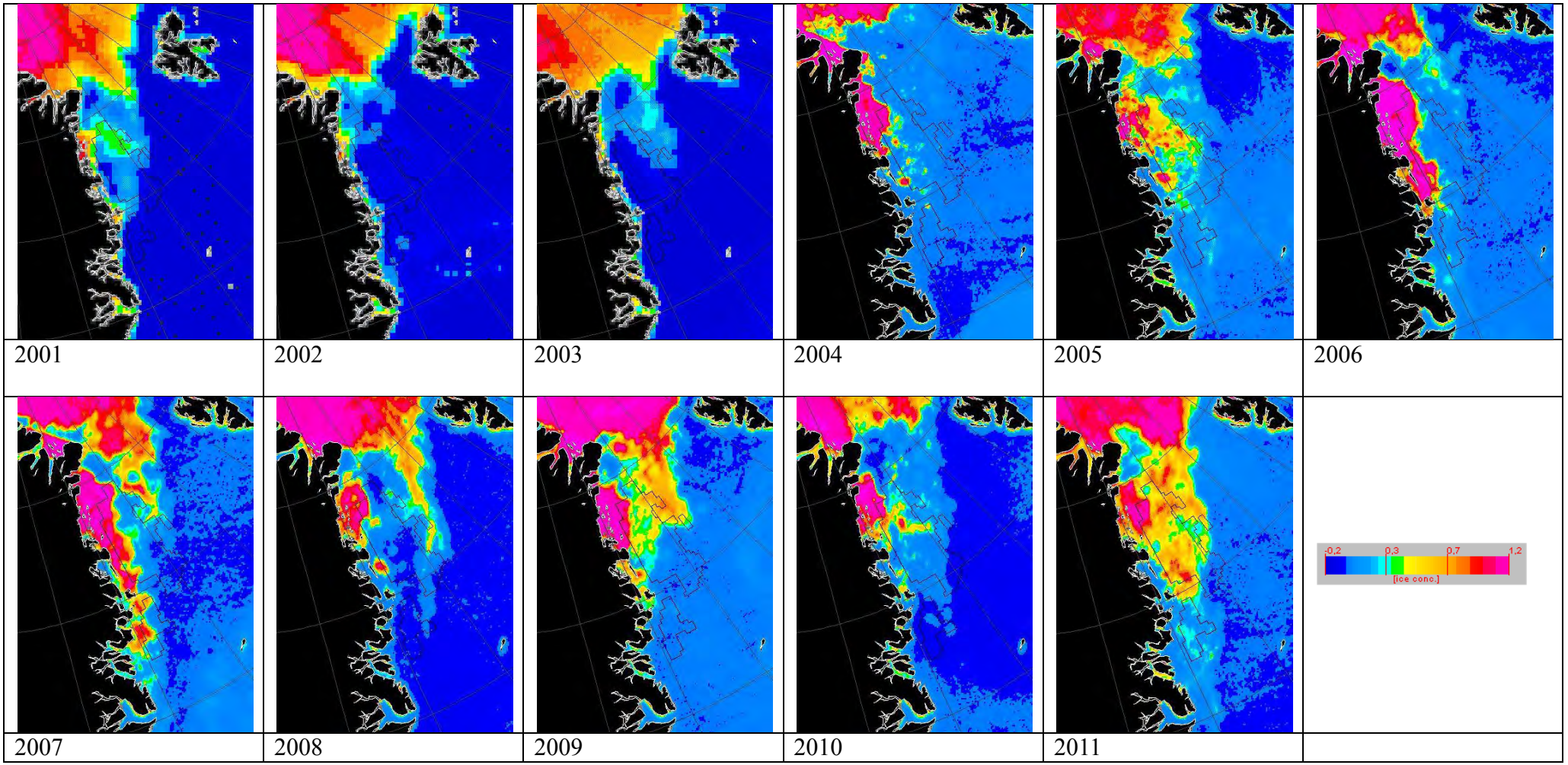

Figure 3.11. August 11 ice conditions 2001-2003 from SSMI, 2004-2011 from AMSR.

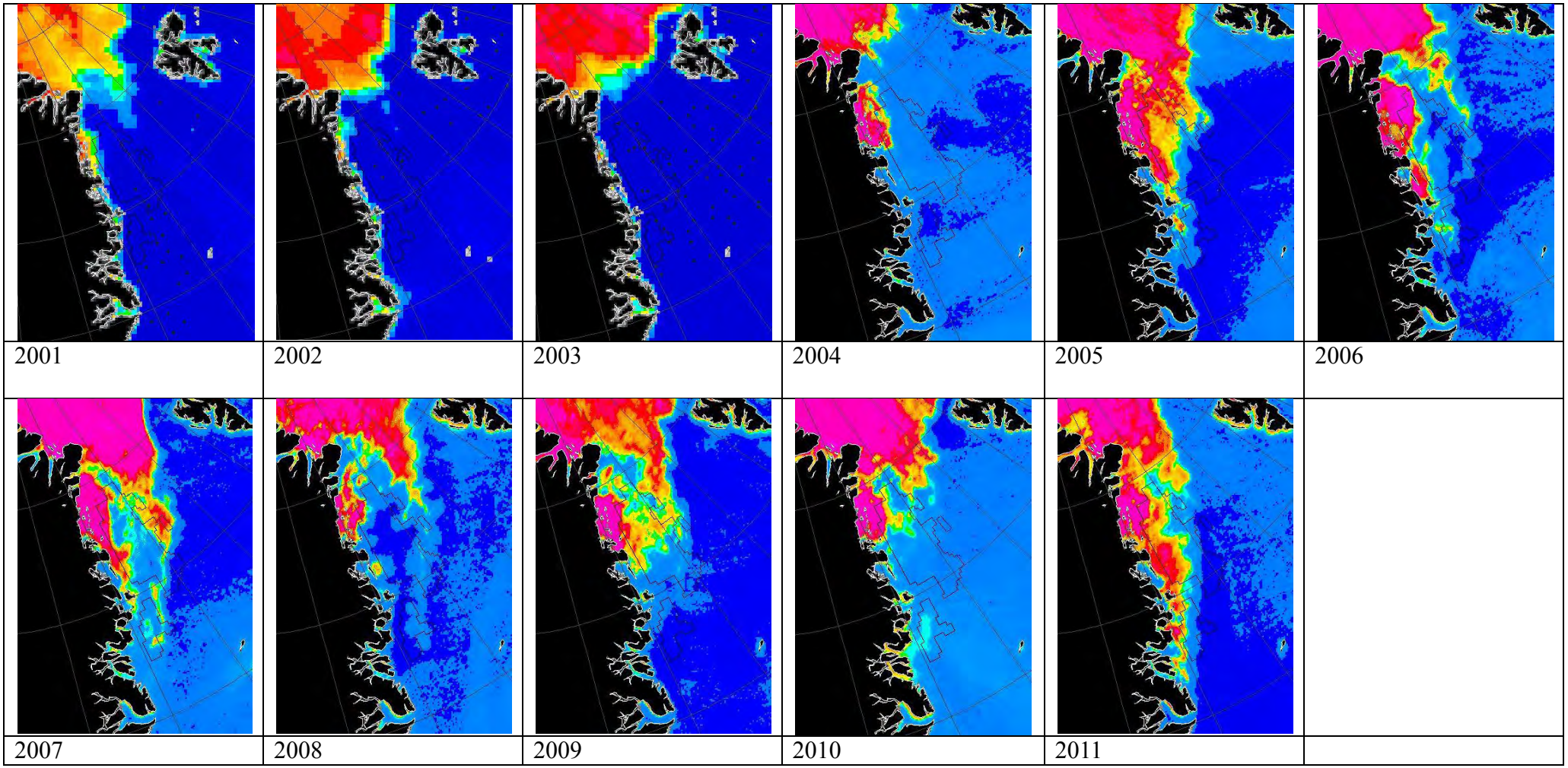

Figure 3.12. September 11 ice conditions, 2001-2003 from SSMI, 2004-2011 from AMSR.

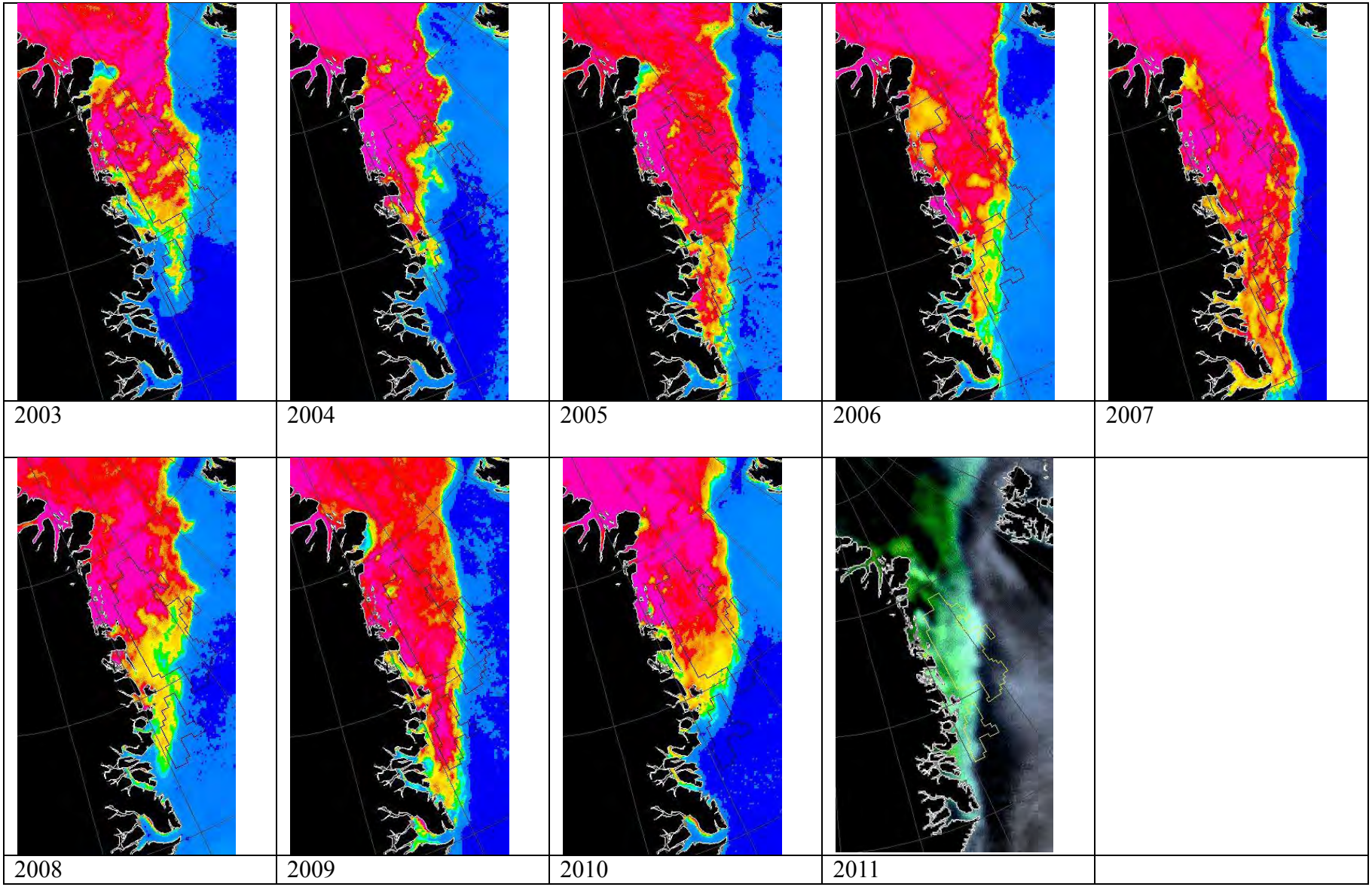

Figure 3.13. Ice conditions October 11 from AMSR-E and AMSU. AMSR-E failed in late September 2011.

4. Ice types/thickness

4.1. Ice type from Scatterometer data

Satellite Radar Scatterometer datasets has proven to be a valuable source on information on large-scale sea ice type discrimination. The frequent, wide-swath coverage allows investigation of sea ice on hemispheric scale on a near-daily basis, but at a low resolution (several kilometers).
The dielectric and scattering properties of sea ice and its surface enables a categorization of first-year ice (FYI) and multiyear ice (MYI) from radar backscatter data. In this study, the distribution of FYI and MYI is estimated from Quikscat and Ascat satellite scatterometer data
The two scatterometers operates at different wavelengths. Quikscat data for the years 1999-2009 has proven well-suited for ice type classification and has a lower noise level and greater sensitivity to ice type, than Ascat data. But the Ascat data allows the scatterometer data record to be extended with the years 2010-11.
The MYI zone (sea ice area with any partial concentration of MYI) and FYI zone (sea ice area where no MYI at all is present) is here delineated using a simple threshold backscatter value, that was found in a statistical study of typical backscatter signatures over sea ice. Due to the low data resolution, the ice type classification is best determined for areas (grid cells) where the concentration of one of the two ice types exceeds 70%.
Ice type classification using backscatter data is difficult during the summer months due to ice surface melting. Backscatter signatures are stable under freezing conditions in the winter months; therefore this study uses daily backscatter data maps in 12.5 x 12.5 km grid cells for a six-day period in the end of February (20^{th}–25^{th}). From this six-day data period for each of the years 2000-2011, the *mode* was calculated in each grid cell to reveal the most frequent occurring of the three classes: MYI, FYI and open water. Also the *max* was calculated in each grid cell, to reveal the *heaviest* ice conditions (MYI before FYI and Open water) possible over the six-day period.

The following **Figures 4.1-6** shows a series of *mode* and *max* distribution plots for ultimo February 2000-2009. The figures to the left show the *mode* and the figures to the right show the *max* or heaviest conditions. The colour code follows the WMO (World Meteorological Organization) sea ice code: FYI is given by the yellow colour, MYI by red, Open Water by light blue and No Data by white (no colour).

As described earlier in this report (**chapter 2**_on general ice conditions) the sea ice drifting in the East Greenland Current along the Greenland East Coast consist in general of multi-year ice from the Central Arctic and first-year ice formed along the Siberian coast and *in-situ*. Both the annual and interannual variability in outflux of MYI and FYI through Fram Strait is high, as is also evident from the Ice Type maps in figure **4.1-6**. As it is seen from the Ice Maps, the inner flow of the East Greenland Current (also called the *main* flow) predominantly consists of MYI, whereas the FYI is the dominant ice type in the marginal ice zone.
Studies made on the Fram Strait sea ice export during the last decade, shows that there is no significant increase in either export or a decrease in the mean thickness of the sea ice exported. The ice in the East Greenland Current may have become thinner, containing a larger fraction winter ice relative to old ice, but there may also be a greater occurrence of ridged ice as a result of increased deformation rates in the Arctic Ocean.
In winter Northeast Greenland coastal zones are characterized by large areas of fastice; predominantly firstyear, but also perennial. Particularly the recurring fastice-plate around 80°N is evident from the Ice Type maps.
New-ice formation along the ice edge in and around the Jan Mayen Current (the so-called Odden feature) is evident on the 2001, 2002 and 2004 Ice Maps.

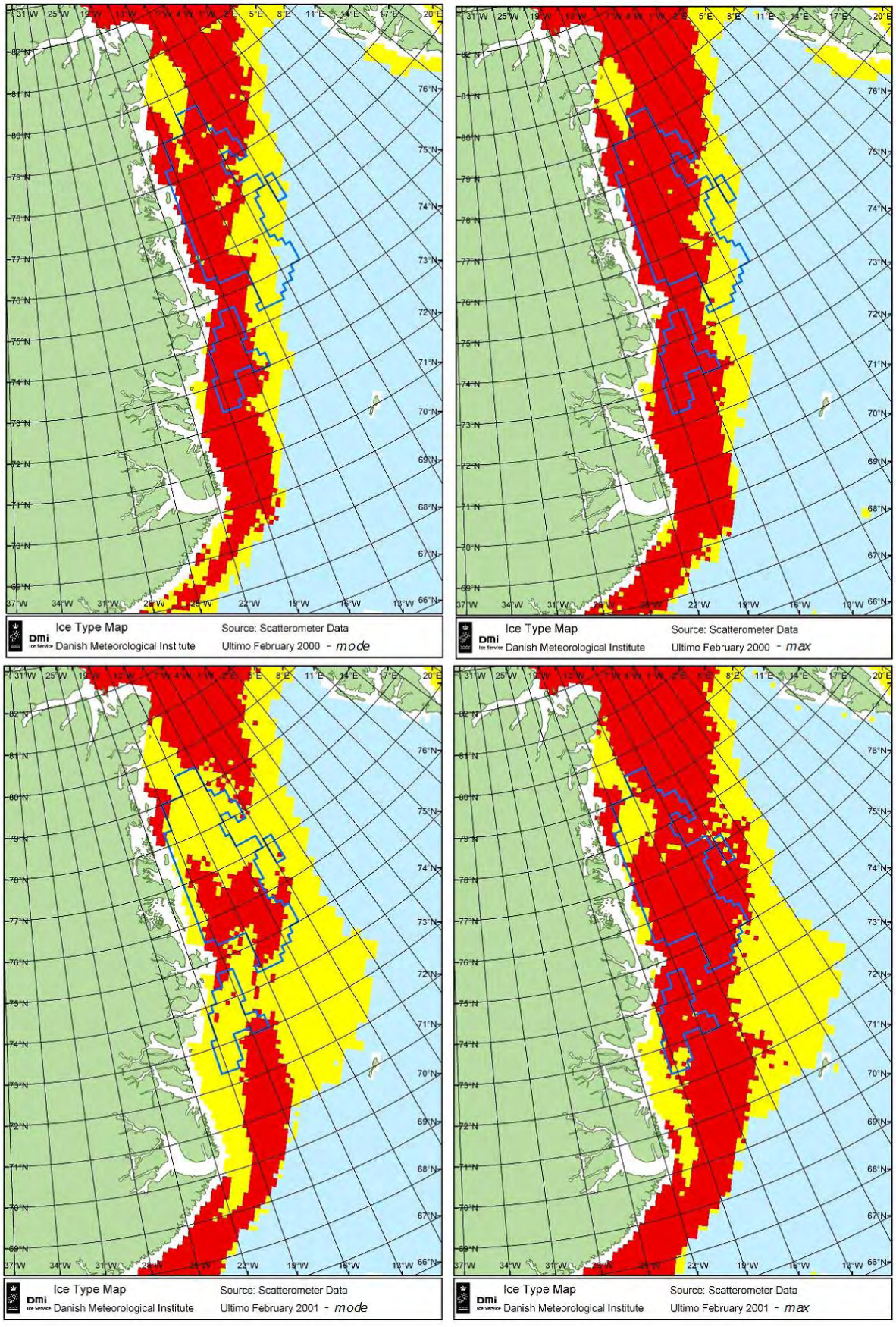

Figure 4.1: Ice Type maps from Quikscat backscatter data showing MYI (red) and FYI (yellow) ultimo February 2000 [top] and 2001 [bottom]

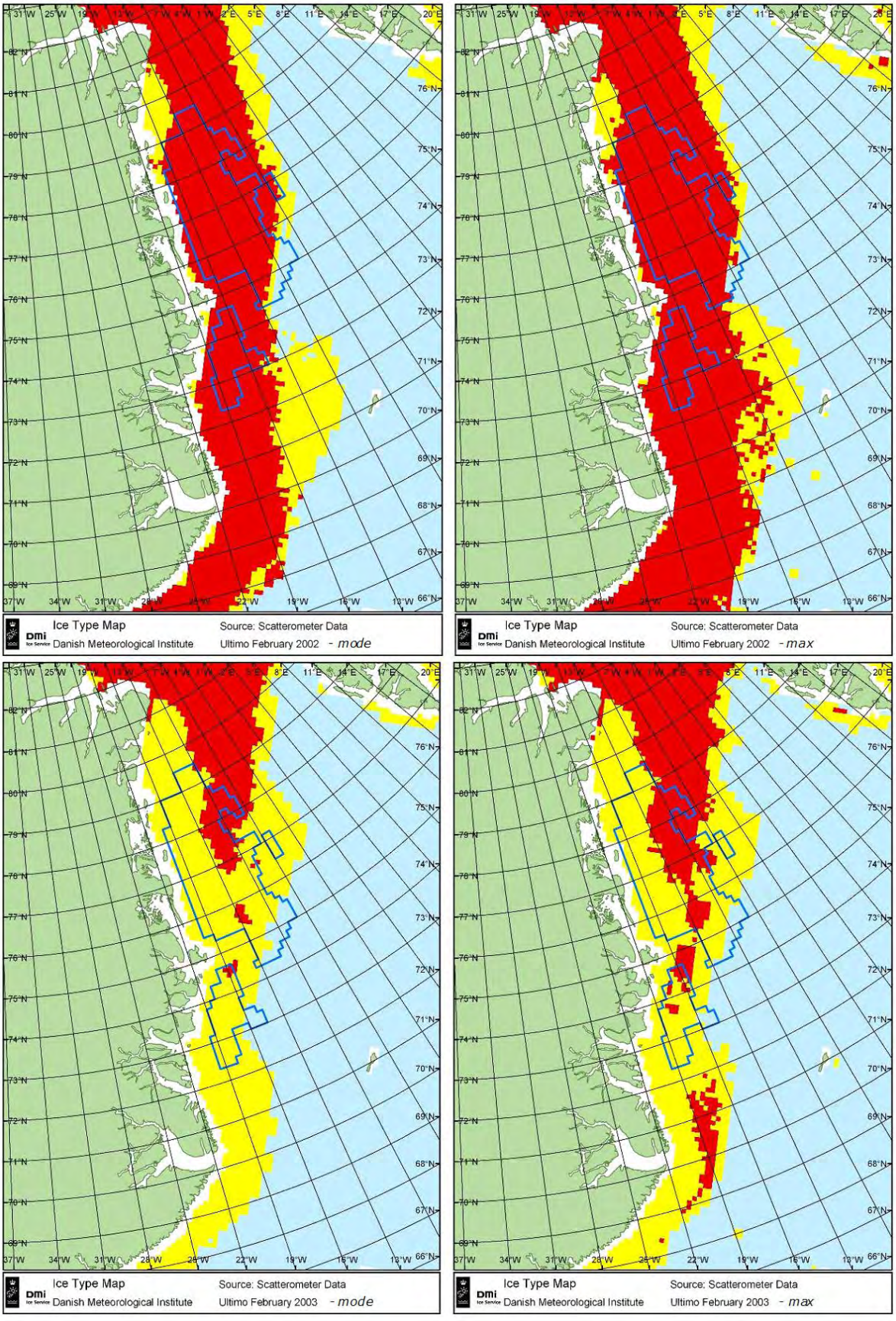

Figure 4.2: Ice Type maps from Quikscat backscatter data showing MYI (red) and FYI (yellow) ultimo February 2002 [top] and 2003 [bottom].

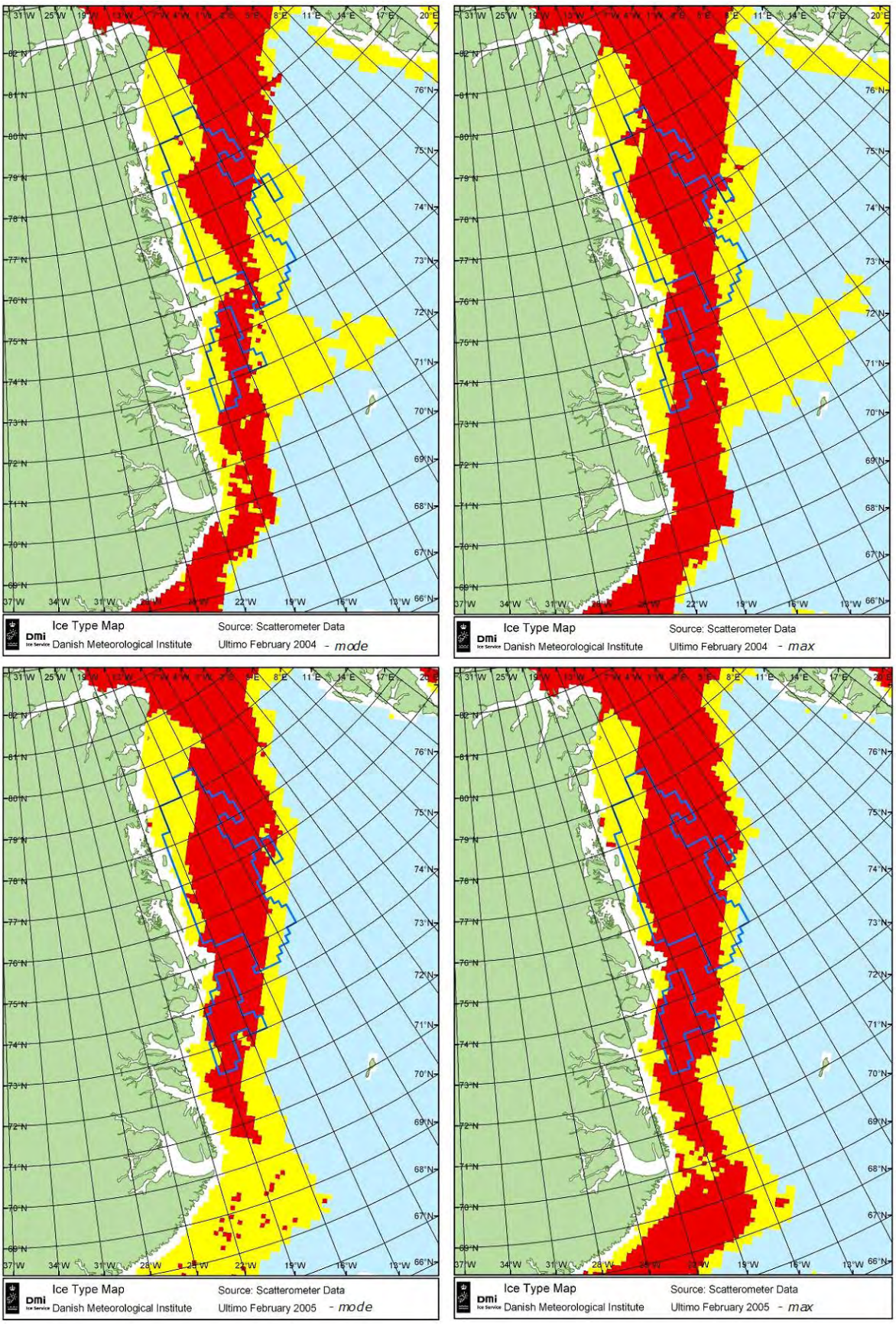

Figure 4.3: Ice Type maps from Quikscat backscatter data showing MYI (red) and FYI (yellow) ultimo February 2004 [top] and 2005 [bottom].

.

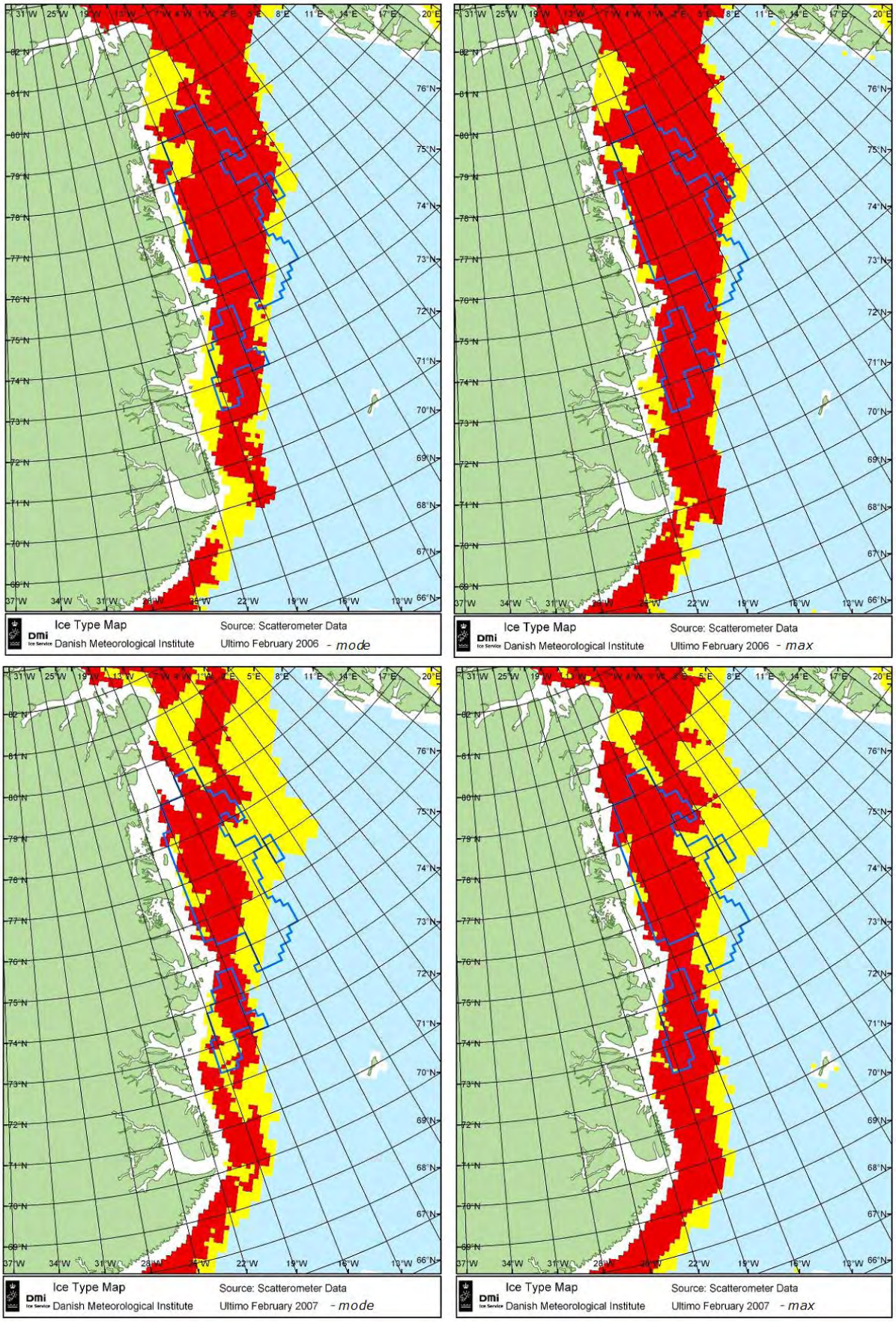

Figure 4.4: Ice Type maps from Quikscat backscatter data showing MYI (red) and FYI (yellow) ultimo February 2006 [top] and 2007 [bottom].

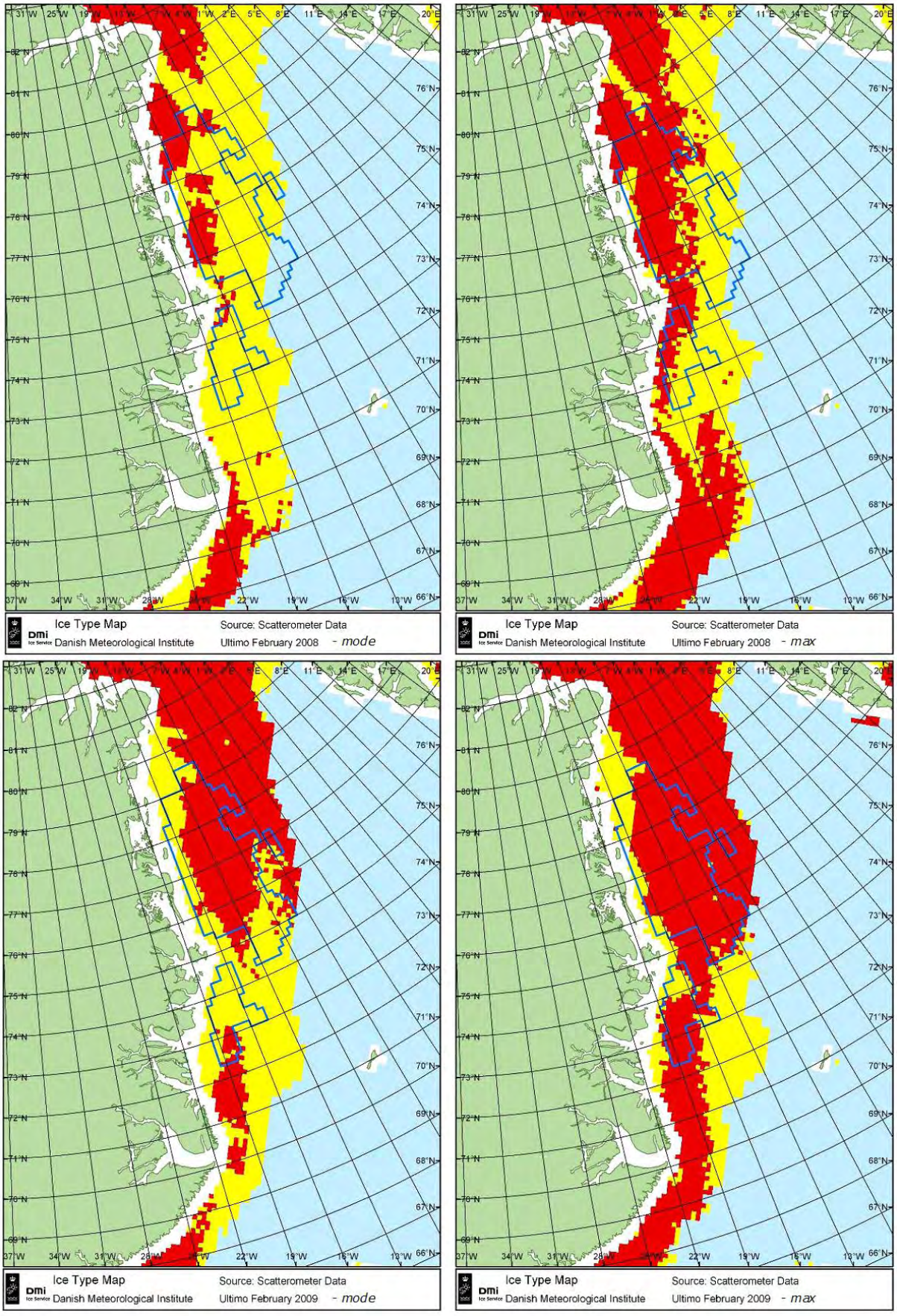

Figure 4.5: Ice Type maps from Quikscat backscatter data showing MYI (red) and FYI (yellow) ultimo February 2008 [top] and 2009 [bottom].

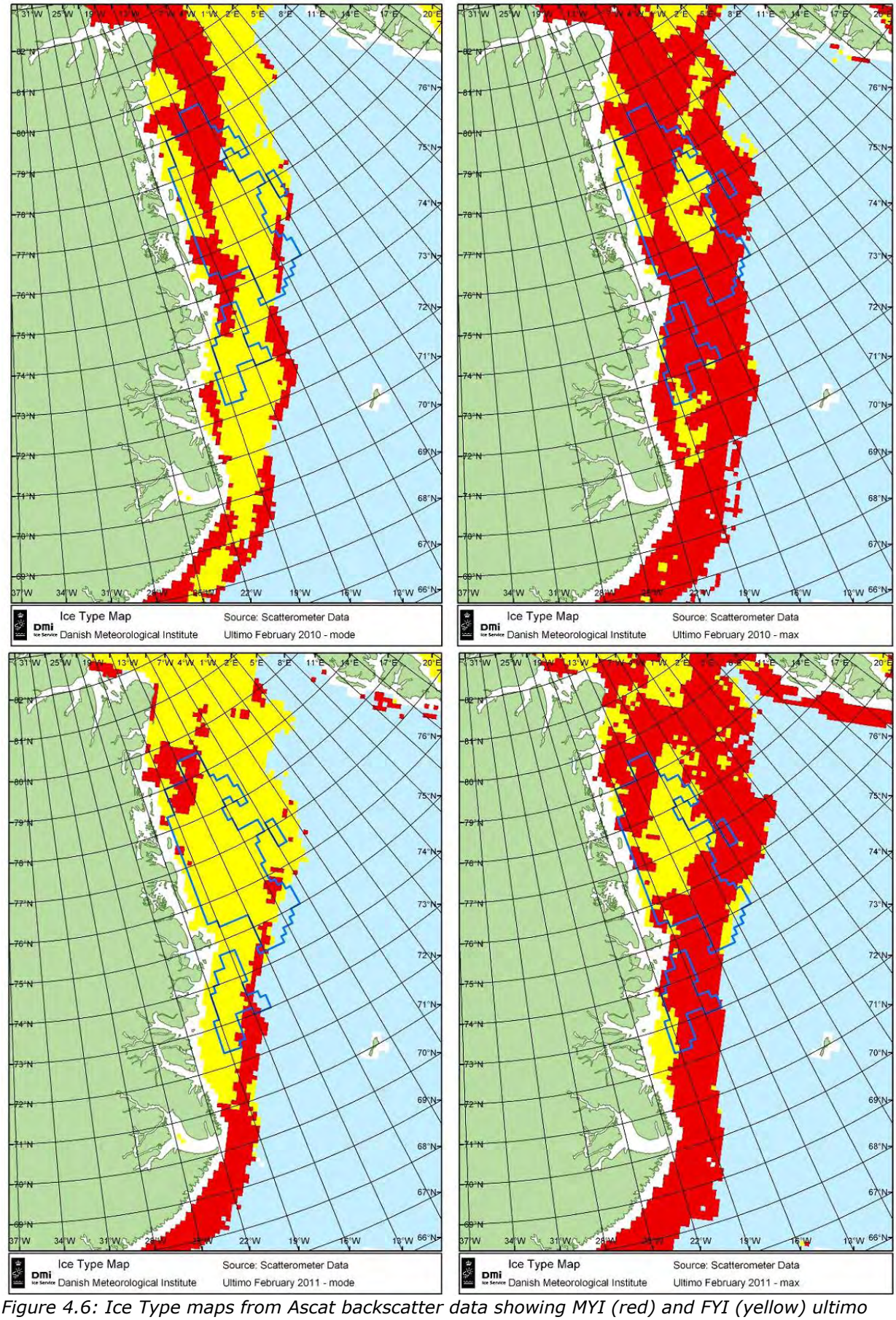

Figure 4.6: Ice Type maps from Ascat backscatter data showing MYI (red) and FYI (yellow) ultimo February 2010 [top] and 2011 [bottom].

4.2. Sea ice freeboard heights from satellite altimetry

Recent studies have proved satellite altimetry to be used for estimating Arctic Ocean sea ice freeboard heights (Skourup (2010), Farrell et al (2009), Giles et al (2008), Kwok et al (2007, 2005, 2004), Forsberg and Skourup (2005), Peacock and Laxon (2004), Laxon et al (2003)).

In this study, we estimate freeboard heights from NASA's Ice, Cloud and land Elevation Satellite (ICESat), which provided laser altimetry measurements of sea ice from January 2003 to October 2009. To obtain sea ice freeboard heights beyond ICESat, ESA launched the Earth explorer satellite CryoSat-2 in April 2010, dedicated to measure the cryosphere of the Earth by advanced radar altimetry. Unfortunately, there are problems with the processing of the special "sea ice mode" used in sea ice covered areas. Reprocessing of data is planned to be carried out by ESA during December 2011, and the improved data set will be available to the users in the beginning of 2012, where sea ice freeboard maps of the Arctic will be estimated accordingly. Some first results of CryoSat-2 data sea ice and related issues are presented and discussed in Poulsen (2011). The only group (Centre for Polar Observation and Modelling, University College London) having access to raw CryoSat data, have been able to process CryoSat to obtain Arctic Ocean sea ice thicknesses for January-February 2011, see **chapter 2.6**. Based on a similar study for the Baffin Bay **seperate report to BMP**, it is concluded that the ice thicknesses in the Baffin Bay are overestimated in the CryoSat ice thickness map (**figure 2.5**).

We have used a lowest-level estimation method to derive sea ice freeboard heights (including the snow layer) for the Fram Strait from ICESat measurements. For a more detailed description of the procedures, see Skourup (2010). We include winter conditions (February-March) for each of the years 2003-2008, where the sea ice is close to the annual maximum see **chapter 2.** The maps of sea ice freeboard heights are shown in **figures 4.8-13** with the licence areas marked by white lines. Each map represents data covering approx. 30 days of observation. ICESat measurements are obtained 40 times a second corresponding to an along-track separation of 172m. Within the 30 days observation period the track spacing is 20km at 75°N. Each ICESat measurement covers a surface spot-size (footprint) of approximately 70m in diameter with a vertical accuracy better than 15cm.

The sea ice freeboard height (f) to thickness (t) conversion ($t = k * f$) is debated in many papers and is highly variable depending primarily on snow conditions and to a less extent on sea ice type and settings. In previous studies of high resolution airborne laser scanner measurements of sea ice in the Fram Strait a k-factor of 5.5 was used, based on *in situ* measurements (Hvidegaard et al, 2008). However, when averaging over footprint areas similar to ICESat, recent studies of the relation between freeboard heights and draft by Doble et al (2011), finds a k-value of 4.4 for level ice and 5.2 for deformed ice in the central Arctic Ocean. Thus, it is suggested to use the value of 5.2 to convert the sea ice freeboard heights of ICESat into sea ice thicknesses in the license areas.

According to definitions of the WMO (World Meteorological Organization) sea ice nomenclature the thickness of multiyear ice (MYI) is defined to be thicker than 2m and firstyear ice (FYI) thinner than 2m. This, corresponds to freeboard heights of 38cm (using k=5.2). Thus, MYI or deformed ice are primarily found in areas with freeboard heights represented by yellow-red colours in figure **figures 4.8-13**, and FYI with freeboard heights represented by blue-green colours.

Visually, the distribution of MYI and FYI based on sea ice freeboard heights show good correlation with the "mode" distribution based on backscatter values from Quikscat scatterometer data with all the distinct ice characteristics for the area, see **chapter 4.1**, even part of the Odden area is present in the 2004 ICESat freeboard map.

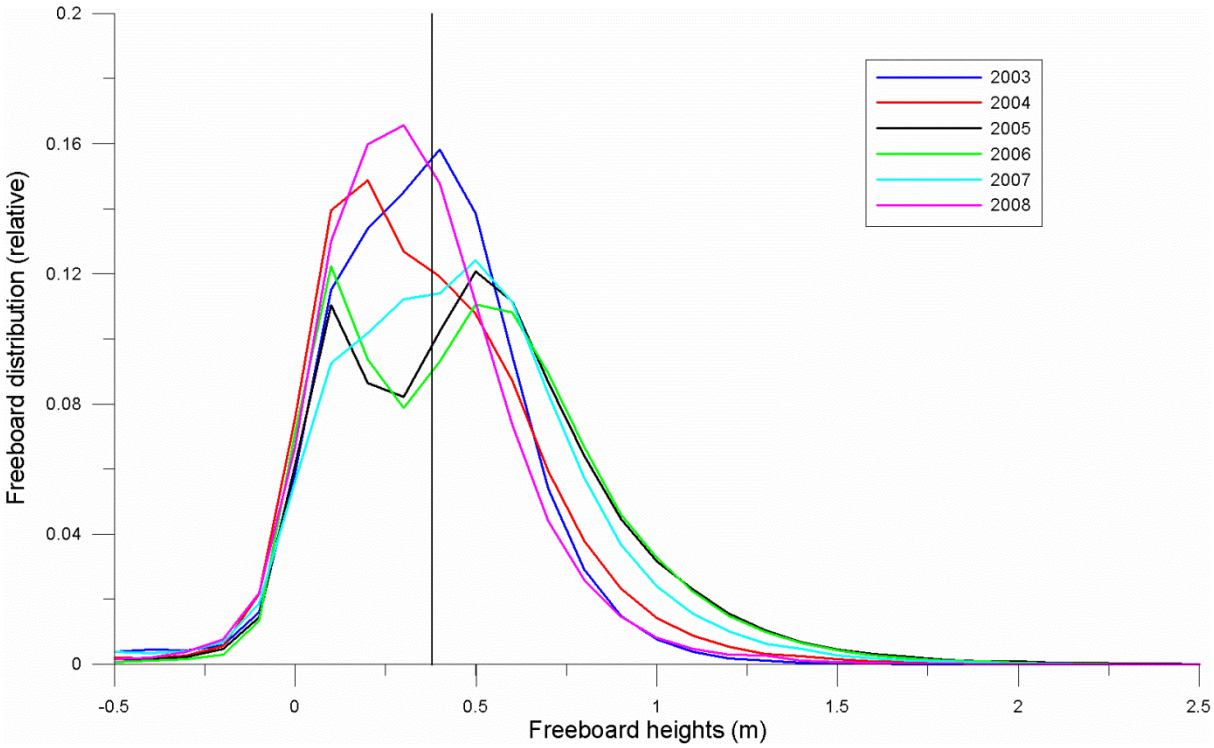

Figure 4.7: Distribution of sea ice freeboard heights in the Fram Strait

The mean and standard deviation of the freeboard heights in the Fram Strait are given below the respective plots. The minimum freeboard height of 29cm is found in 2008 and the maximum of 45cm is found in 2005. Using a k-factor of 5.2 this corresponds to an average ice thickness of 1.5 and 2.3m, respectively. This is less than the Fram Strait average thickness of 3.25m **(chapter 2).** However, the lowest-level estimation method is dependent on open water leads and tends to underestimate ICESat sea ice freeboard heights in areas of thick ice or ice of high concentration. For a further discussion, see **chapter 7.2.**

ICESat freeboard distributions are plotted in **figure 4.7** with freeboard resolution of 0.1 m. Each histogram represents one ICESat period in the Fram Strait area. In general, the freeboard distributions have an asymmetric shape with a sharp increase in the leading edge and a long tail. This shape is characteristic for sea ice freeboard heights, drafts and thicknesses, where the long tail represents the presence of thick MYI and deformed ice due to ridging and rafting processes. The vertical black line represents the freeboard height separating FYI from MYI. The years 2005 and 2006 have distinct peaks for both MYI and FYI, and both distributions have a large amount of thick ice. The sea ice conditions in 2007 still have a larger amount of MYI, whereas the freeboard distributions of 2003, 2004 and 2008 have less deformed ice and a larger amount of FYI. This is consistent with the distribution of FYI and MYI in the Quikscat scatterometer data (**chapter 4.1**).

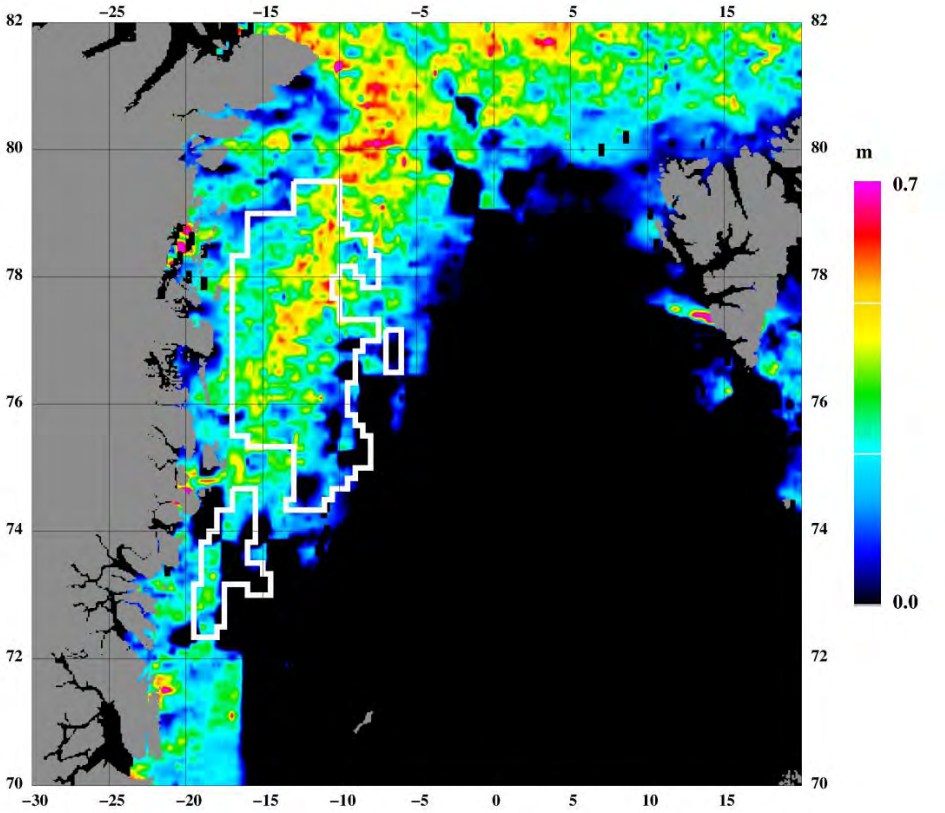

Figure 4.8. Sea ice freeboard heights
Mean: 0.30m, std: 0.27m
FEB 20 – MAR 29, 2003
Source: ICESat

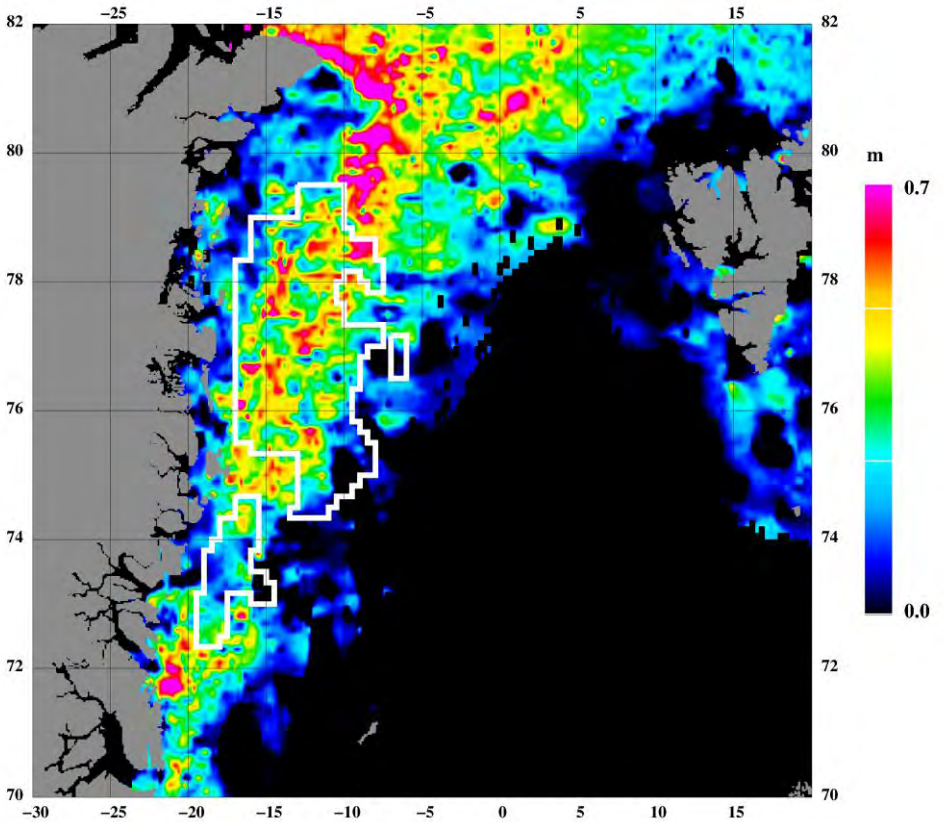

Figure 4.9 Sea ice freeboard heights
Mean: 0.32m, std: 0.31m
FEB 17 – MAR 21, 2004
Source: ICESat

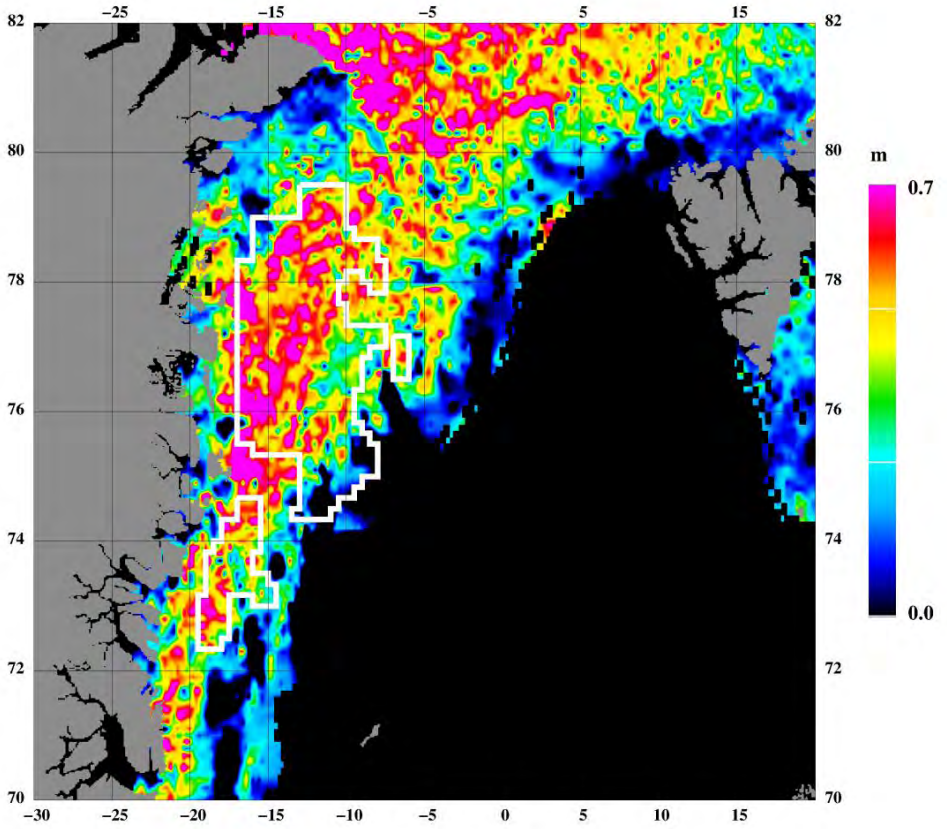

Figure 4.10. Sea ice freeboard heights FEB 17 – MAR 24, 2005
Mean: 0.45m, std: 0.37m Source: ICESat

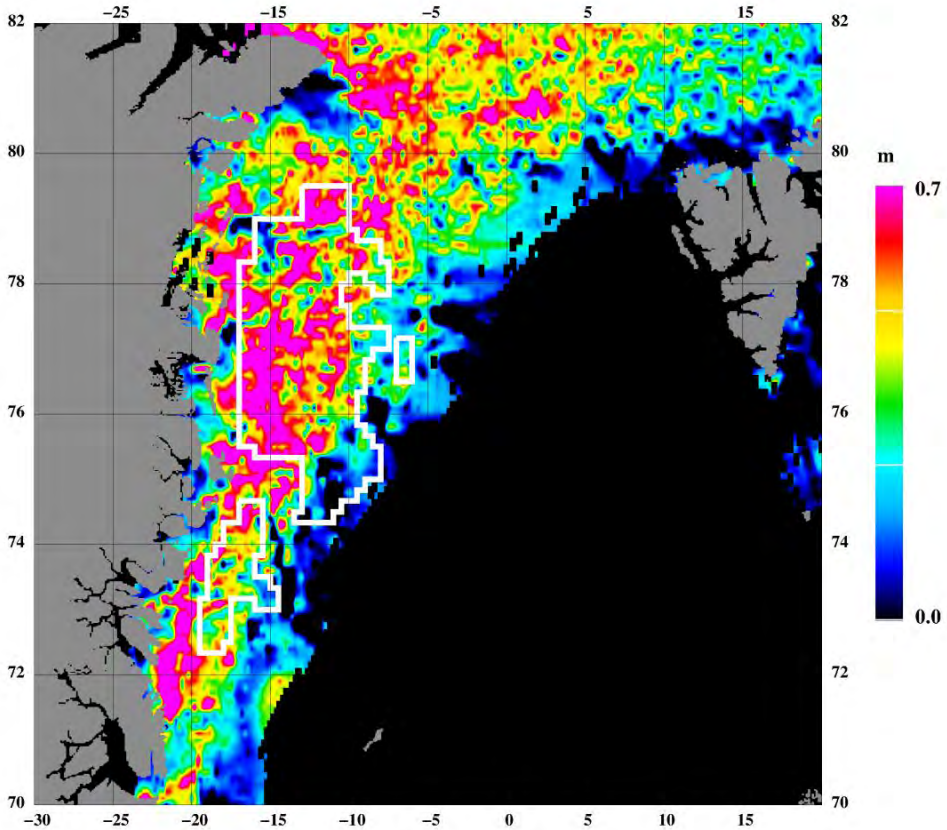

Figure 4.11. Sea ice freeboard heights FEB 22 – MAR 27, 2006
Mean: 0.44m, std: 0.36m Source: ICESat

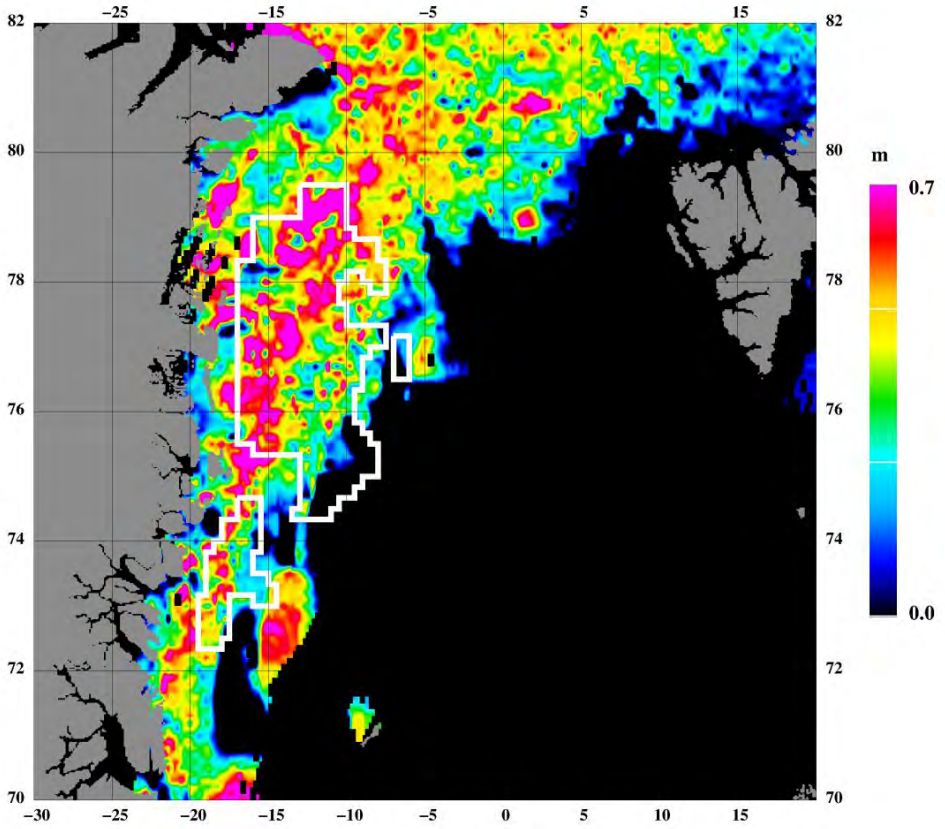

Figure 4.12. Sea ice freeboard heights *MAR 12–APR 14, 2007*
Mean: 0.40m, std: 0.34m *Source: ICESat*

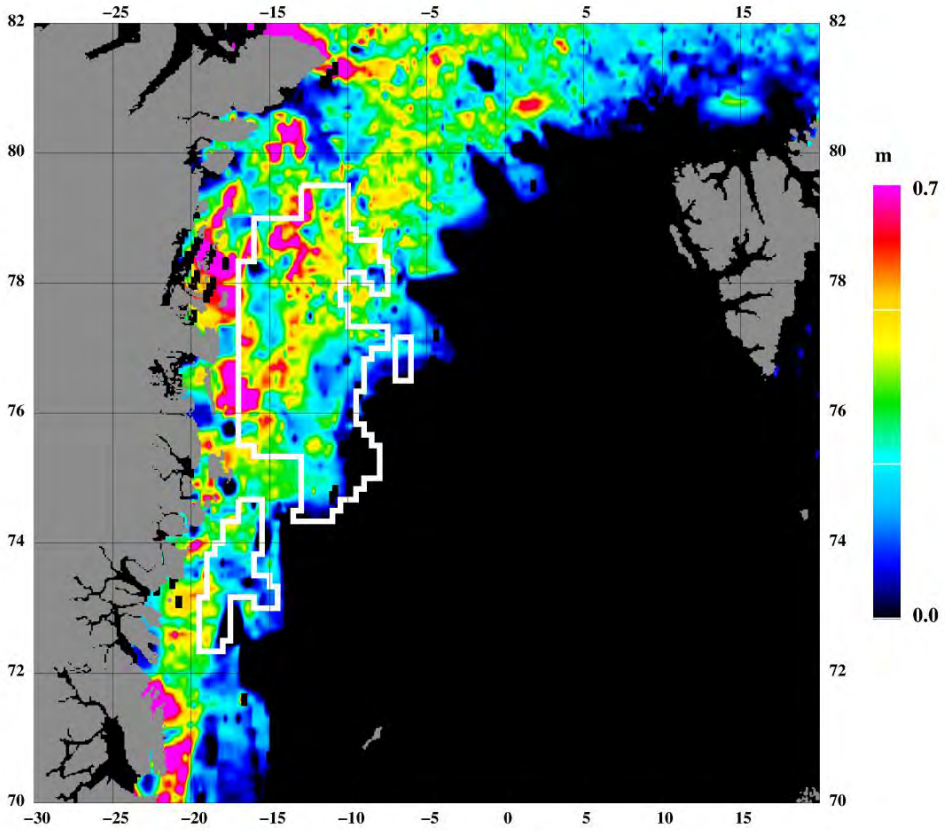

Figure 4.13. Sea ice freeboard heights *FEB 17 – MAR 21, 2008*
Mean: 0.29m, std: 0.27m *Source: ICESat*

5. Ice drift

5.1. Ice drift and wind interactions.

The drifting of sea ice is caused by wind and ocean currents. Of these forcing parameters the surface wind is dominating. The specific sea ice response to surface winds is mainly determined by the sea ice roughness and strength/thickness, hence the sea ice response to the surface wind is varying with time and place. In this section essential characteristics of the ice drift and wind interaction are analysed in the oil concession areas in the Baffin Bay and in the Greenland Sea.

The ice drift data used in this analysis consist of a coarse resolution data set, based on passive microwave data and a fine resolution data set, based on radar data, subsequently denoted the AMSR and the SAR ice drift data sets, respectively.

The AMSR data covers the past 9 years (no summer data) of ice drift on a daily basis and in a full Northern Hemisphere grid. This period coincides with great changes in the Arctic sea ice, including the record low ice extent in September 2007. Besides full temporal and spatial coverage the AMSR data set is of highest quality (Hwang and Lavergne, 2010) and therefore a well suited data set for trends analysis of the ice drift behaviour.

The SAR data set covers the 4 most recent years of ice drift particular in the areas of interest here. This data set is the most accurate ice drift data set available and at the same time one of the few data sets with full-year coverage. The SAR data are well suited for fine scale ice drift analysis and an essential reference of quality for the coarser resolution AMSR data.

The applied methodologies used for both ice drift data sets are variations of the Maximum Cross Correlation technique (MCC). The principle of the MCC methodology is to track features from one satellite imagery to a later satellite imagery. The geographical shift between the matching features in the two subsequent satellite imagery determines the ice drift.

Each ice drift data vector from the two drift data sets is matched with a wind speed vector from the - at any time - operational Numerical Weather Prediction (NWP) model from the European Centre for Medium-Range Weather Forecasts (ECMWF). The matched ice drift and wind data are separated by maximum 25km. The associated wind speeds are weighted mean wind speeds from bi-daily nwp analysis fields.

5.2. Statistics (average and extreme ice drift)

The **figures 5.1-5.2** show ice drift statistics (maximum and mean) derived from all matching pairs of ENVISAT SAR images from 2007- 2011 for January and June respectively.

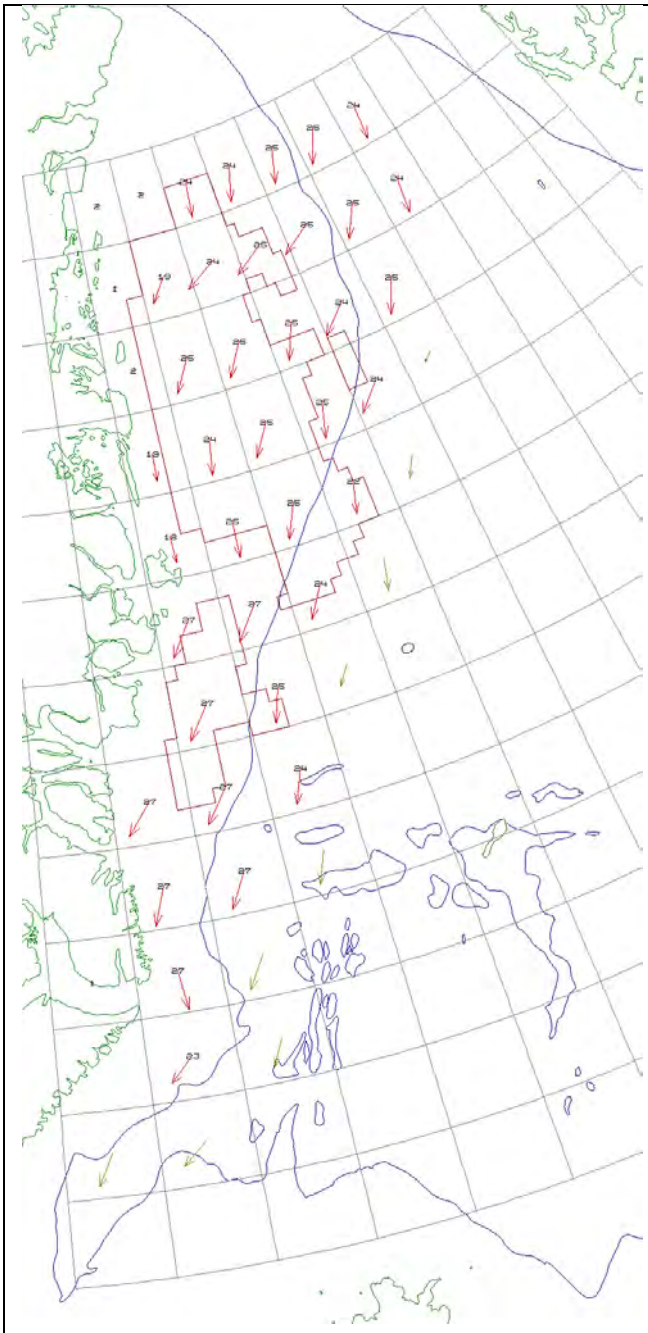

Figure 5.1 January max ice drift (cm/sec averaged over 24 hours)

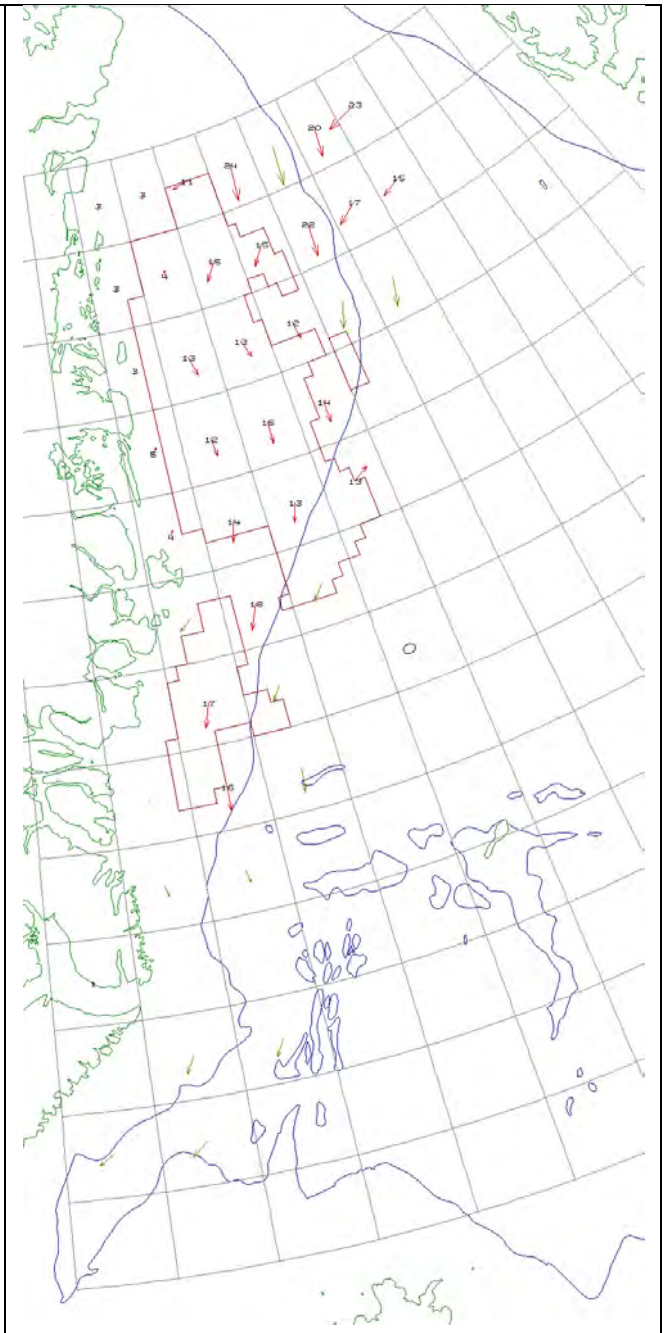

June max ice drift (cm/sec averaged over 24 hours)

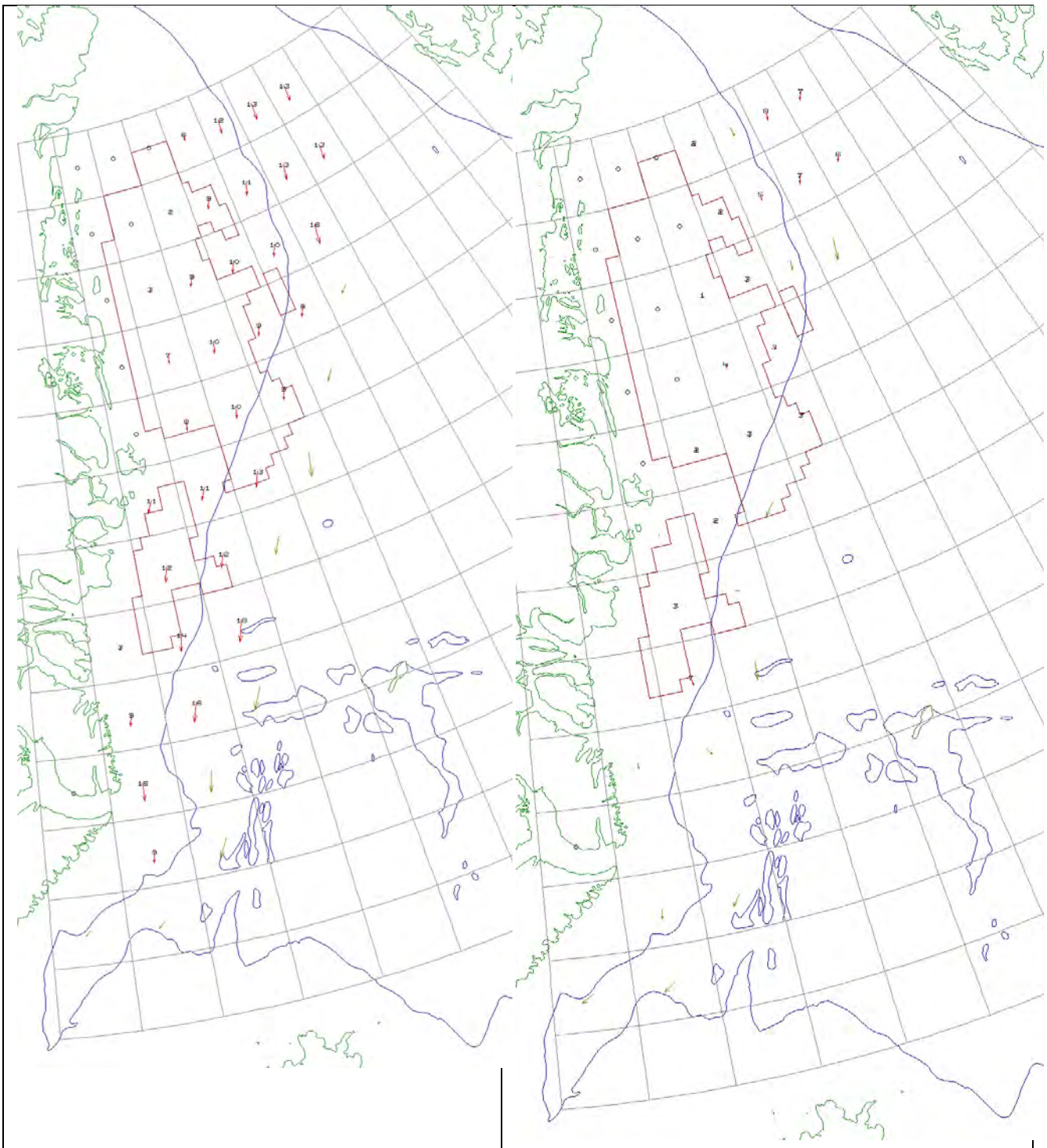

Figure 5.2. January mean ice drift (cm/sec averaged over 24 hours and averaged over all Januarys)

June mean ice drift (cm/sec averaged over 24 hours and averaged over all Junes)

Tables with data for all months of the year can be found in **chapter 9**.

The plots in **figure 5.3 and 5.4** show histograms of ice drift in 2 selected areas. Drift is average speed over 24 hours. Faster speeds can occur during shorter periods.

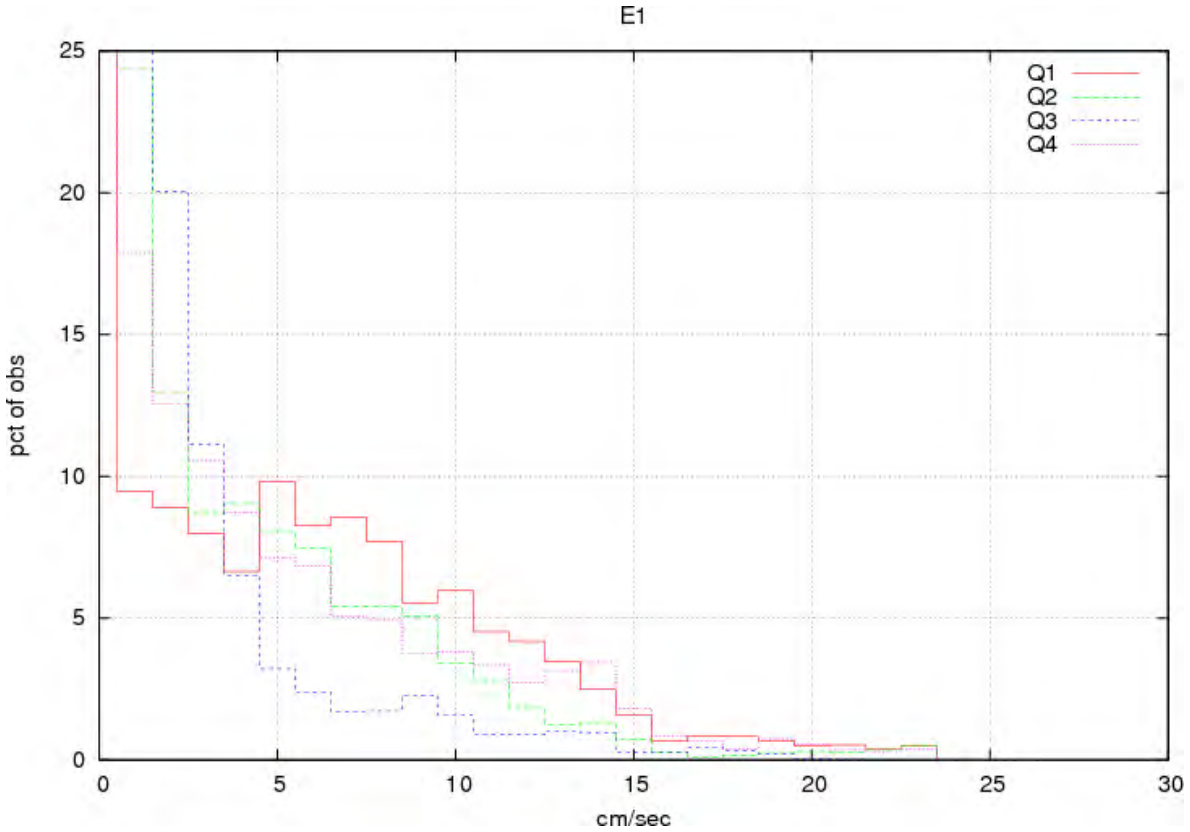

Figure 5.3. Histogram of all ice drift vectors in Area 1. The 4 curves correspond to the 4 quarters of the year. (Area: 77-80N, 13-19W)

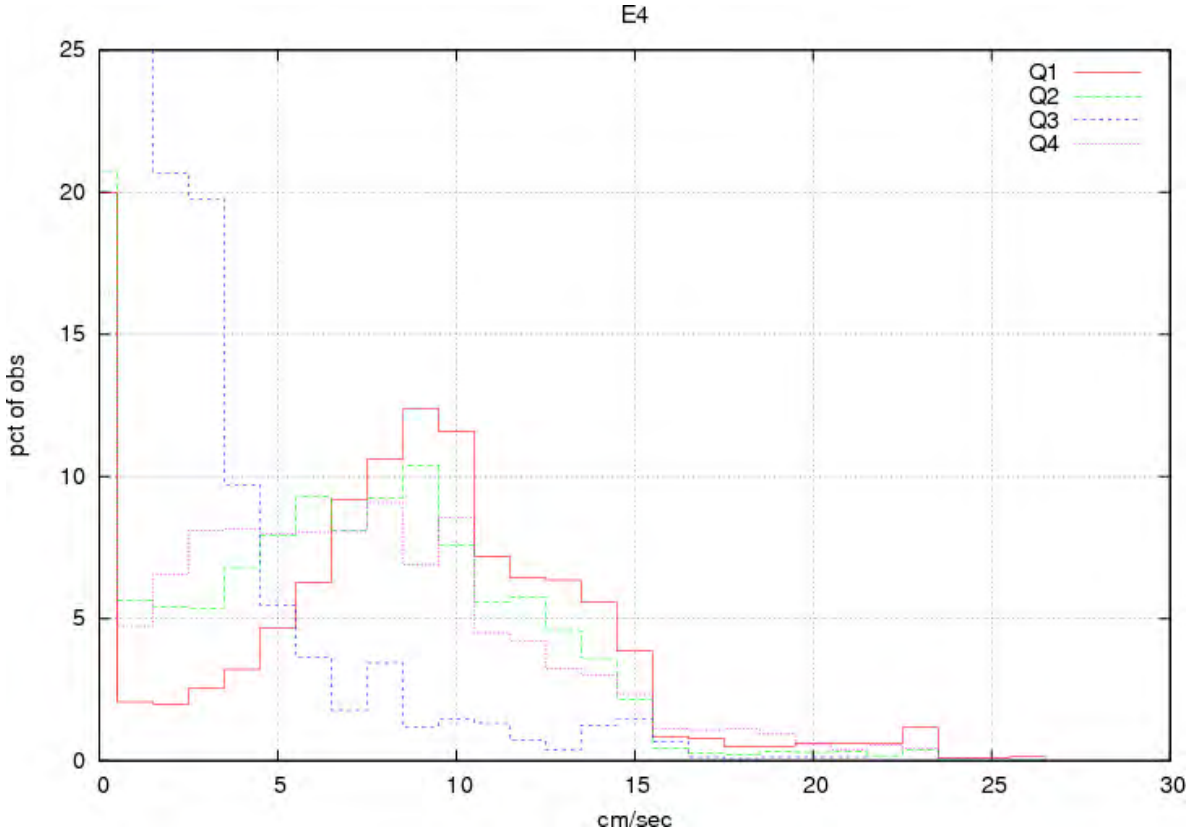

Figure 5.4. Histogram of all ice drift vectors in Area 4. The 4 curves correspond to the 4 quarters of the year. (Area: 74-77N, 13-19W)

5.2.1. Area description and mean drift plots

The ice drift and wind analysis presented here is split into 2 sectors in the Greenland Sea, together covering most concession areas in question here. The sectors are denoted E1big and E2big and plotted in **figure 5.5**. The March mean ice drift vectors through out the entire AMSR data period is also plotted in the figures, showing very coherent southward ice drift in both sections.

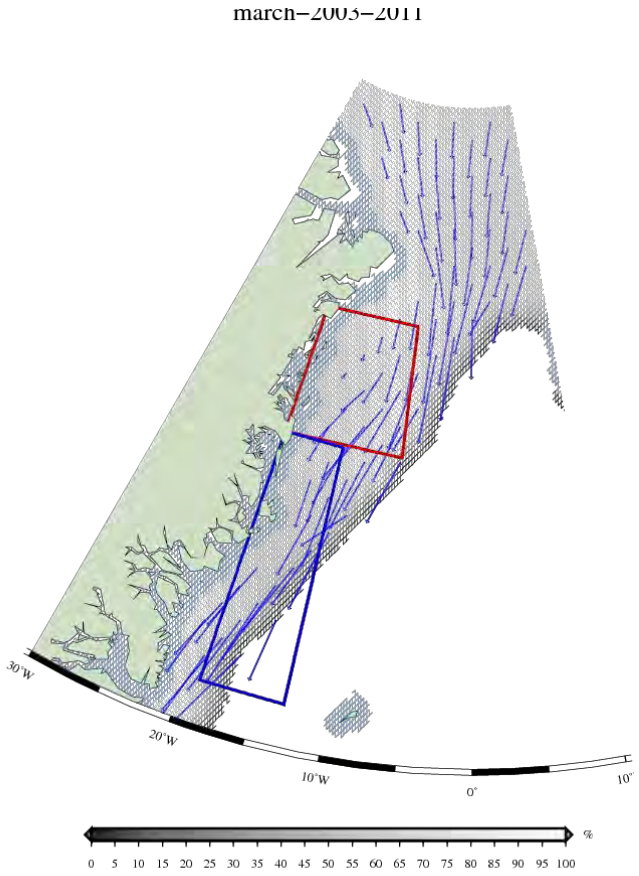

Figure 5.5. March mean ice drift in the Greenland Sea 2003-2011. The blue edge along the coastline is a coast mask. Red and blue squares are the areas E1big and E2big, respectively.

The general March ice drift pattern in the Greenland Sea is equally strong in North and South and driven by the transpolar drift. However, slower drift is observed in areas sheltered from North. The sea ice characteristics in the Greenland sea has changes drastically over the past decade. Before the sea ice extend minimum in September 2007 the ice exported through the Fram Strait consisted mainly of Multi Year Ice (MYI) and since that event the exported ice is mainly First- and Second Year Ice (FYI/SYI).

5.2.2. Ice drift vs wind – ratios

The ratio between ice drift speed and wind speed (Drift Ratio, DR) is related to the term 'drag-coefficient', with the difference that DR is independent of ice and wind direction. In **figure 5.6** the monthly mean DR values for both AMSR and SAR drift data are plotted against time for both sectors. One note coherency in DR values between the AMSR and SAR data in the period of overlap. This indicates that the DR data for the 2 data sets are comparable and that the more

detailed SAR data series can be extended backwards in time using the AMSR data. An exact match between the 2 data sets in the overlapping period is not expected as temporal and spatial characteristics of the data sets are different.

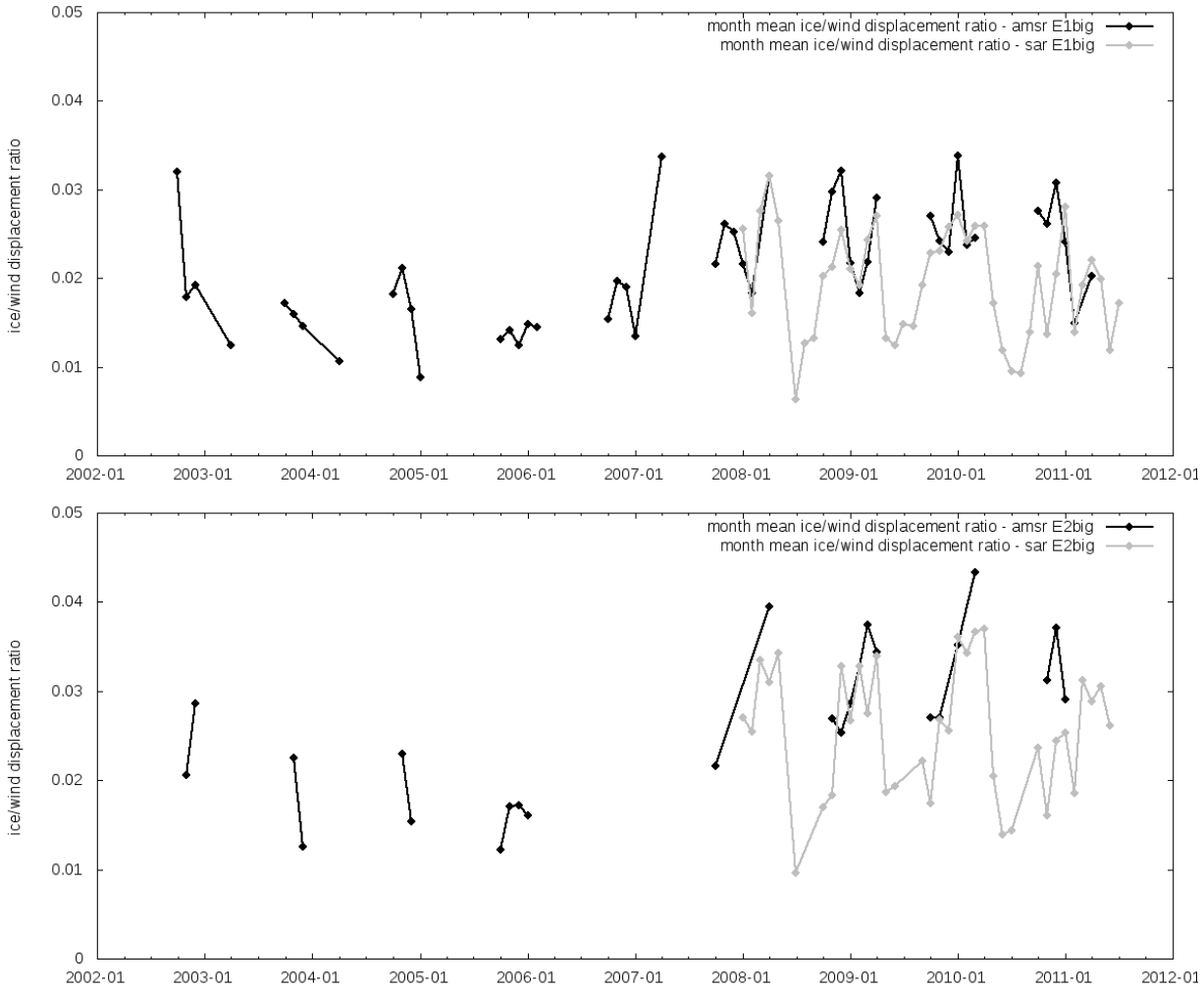

Figure 5.6 Monthly values of ice/wind displacement ratios (DR) as a function of time. DR values from AMSR and SAR drift data are plotted as black and grey curves, respectively. Order of plots from the top: Area E1big, E2big.

Two ice variables affect the DR value, namely ice thickness and ice surface roughness. The ice thickness/strength increases during the winter season and DR will consequently decrease, as thin ice deforms easier than thick ice. Surface roughness also increases throughout the winter season as a consequence of a build up of sea ice deformation ridges. Increased surface roughness increases DR because of larger friction between ice surface and surface wind.

DR is also a function of the absolute wind force, as illustrated in **figure 5.7**. Here the 'with ice interaction' -curve illustrate the concept of wind force dependency through the fact that it takes a minimum wind force to initiate ice drift. Subsequently this is called the initial wind speed. The initial wind speed is depending on the ice's ability to resist deformation (i.e. Ice thickness), and therefore its ability to resist displacement. As the wind speed approaches the initial wind speed DR approaches zero.

Monthly mean wind data for both sectors are plotted in **figure 5.8** and these data show no trend, in agreement with other trend analysis for Arctic regions. Provided that the wind conditions in the past decade is trend less, trends and/or changes in the general DR patterns in the sectors are caused by

changes in the general ice thickness.

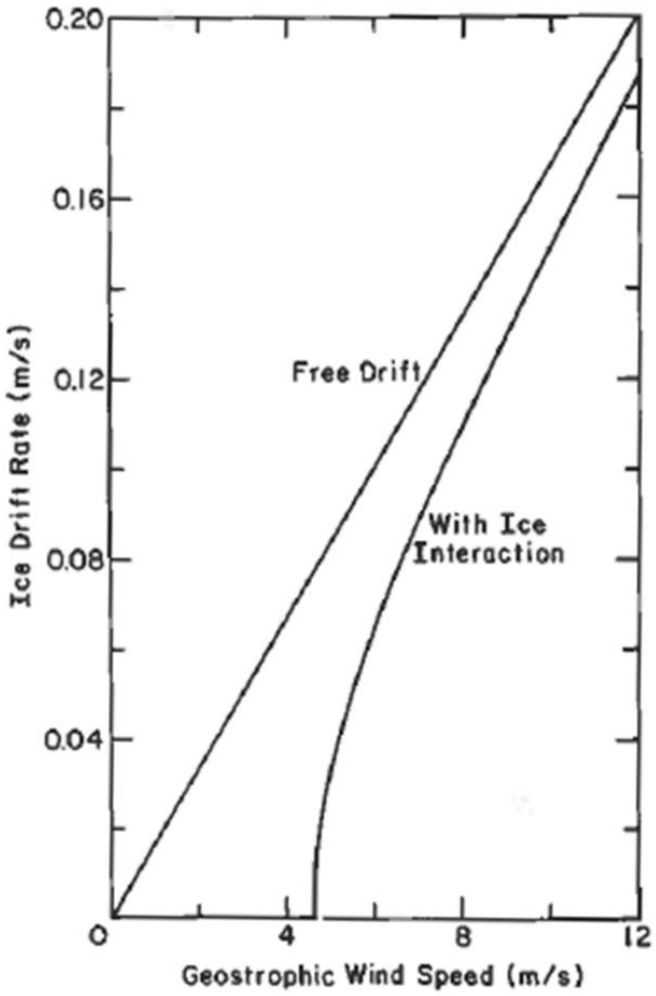

Figure 5.7. Conceptual graph of sea ice and wind interaction. From Untersteinar (1981)

An important uncertainty to this reasoning is the influence of ocean currents. This is not discussed here.

DR in Greenland Sea

Figure 5.6 represent DR values in the Greenland Sea sectors, E1big and E2big. Here a positive trend in the AMSR data series is suggested or alternative a shift to generally higher DR levels after the summer of 2007. This agrees with the fact that the ice exported through Fram Strait is generally younger (FYI and SYI) today than before 2007. The inter annual DR variations are illustrated by the SAR data, showing that DR values are very low during summer. As the ice thickness also is lower in the summer period the low DR values must be explained by wind forces approaching initial wind forces values and thus leaving less wind to move the ice. This is also the case for the seasonal data in **table 2** and also indicated by the monthly mean wind data in **figure 5.8**.

5.2.3. Ice drift and wind speed

The general picture of ice drift and wind speed statistics in **figure 5.8**, basically tells the same story as the DR plots in **figure 5.6**. A general elevated level of mean ice drift in the Greenland Sea sectors after 2007. Low mean ice drift values during summer, caused by weaker winds, agree with the associated low DR values discussed above.

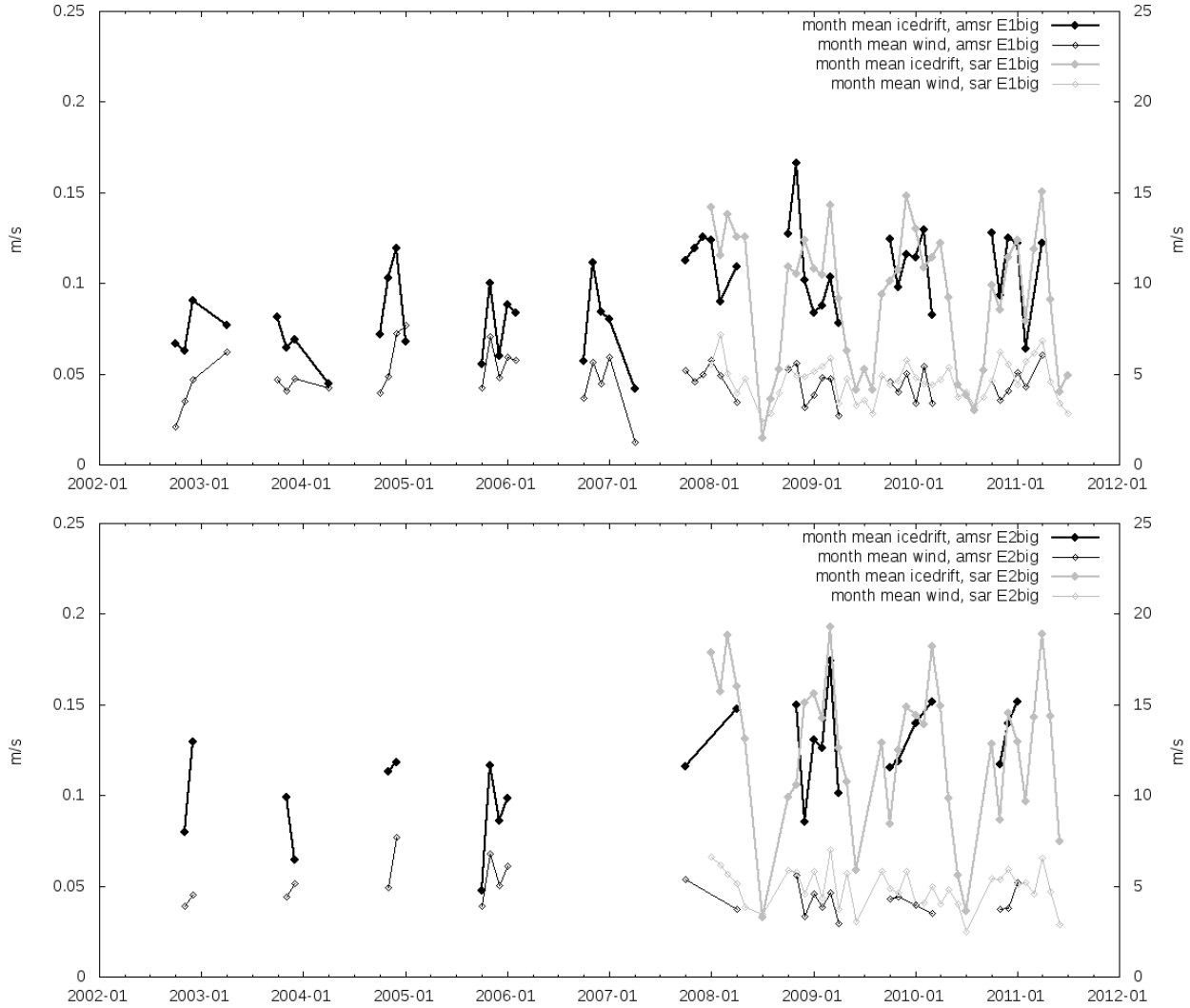

Figure 5.8. Ice and associated wind displacements plotted as speed as a function of time. The left y-axis is associated with ice drift and the right y-axis is associated with wind speed. Black curves is ice drift based on AMSR data and grey curves is ice drift based on SAR data, thick lines are ice drift and thin lines show the associated wind speed. Order of plots from the top: Area E1big, E2big

5.2.4. Seasonal ice drift and wind speed, scatter plots

In the **figures 5.9, 5.10 and 5.11** all ice drift and wind speed pairs for the summer (July, August and September) and winter seasons (January, February and March) are plotted to illustrate the correlation of the two parameters and the initial wind speed estimate. To all scatter plots the best fitted line is superimposed and the fitting parameters (slope and intercept) determine the seasonal 'initial wind speed' parameter and a value similar to the DR parameter, namely drag ratio between ice drift and the available wind energy (ADR), after subtracting the wind used to deform ice. The ADR values are naturally higher than the DR values as the initial wind speed is subtracted from the actual wind speed used to calculate the DR value. The statistics for this seasonal analysis is written in **table 1 and 2**.

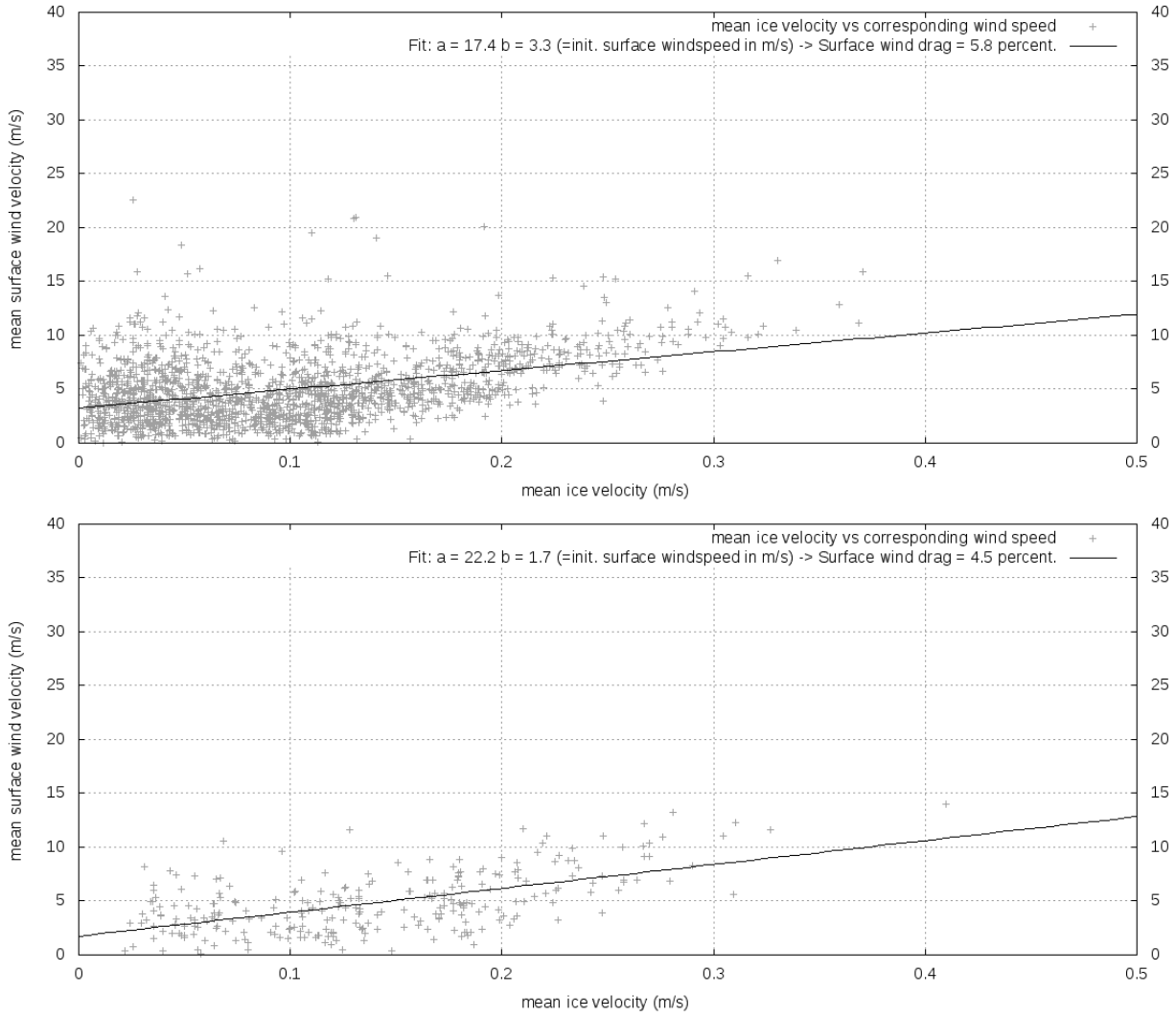

Figure 5.9 Scatter plots of ice drift speeds vs. wind speeds as a function of time for AMSR data during winter (January-February-March; 2002-2011). The black line is the best fitted line to the data with non fixed offset. Order of plots from the top: Area E1big, E2big

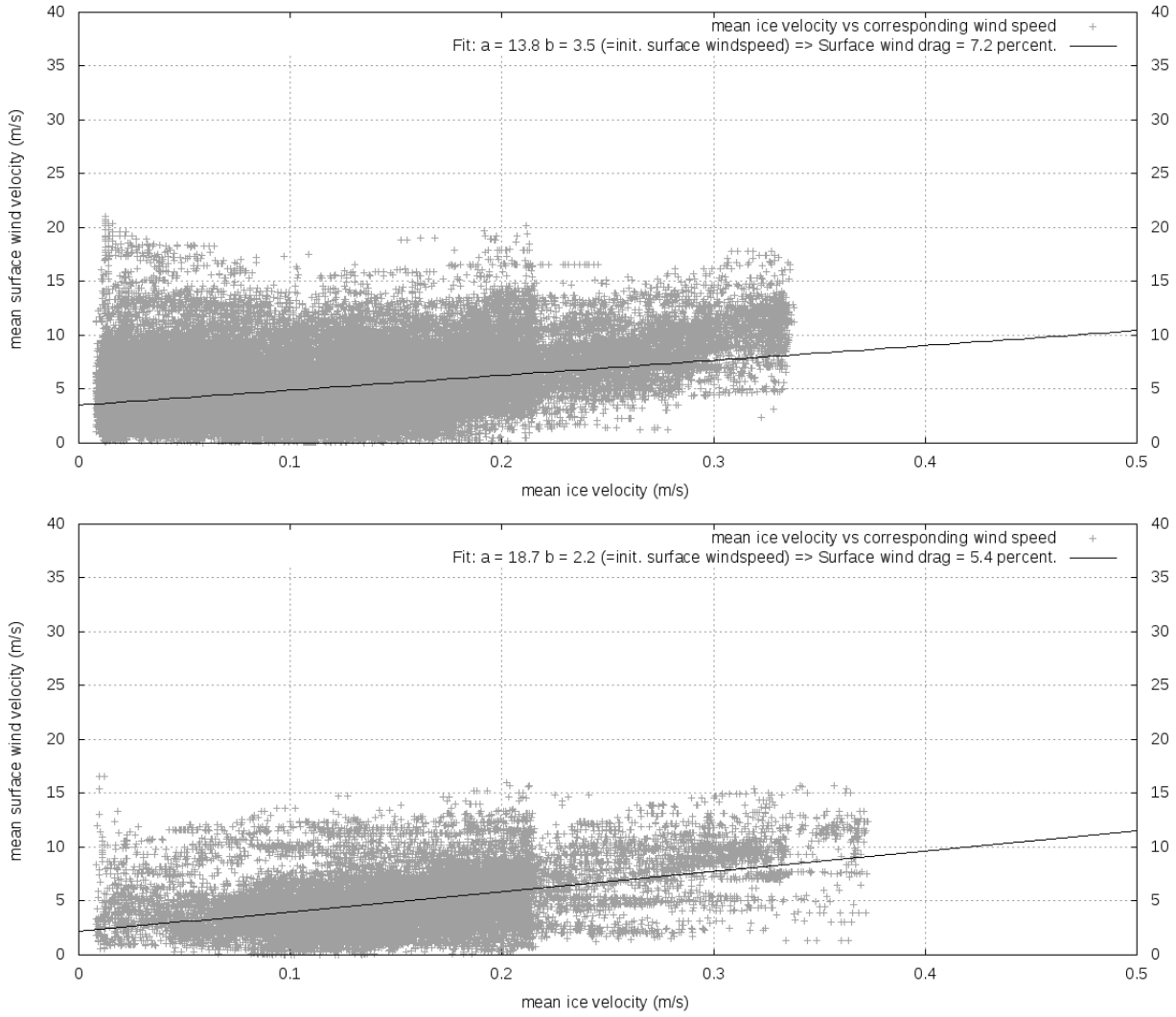

Figure 5.10. Scatter plots of ice drift speeds vs. wind speeds as a function of time for SAR data during winter (January-February-March; 2002-2011). The black line is the best fitted line to the data with non fixed offset. Order of plots from the top: Area E1big, E2big

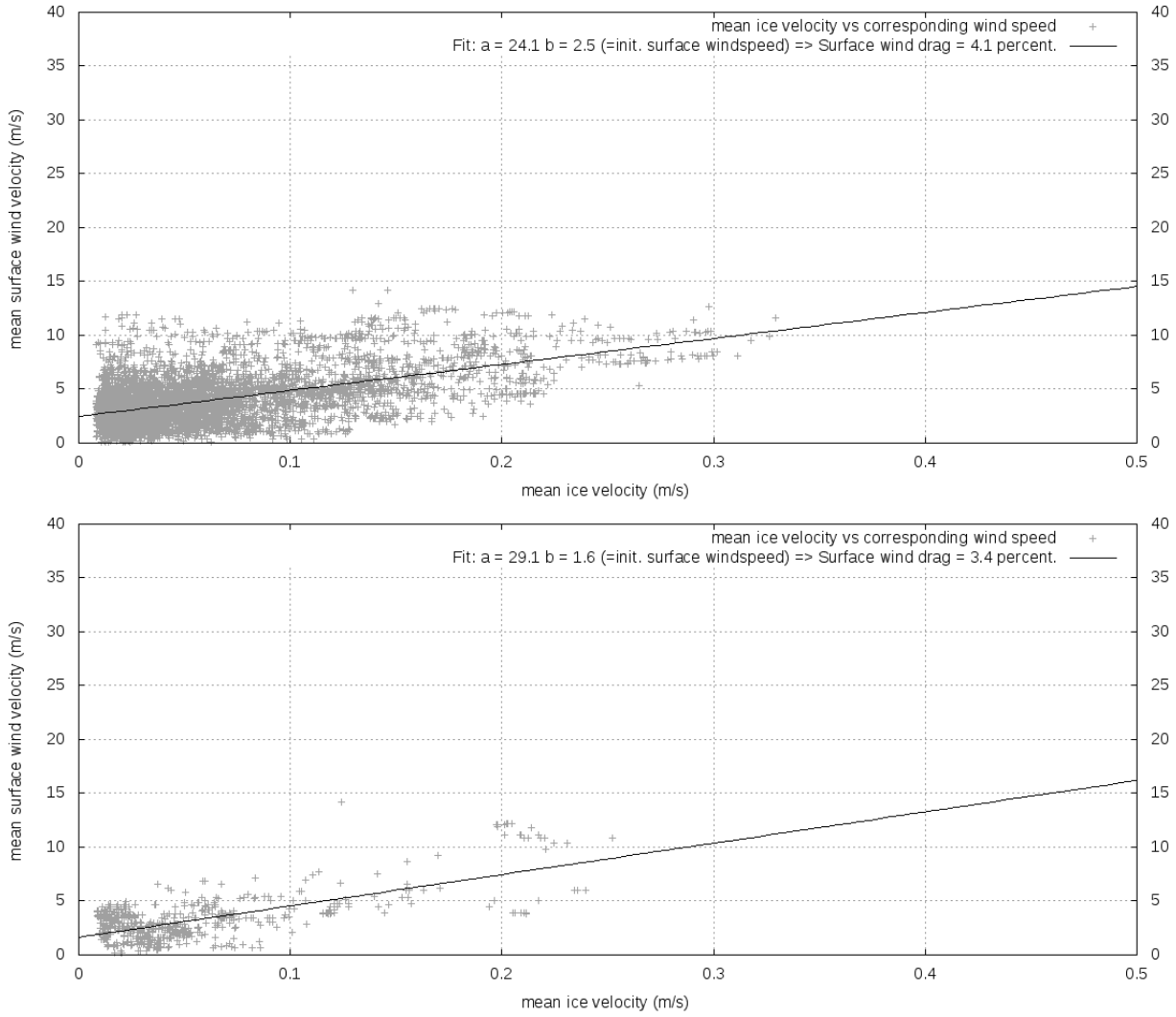

Figure 5.11 Scatter plots of ice drift speeds vs. wind speeds as a function of time for SAR data during summer (July-August-September; 2002-2011). The black line is the best fitted line to the data with non fixed offset. Top plot is area E1big and bottom plot is area E2big.

Tabel 1 Statistics for seasonal AMSR ice drift and wind data. Statistics for records less than 100 are set to 'nodata'. Summer season correspond to July, August and September and the winter season correspond to January, February and March. The areas are plotted in figures 1 and 2.

season	area	records	mean ice speed (m/s)	std ice speed	mean wind speed (m/s)	std wind speed	correlation	Init wind Speed (m/s)	ADR
summer	E1big	nodata	nodata	nodata	nodata	nodata	nodata	nodata	nodata
summer	E2big	nodata	nodata	nodata	nodata	nodata	nodata	nodata	nodata
winter	E1big	1,926	0.10	0.07	4.97	2.94	0.41	3.30	0.06
winter	E2big	272	0.14	0.07	4.83	2.75	0.57	1.70	0.05

Tabel 2 Statistics for seasonal SAR ice drift and wind data. Statistics for records less than 100 are set to 'nodata'. Summer season correspond to July, August and September and the winter season correspond to January, February and March. The areas are plotted in figures 1 and 2.

season	area	records	mean ice speed (m/s)	std ice speed	mean wind speed (m/s)	std wind speed	correlation	Init wind Speed (m/s)	ADR
summer	E1big	6,780	0.06	0.05	3.88	2.30	0.55	2.50	0.04
summer	E2big	643	0.05	0.05	3.17	2.09	0.68	1.60	0.03
winter	E1big	104,551	0.12	0.06	5.13	2.77	0.32	3.50	0.07
winter	E2big	29,040	0.15	0.06	4.98	2.66	0.44	2.20	0.05

6. Met/Ocean

6.1. General conditions

The pressure pattern is strongly influenced by the distribution of cold and warm surfaces with a tendency of high pressure over cold surfaces (sinking air) and low pressures over warm surfaces (rising air).

Another parameter which has a highly influence of the weather patterns is the polar front which is the boundary between cold arctic and warm tropical air masses. Along the polar front mid-latitude lows has their track followed by unsettled conditions. The position of the polar front has a seasonal variation which leads to a variation in weather patterns in the summer and in the winter which will be described below.

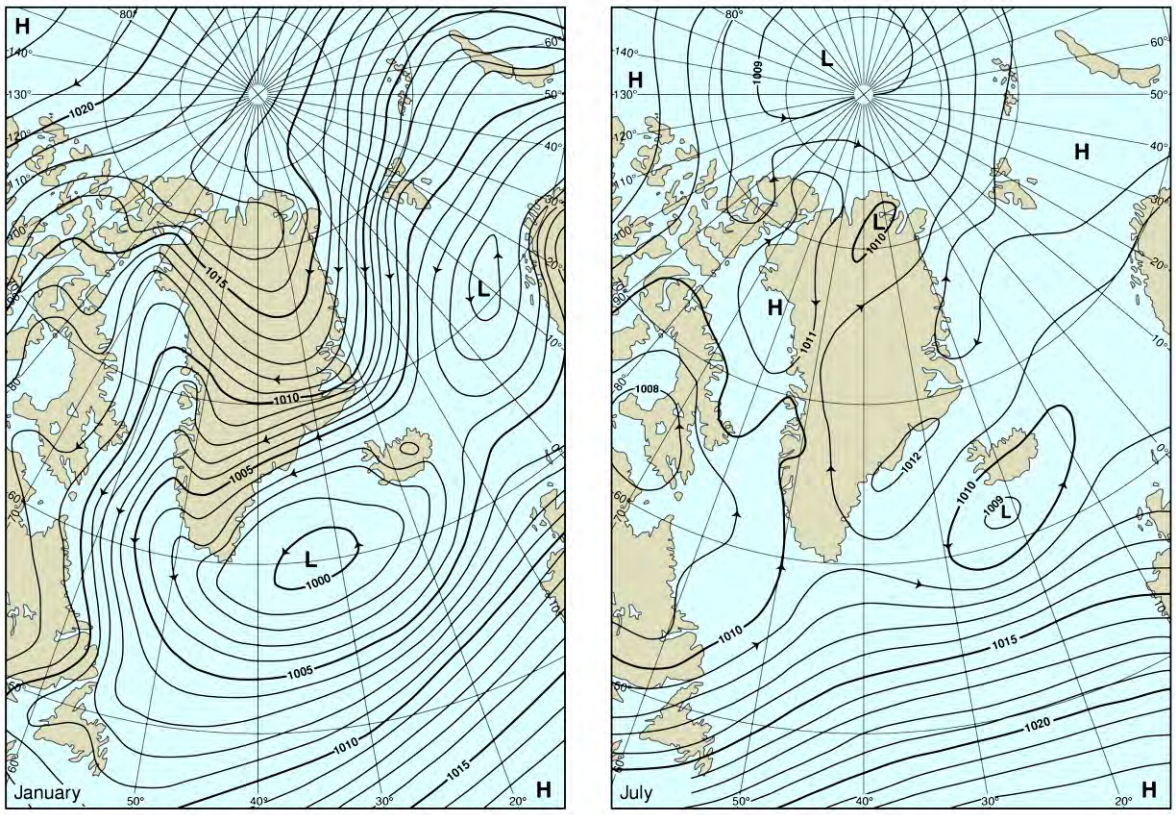

Figure 6.1 Mean sea level pressure (hPa) winter and summer.

In the winter an area of high pressure normally exists over the northernmost part of Greenland (over the icecap) and a low pressure area often occurs over the Norwegian Sea. These systems generate prevailing northerly winds over Northeast Greenland.

In the summer the surface temperature differences are small and therefore the pressure gradient and the thermal wind are weak and a prevailing wind direction is therefore not that unambiguous. Over the northern part of the northeast coast the tendency is a southerly flow but over the southernmost part a northerly flow tends to occur both in the winter and in the summer due to track of lows.

Katabatic winds occur as well along northeast Greenlandic coastline which is high density (cold) air

moving/falling down from the elevated icecap under the force of gravity. These winds can occasionally be quite strong and gusty due to the flow is canalised in the fjords but typically weakens when it is spread at the mouth of the fiords. The strong flow will seldom occur far at sea but often it will transport the coastal ice at sea.

6.2. Low tracks

During the winter the Polar front moves southwards often leading the lows to pass south of Greenland. Thereafter a typical track is through the Denmark Strait because the polar front often tilts in a southwesterly-northeasterly direction. Due to relatively cold air over warm sea surface the lows are very often rather intense and severe conditions often occurs over the southern part of the northeast coast with gale force winds and moderate to heavy snow.

The northern part of the Greenlandic ice sheet if often dominated by a high with sinking air and no convection over the cold land areas. When an extensive high is established and a low is over the Norwegian Sea a strong pressure gradient occurs over Northeast Greenland with prevailing northerly winds. Often the flow is of strong gale force and continues for days. When the high extends to the northern part of Canada it usually opens up for lows from the Norwegian Sea to approach Northeast Greenland and associated front zones will approach the area leading to bad weather with poor visibility and even stronger flow in coastal regions.

Normally during the summer the polar front is quite far north which typically leads to a track of lows arriving to the South Greenland from southwest. Thereafter they often take the trajectory south of Iceland and continuing east-north-eastwards towards the southern part of Norwegian Sea or becoming almost stationary over waters between southeast Greenland and Iceland.

Under special conditions the low could take the track through the Denmark Strait and proceed to Norwegian Sea. Under these circumstances it normally affects only the southernmost part of the Northeast Greenlandic area by the associated front zone with a moderate and at times a strong northerly flow and unsettled conditions. The areas further north will not be that affected in these situations and the relatively cold waters over the Greenland Sea and the northernmost part of the Norwegian Sea often establish a weak high which guides the lows towards Scandinavia and Northern Europe. Due to this ridge of high along the Northeast Greenlandic coastline calmer conditions often occurs in that area with relatively weak southerly flow over the northern parts. This flow is also prevailing over the southern part when fronts are not passing.

Another option is a track along the west coast of Greenland which will not be discussed here. A division/split of a low near Cape Farewell is as well a possibility. The tracks will under normal circumstances be as described above but the energy will then be stored in two systems in stead of a single one.

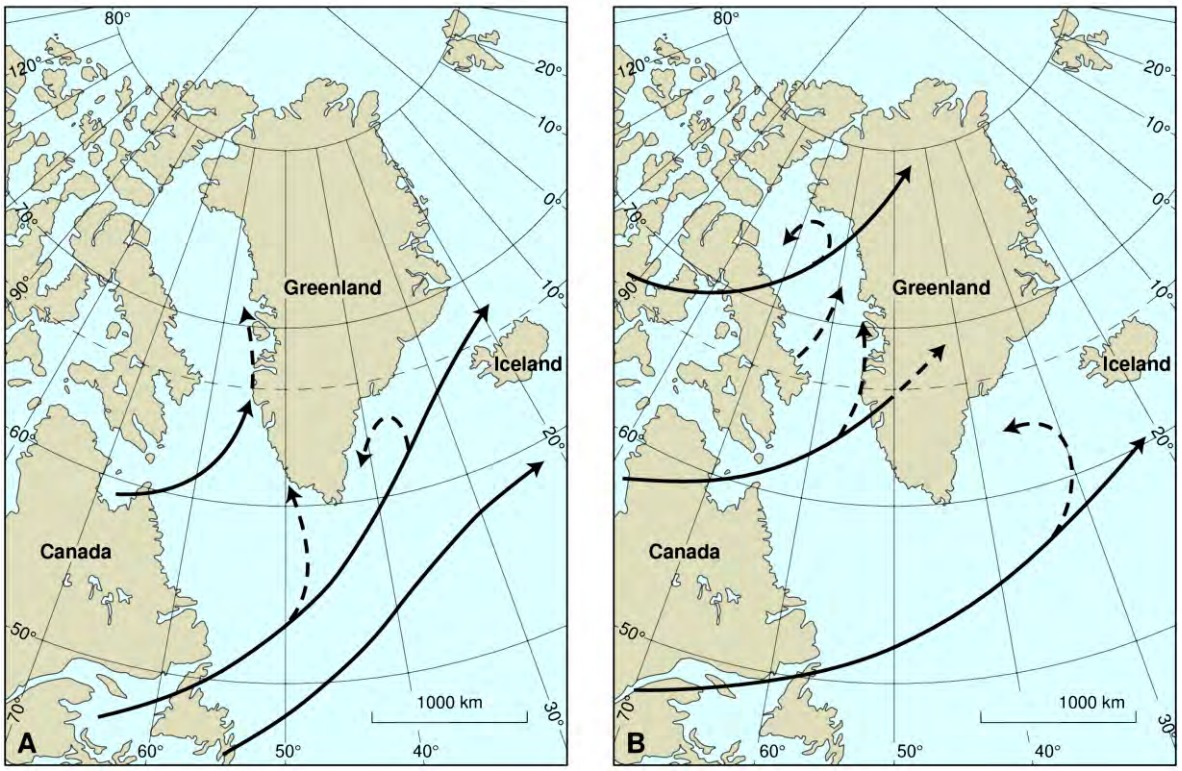

Figure 6.2 Typical tracks for major cyclones in winter (A) and summer (B).

In rare situations a low can take an easterly track from the Baffin Bay or the Davis Strait to the Greenland Sea and often they weaken during the passage over the icecap. However they may regenerate over the Greenland Sea under special circumstances leading to severe weather – especially close to the coast line.

Lows on small scale could develop any time of the year but the intensity will vary a lot and you have two types - lee lows and polar lows.

Lee lows are a result of local orographic influence where circulation is generated on the lee side of a mountain (thereby the name) and is often not that intense.

Polar lows are quite different. It develops often in the winter over open water with a combination of very cold air aloft. Polar lows are not very extensive but very intense with gale force winds and heavy snow or snow showers occur. They often develop near the ice edge or further at sea but on rare occasions they are also seen near the coast line if sufficient cracks in the sea ice occurs. Occasionally a polar low in its mature stage shows a structure resembling that of a tropical storm.

6.3. Wind

In the area of interest winds from north are by fare the most common in winter. Compared to summer, winter is also the windiest period. Especially the southern parts are frequently exposed to gale force or higher winds, which occur 15-20% of the time. Storm force winds (24.5 m/s or higher) are seen occasionally. In northern parts gale force winds are also present in the winter, however not as frequent as in southern parts and wind speeds at storm force are rarely seen.

During summer southerly winds are almost as frequent as northerly winds and in northern parts of the area southerly winds occurs more often than northerly winds. In the north gale force winds or

higher are also not that common, however they are seen now and then. In southern parts gale force winds occur more frequently than in the north, however still significantly less frequent than in the winter.

Wind analyses for the period 1999-2010 based on DMI's high resolution area model (HIRLAM) have been made for four points in the Greenland Sea (see **figure 6.3**). The analyses have been divided in to winter (November to March) and summer (June –August). In **Figure 6.4Error! Reference source not found.** are shown frequency of winds speed in the following intervals; below 5 m/s, between 5 m/s and 13.8 m/s as well as above 13.8 m/s (gale force) in relation to wind direction. Please note that the scale in the winter is twice the scale in the summer.

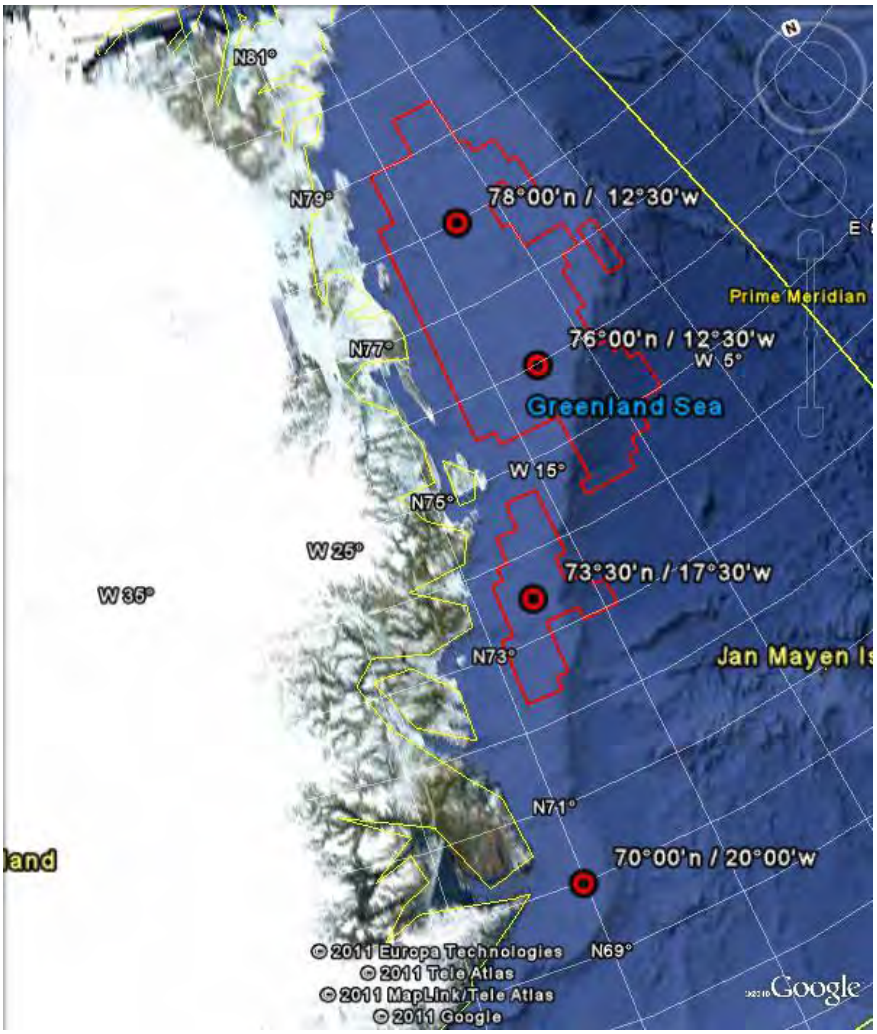

Figure 6.3 Positions where wind analysis has been made.

78°00'n / 12°30'w
Winter

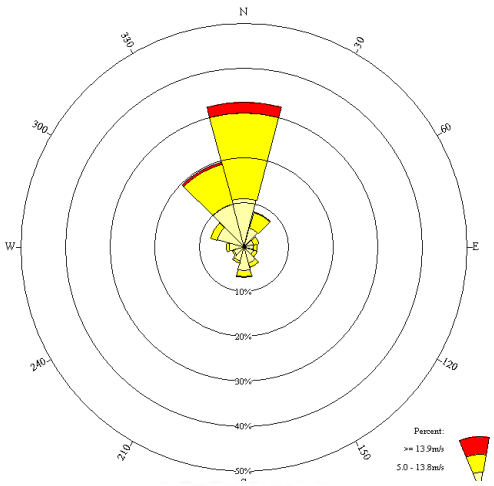

76°00'n / 12°30'w
Summer

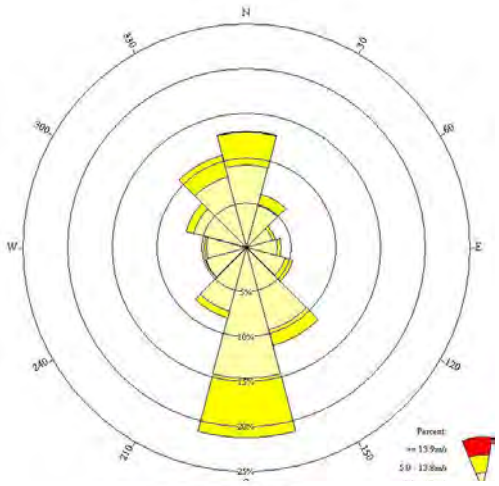

76°00'n / 12°30'w
Winter

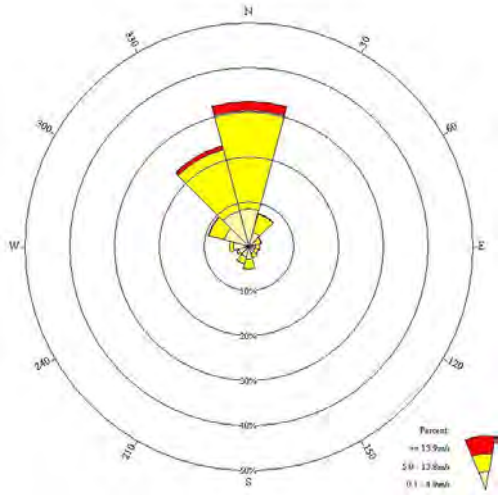

76°00'n / 12°30'w
Summer

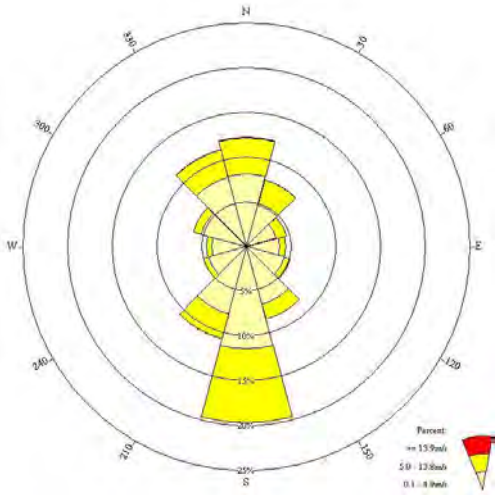

73°30'n / 17°30w
Winter

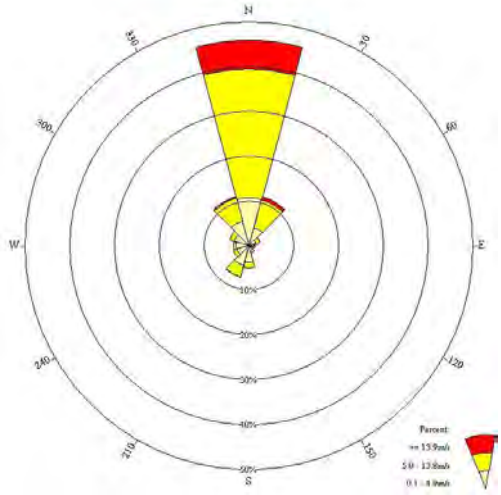

73°30'n / 17°30w
Summer

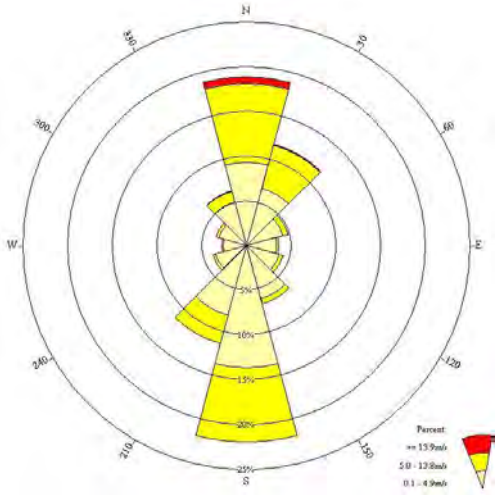

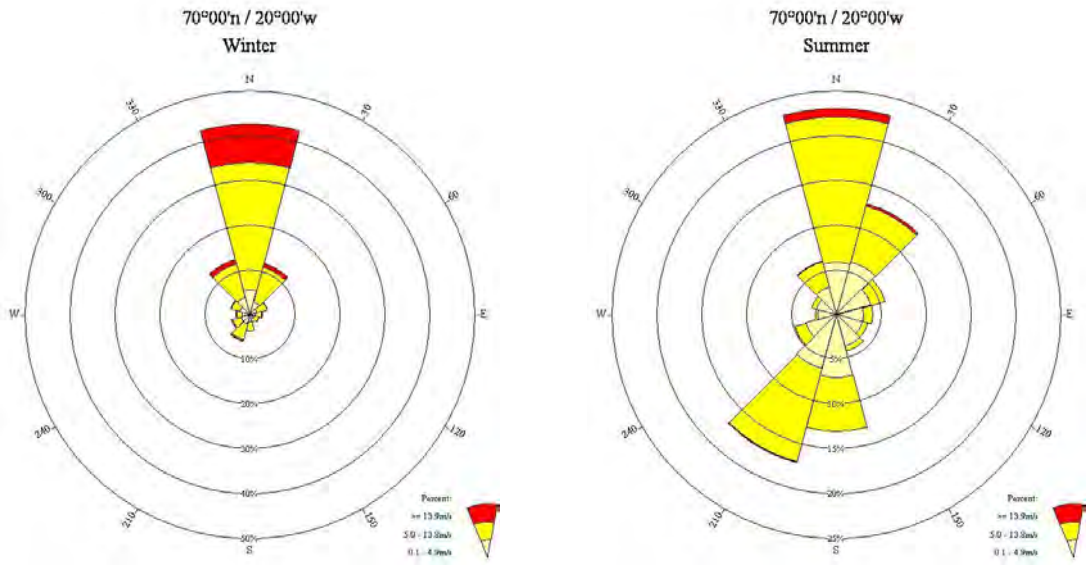

Figure 6.4 Wind analyses for four positions in the Greenland Sea. (Winter [left], Summer [right]).

6.4. Visibility

Visibility is influenced mainly by the occurrence of fog, although precipitation, particularly snow, is another important cause as well as drifting snow which mainly occurs in coastal / fast ice regions.

In the winter, snow showers are present much of the time over open water causing moderate to poor visibility. Another form of wintry precipitation which causes reduced visibility is diamond dust. That is ice crystals formed in very low temperatures normally under stable conditions. The sun is visible trough the layer but the ice crystal scatter the light is such a way that "white out" often occurs. As very low temperature are required diamond dust are not seen over open water, but only onshore and over fast ice.

Rain does often not reduced the visibility that much due to the clear Arctic air but drizzle often gives moderate visibility due to smaller and a lot more particles which scatter the light.

Fog (visibility less than 1km) is primarily a summer phenomenon and the sun will often be visible through the fog. The frequency of fog increases during May and has its peak value in June/July and it fades out in late August/early September. Fog is less frequent in the coastal region in the afternoon due to heating of land areas but the daily variations are not that significant at sea due to waters higher heat capacity compared to soil.

Summer fog is of the advection type frequently formed when relatively warm and humid air masses move to a colder surface (cold sea water in spring and early summer or cracked sea ice). Once formed over sea, fog may persist with increasing wind or gradually becoming patchy. Advection to a warmer surface will make the fog evaporate or lift to a low cloud cover – for example advection to land areas where sun heating has occurred. Temperatures within fog will, with clear skies above, often be a few (typically 1-2) degrees below that of the sea surface, due to radiation cooling. So freezing temperatures within fog over a cold water surface are not unusual, and icing with rime ice or clear ice may occur.

Radiation fog is normally seen over land and in near coastal regions developed under calm conditions. The fog over sea will thereby be regenerated in these areas during evening and nights when surface cooling exist.

In the winter, advection fog may form occasionally within a warm and moist air mass advection from the south similar to the summer fog appearance. Radiation fog may develop under clear calm conditions over snow covered and solid ice. The air will often be too dry for the fog formation, unless there is a source of moisture, such as an open lead nearby/cracks in the sea ice and sublimation of rime on the cold surface will occur. Here the sea water evaporates into the cooler surroundings and the moisture will condense into fog called steam fog/sea smoke. Another way to form sea smoke is when cold air flows from cold land areas over open (relatively warm) waters.

The occurrence is often very local and it seems patchy especially when only small cracks are in the ice. However in a very cold air mass it may be more widespread and it looks dense from the distance.

6.5. Icing

Icing occurs with air temperatures below 0ºC. It is caused by freezing rain, fog or sea spray. Freezing rain occurs with warm air aloft and a shallow layer of cold air with freezing temperatures at the surface. This pattern often occurs with the advection of warm air from the south in the winter. Icing due to freezing rain demands a cold surface (preferably 0ºC or colder). It is unlikely to occur over a sea surface warmer than 5ºC. Freezing rain will cover a ship with clear ice. It accompanies changeable weather and the duration will generally be short. The accumulated weights are unlikely to be sufficient to endanger the vessel directly.

Freezing fog may cause the formation of clear ice (at temperatures just below 0ºC) or rime ice (at lower temperatures). Here, too, the accumulated weights are generally small, but within persistent fog considerable amounts of ice may be accumulated. Accumulation on vertical structures, such as cranes, can be more than twice as heavy as on flat surfaces. Persistent freezing fog is typically a summer phenomenon, occurring over vast ice fields. It is not likely to occur over open water with a water temperature above +1ºC. Freezing sea spray is the most dangerous form of icing. The spray freezes on exposed surfaces to produce clear ice. At low air temperatures the ice may be opaque. At extreme low temperatures (below -15ºC), the spray may freeze in the air, so that it does not adhere to the surface. In open waters icing caused by sea spray will be frequent from November to April but rare in October and May. Heavy icing may occur with persistent strong northerly and north-easterly winds. Strong winds from other directions (particularly south and southeast) may cause heavy icing as well, though of short duration due to typically advection of warmer air. The rate of icing depends on wind speed, air temperature, sea surface temperature and characteristics of the vessel. The relationships are described in figure below.

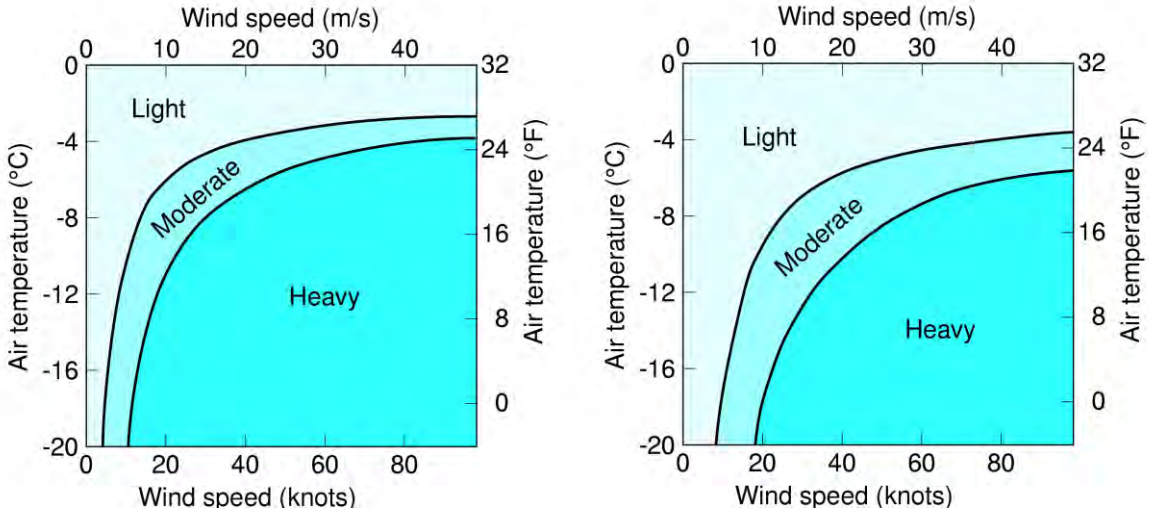

Figure 6.5 Icing conditions for vessels heading into or abeam of the wind for water temperatures of +1°C (34°F) [left] and +5°C (41°F) [right]. (Overland et al, 1986)

6.6. Ocean Currents

The oceanography of the Nordic Seas including the western Greenland Sea is dominated by two primary water masses, the Atlantic water and Polar water. Warm (6 to 8 °C), saline (35.0 to 35.2 psu) Atlantic water enters the Nordic seas in three branches crossing the Greenland Scotland Ridge. The second major watermass is the light, low saline (31.0 to 34.8 psu) and cold (-1.8 to -1.4 °C) polar water mass deriving from the upper Arctic Ocean and being exported south along with first year- and multi year mobile pack ice. Atlantic water circulates cyclonic in the Nordic seas loosing a significant amount of heat to the atmosphere while it in the form of the Norwegian Atlantic Current moves northward to the east. In the Fram Strait region, part of the Atlantic water recirculates and returns south along the East Greenland shelf break with a high salinity warm core aligned with the steepest part of the slope near the 2000m isobath occupying the depth interval between 100 to 500m. Geostrophic velocity estimates yields average current speeds up to 10-20 cm/s. The warm core with temperatures up to 2°C may seasonally be partly capped by polar water which also covers the entire shallow shelf region. In contrast to the conditions off shelf, the on shelf water column is highly stratified due primarily to salinity changes. Warm Atlantic water is found to penetrate onto the shelf as a near bottom layer below the Polar water partly explaining the strong layering in density here. The thickness of this layer is typically 50-75m but its variation, extend and seasonality is unknown. The circulation on the shelf is on average southward. Geostrophic velocity estimates yields relatively weak circulation (0-10 cm/s) which may contrast much higher estimate based on sea-ice drift. There are some evidence for a general intensification seasonally near the coast (0-30km) forming a coastal summer jet with. Drifter data from the shelf region have demonstrated very variable currents related to storm activity with peak currents reaching 100-200 cm/s. The topography on the shelf is relatively complex favoring formation of eddies and closed circulation loops. These are evident from sea-ice drift data and may persist for weeks in the summer period, altering the general southward drift pattern.

Figure 6.6: General ocean surface circulation around Greenland. Modified from Oceanographic Atlas of the Polar Seas (US N.H.O).

6.7. Waves

Waves in the Greenland are a combination of wind driven waves as well as swells. Sometime swells are the domination factor, at other times wind driven waves are the main factor, and then again at other times they contribute equally to the combined waves. Swells coming from low-pressure activity over the north Atlantic affect the area from time to time.

Waves in the Greenland Sea are obvious affected by the distribution of sea ice. In cases where winds blow from the ice, the distance to the ice edge has influence on how high the waves may be, as the ice edge more or less can be treated as a coastline. Wind driven waves need a certain distance to the ice edge/coastline as well as a persisting wind direction to reach the maximum height at a given wind speed.

Another way the ice affects the wave height is the damping effect when the sea is partly covered by ice. How much the damping influence wind driven waves and swells has not been a subject to a lot of investigation.

During summer the significant waves (in open waters) are relative low compared with the significant waves in the winter. This is caused by weaker winds in the summer than in winter combined with lower swells due to weaker low-pressure activity the North Atlantic. During autumn the average swell height increases due to the increasing low-pressure intensity over the North Atlantic, and increasing northerly winds over the Greenland Sea also. That is resulting in higher significant waves. The highest significant waves are usually seen in south parts of the area.

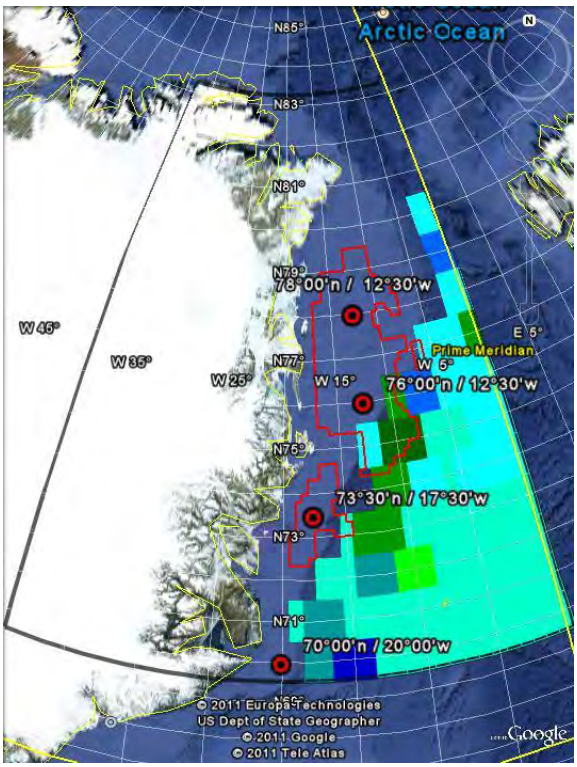

January

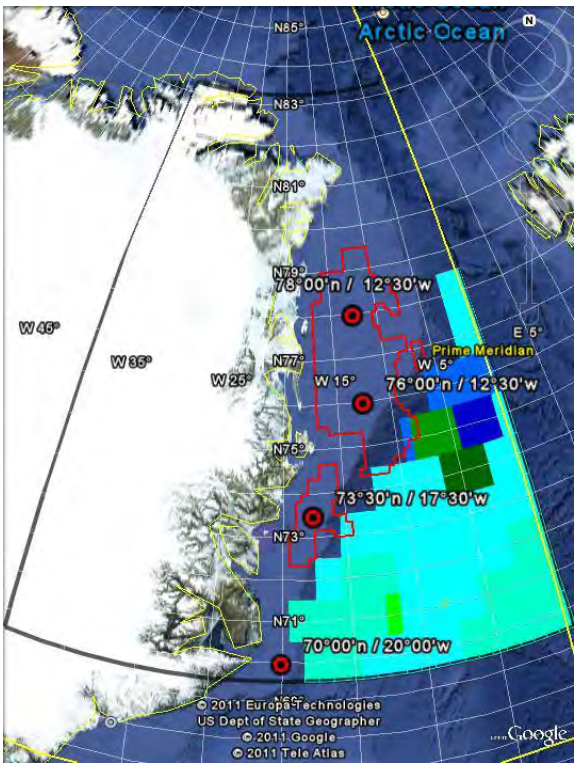

February

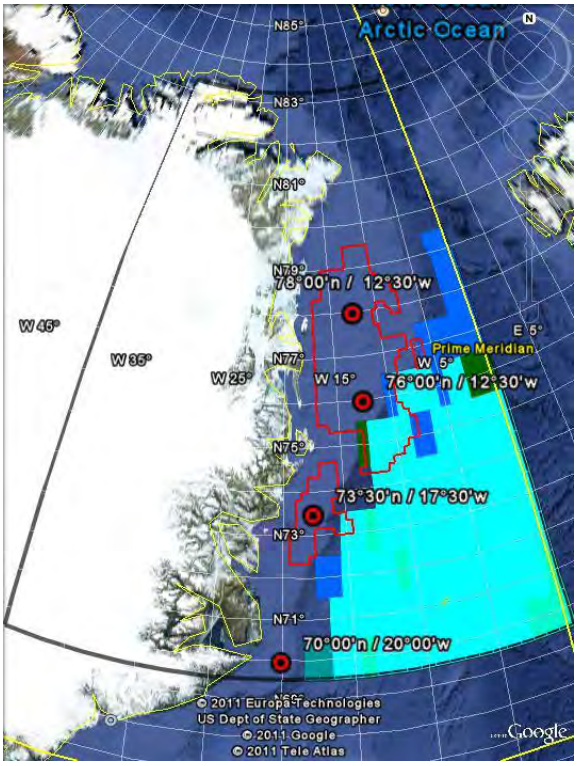

March

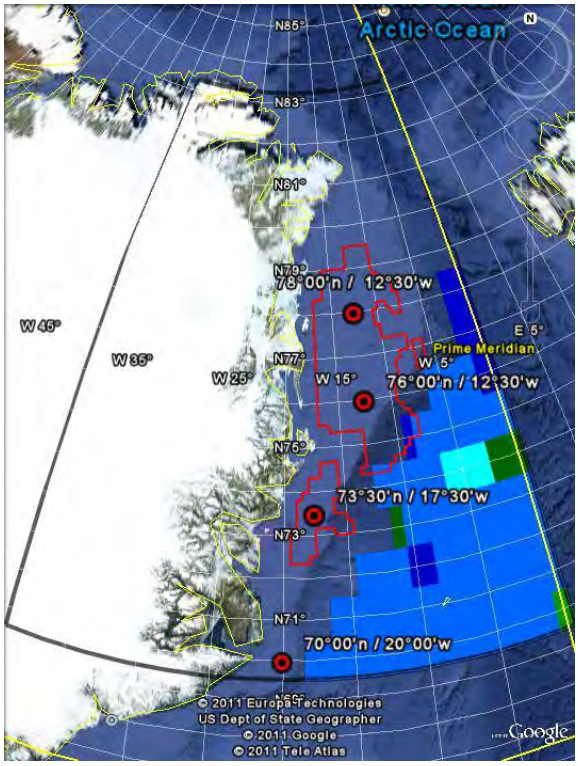

April

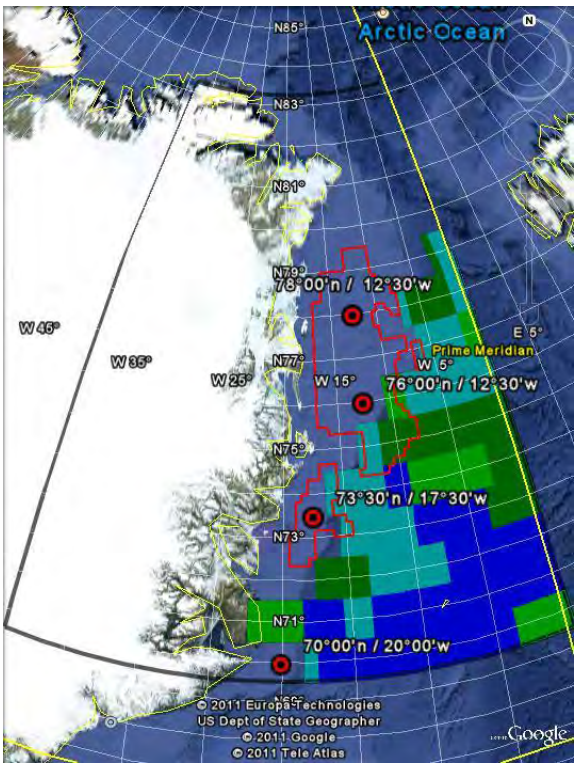

May

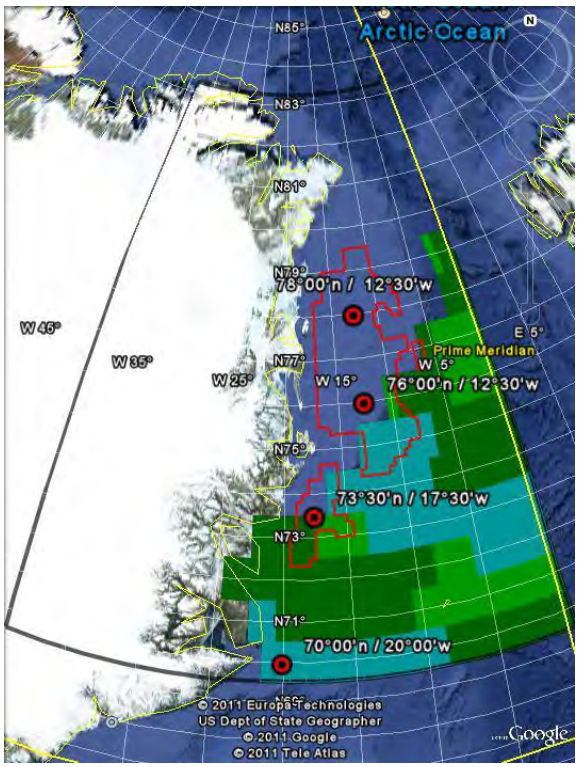

June

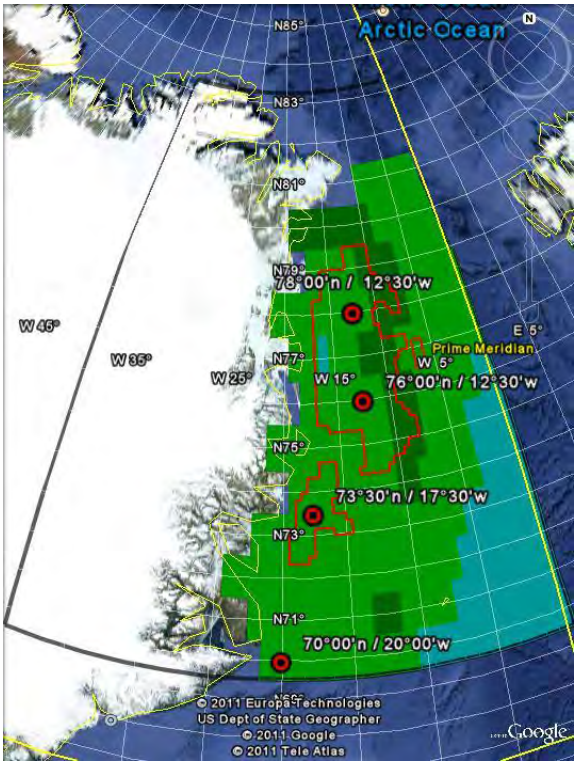

July

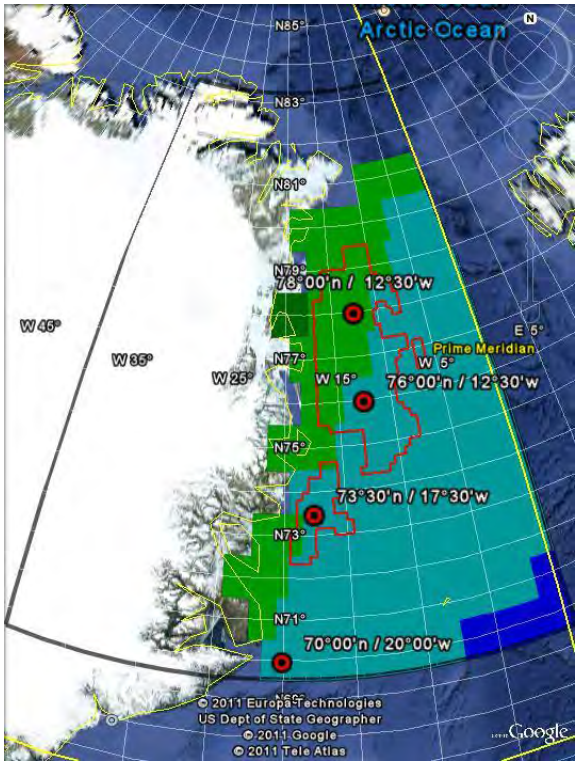

August

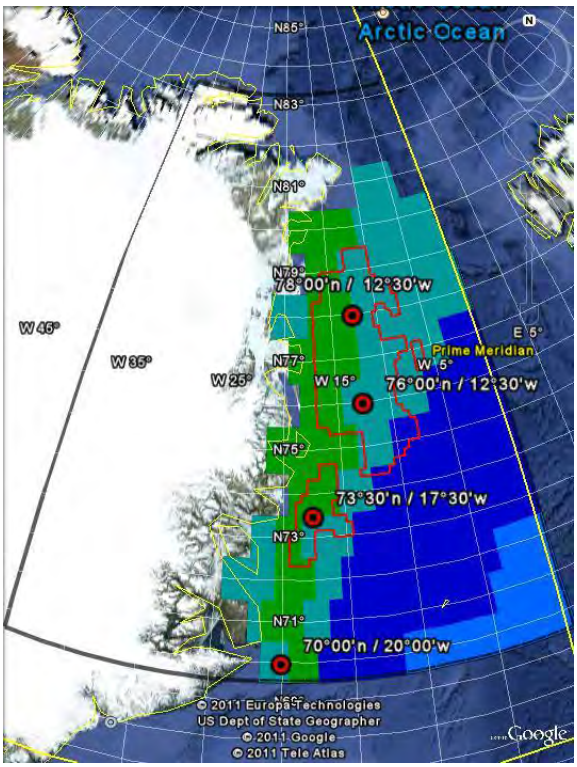

September

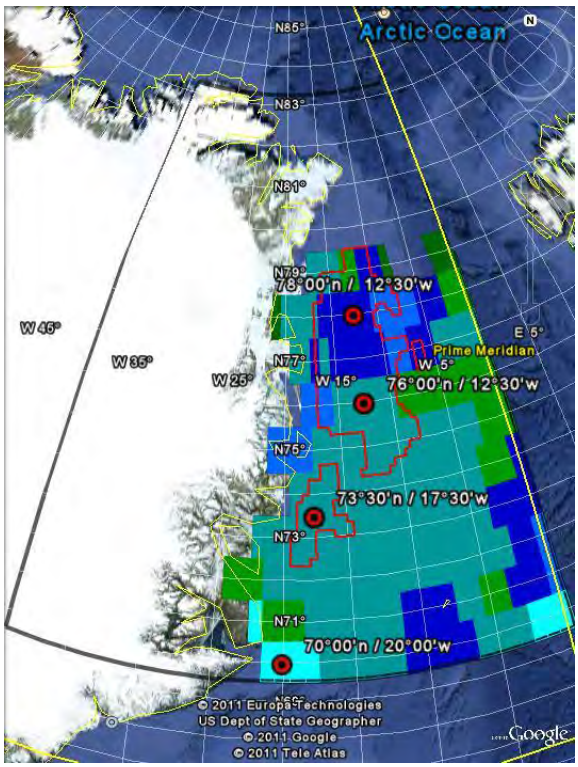

October

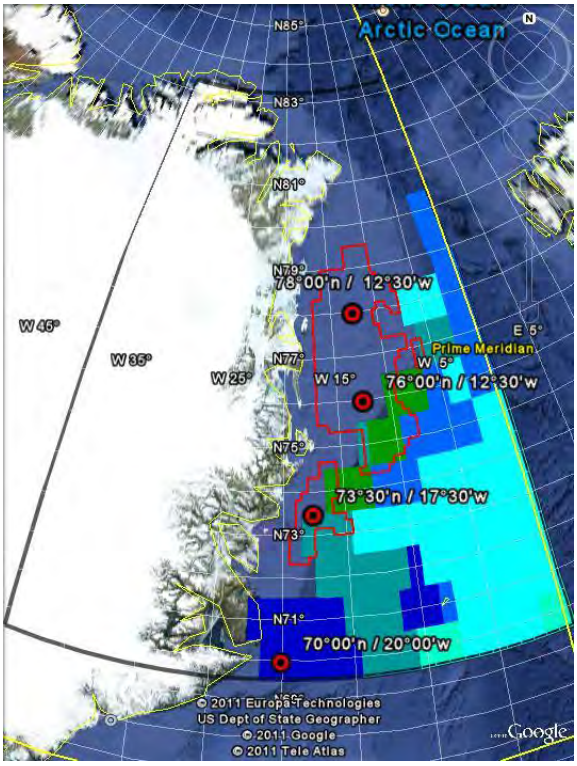

November

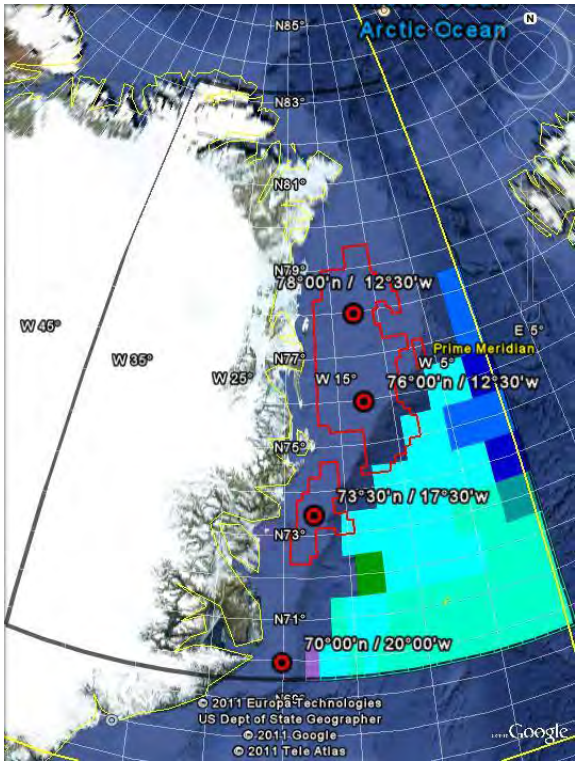

December

Figure 6.7 Monthly average significant wave height base on ECMWF's ERA-interim reanalysis 1979-2010 Due to the resolution of data some data points partly covers land areas when displayed.

7. Detailed ice freeboard measurements

7.1. Airborne laser measurements of sea ice freeboard heights

DTU Space coordinated an airborne campaign in April 2011, to obtain high-resolution laser scanner measurements for estimation of sea ice freeboard heights in the Fram Strait. The tracks were selected to match flight tracks from a similar survey conducted in April 2008, see **Figure 7.1**.

The Fram Strait campaign was carried out in connection with mobilization of ESA's CryoSat-2 Validation Experiment (CryoVEx-2011), thus the aircraft was equipped with an advanced 13.5 GHz radar altimeter (ASIRAS), which is an airborne version of the radar altimeter carried onboard CryoSat-2. Processing of the ASIRAS data is ongoing, however, it is rather time consuming and the processed data will not be available until the beginning of 2012. To support the analysis of laser scanner and ASIRAS data, vertical photography and video recordings were collected during flight.

In this study, we present sea ice freeboard heights (including the snow layer) obtained from the laser scanner measurements of the 2011 survey flights. The data is compared to the 2008 airborne survey to demonstrate relative changes in the sea ice freeboard heights. As the airborne laser scanner measures the surface height with higher resolution and precision, than by the use of satellite altimetry, the airborne measurements are used to validate the ICESat freeboard heights, see **chapter 7.2**

The 2011 campaign was a success. The first attempt, to repeat the 2008 survey tracks, was made on April 28 (blue line), see **figure 7.1**. However, the survey was cut short, due to low clouds and fog (less than 300m) in the area. To finish the planned tracks, a successful flight was carried out on May 3 (green line) in excellent weather conditions. The major part of the 2008 survey was measured on April 24 (green lines) and on April 21 only the south-eastern corner was measured (blue line). For a more detailed description of the 2008 survey, see Hvidegaard et al (2008).

2011 2008

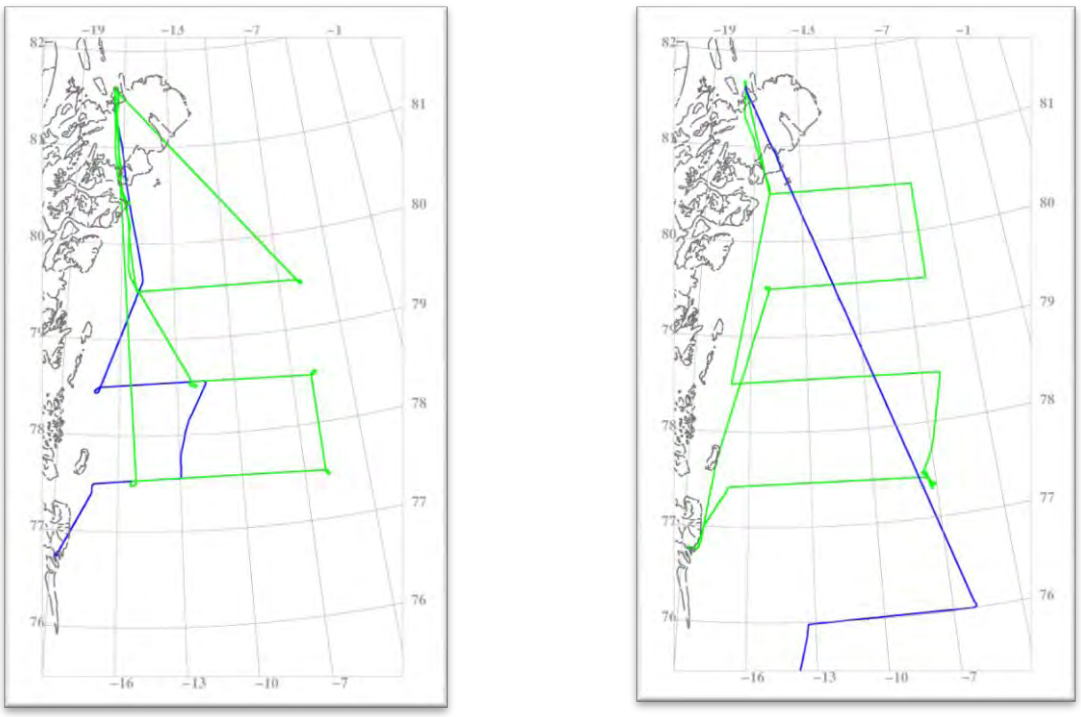

Figure 7.1: Flight tracks in the Fram Strait 2011 (left) and 2008 (right)

In general the sea ice was broken up with lots of open water leads and leads covered by thin ice (grey-white), see **figure 7.2**. Icebergs were primarily frozen into the fast ice near the coast. The shape of the icebergs are best described as large flat tabular or wedged, see **figure 7.3.**

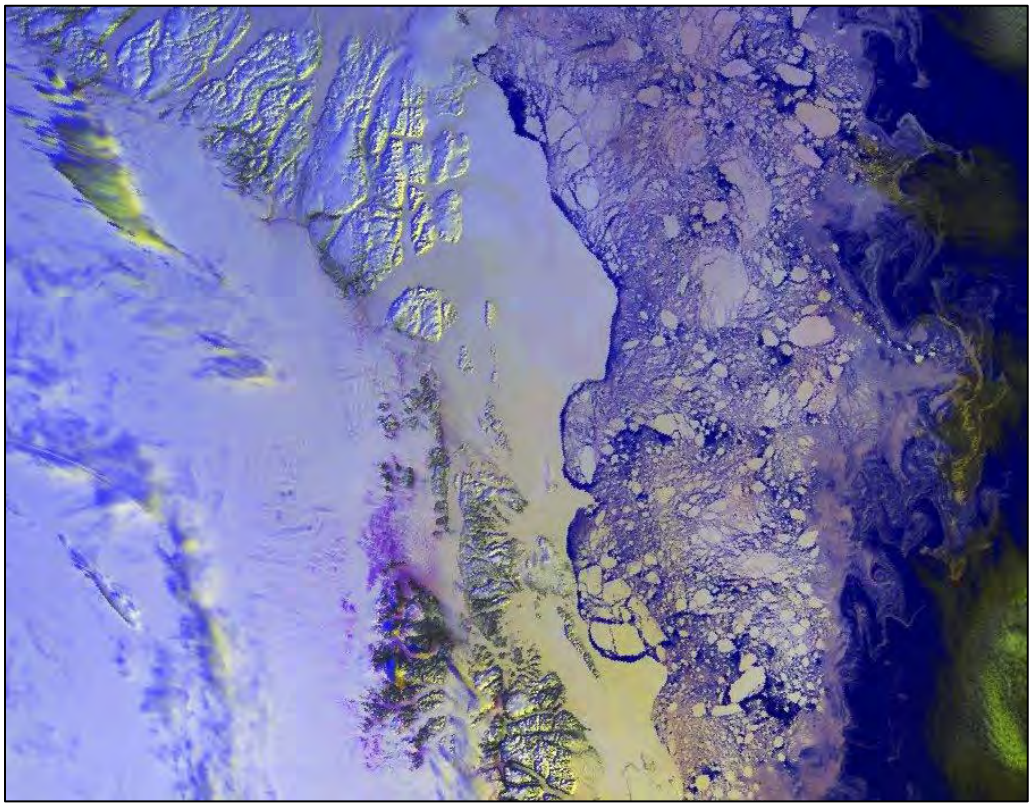

Figure 7.2: sea ice in the Jøkelbugt, NOAA AVHRR satellite image, 2011-05-03 11:18 UTC. By courtesy, DMI

The airborne laser scanner used here, is a laser scanner (Riegl LMS Q240i) measuring with a horizontal resolution of 0.75m x 1m at a flight height of 300m and a ground speed of 250 kph. This is the same scanner as used in the 2008 flights (Hvidegaard et al, 2008). The across-track swath width is roughly equal to the flight height, and the vertical accuracy is in the order of 10 – 20cm depending primarily on uncertainties in the kinematic GPS-solutions, due to long baselines (Krabill et al, 1995). For more information on the airborne instrumentation and the system setup, see Hvidegaard et al (2006).

The freeboard heights are obtained by using a lowest-level estimation method, similar to the method used for the ICESat altimeter. However, it is adapted to the higher resolution of the laser scanner system (Hvidegaard and Forsberg, 2002). An example of sea ice freeboard heights from a full resolution laser scanner swath is shown in **figure 7.4**. For consistency, we use the same freeboard to thickness conversion, k=5.5, as used in 2008 for the Fram Strait (Hvidegaard et al, 2008).

Sea ice freeboard distributions from the laser scanner measurements are plotted in **figure 7.5**. Each distribution represent sea ice along a latitude (77.5°N, 78.5°N and 79.5°N), thus each distribution includes both fast ice, drifting MYI, as well as marginal ice. The dominant ice has freeboard heights of 60-75cm corresponding to an ice thickness of 3.3-4.1m, which is characterized as MYI or deformed ice. A smaller peak of about 15-35cm is present in the northernmost and southernmost tracks representing FYI.

Figure 7.3: Photo of typical ice bergs (Photo: H. Skourup)

For comparison the freeboard distributions covering the same tracks from 2008 are shown in **figure 7.6**. Here the dominant ice type is FYI, with a peak freeboard height of about 15-25cm corresponding to thicknesses of 0.8-1.4m. The small amount of MYI in the Fram Strait in 2008 is supported by the ice type distribution of scatterometer data (**chapter 4.1**) and sea ice freeboard heights from ICESat (**chapter 4.2**), whereas the large amount of MYI in 2011 seems to represent years with a large distribution of thick ice such as 2005 and 2006. A more detailed comparison of sea ice freeboard heights from airborne laser scanner measurements and ICESat is given in **chapter 7.2**.

The average ice thickness (using k=5.5) for the 2011 flight, together with the sea ice distribution of ice thicker than 80cm, are shown in **Figure 7.7**. Each value represents all data within blocks of 3 degrees longitude x 1 degree latitude. This plot also reveals the differences in distribution of MYI and FYI between 2011 and 2008, when compared to a similar plot from 2008 (Figure 23 in Hvidegaard et al, 2008).

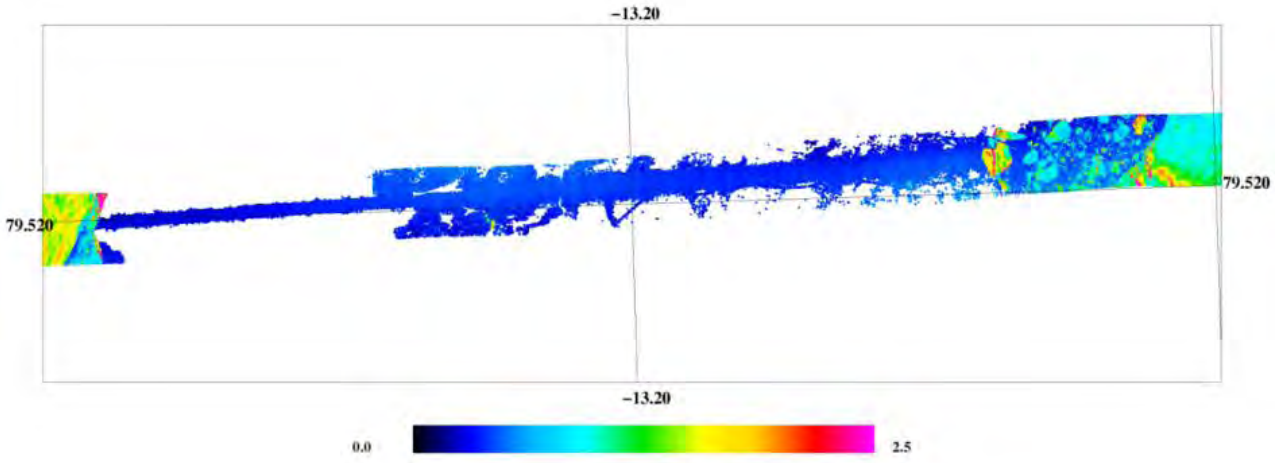

Figure 7.4: Full resolution sea ice freeboard heights from airborne laser scanner (unit is given in m)

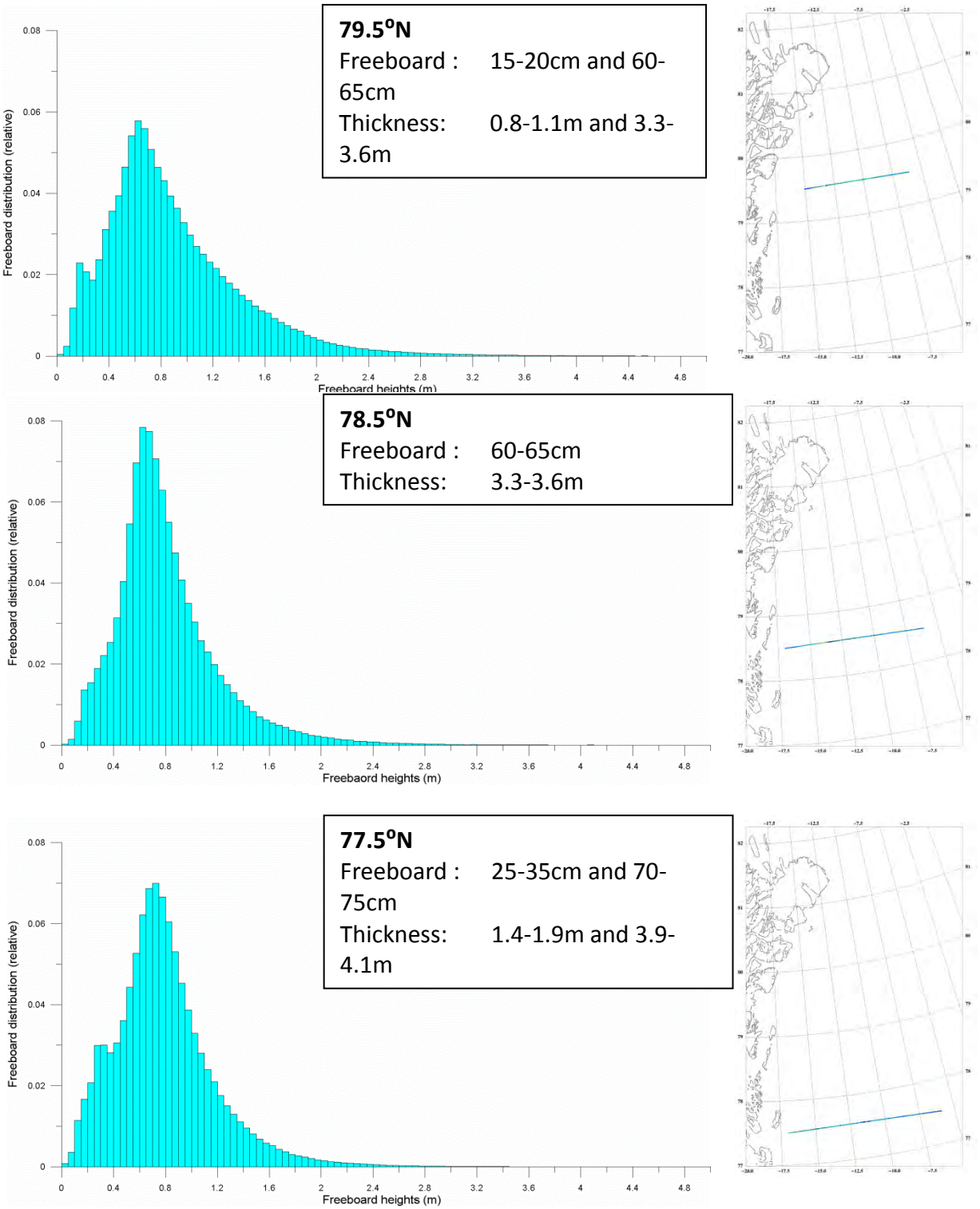

Figure7.5: Distribution of sea ice freeboard heights from airborne laser scanner measurements from May 3, 2011

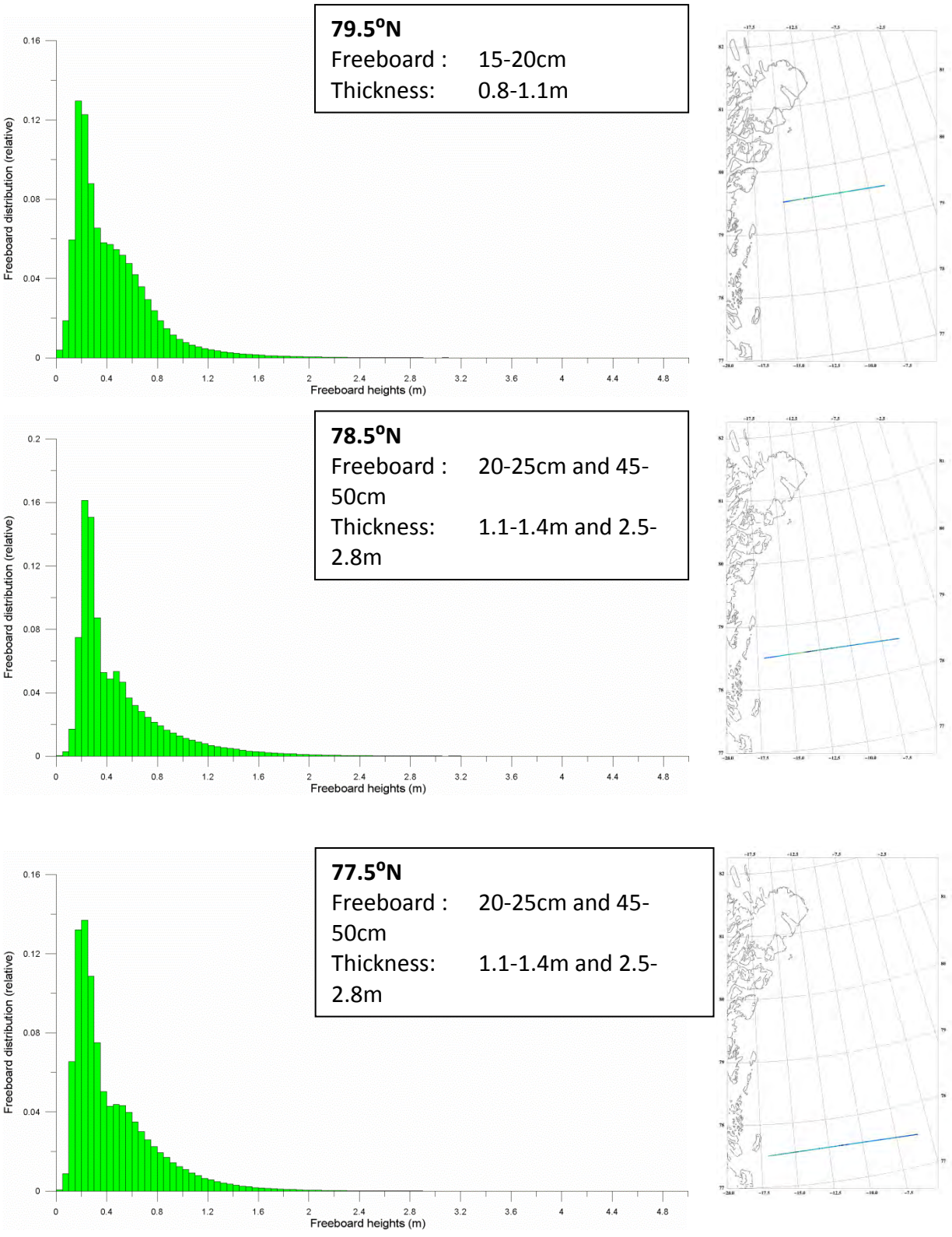

Figure 7.6: Distribution of sea ice freeboard heights from airborne laser scanner measurements from April 24, 2008

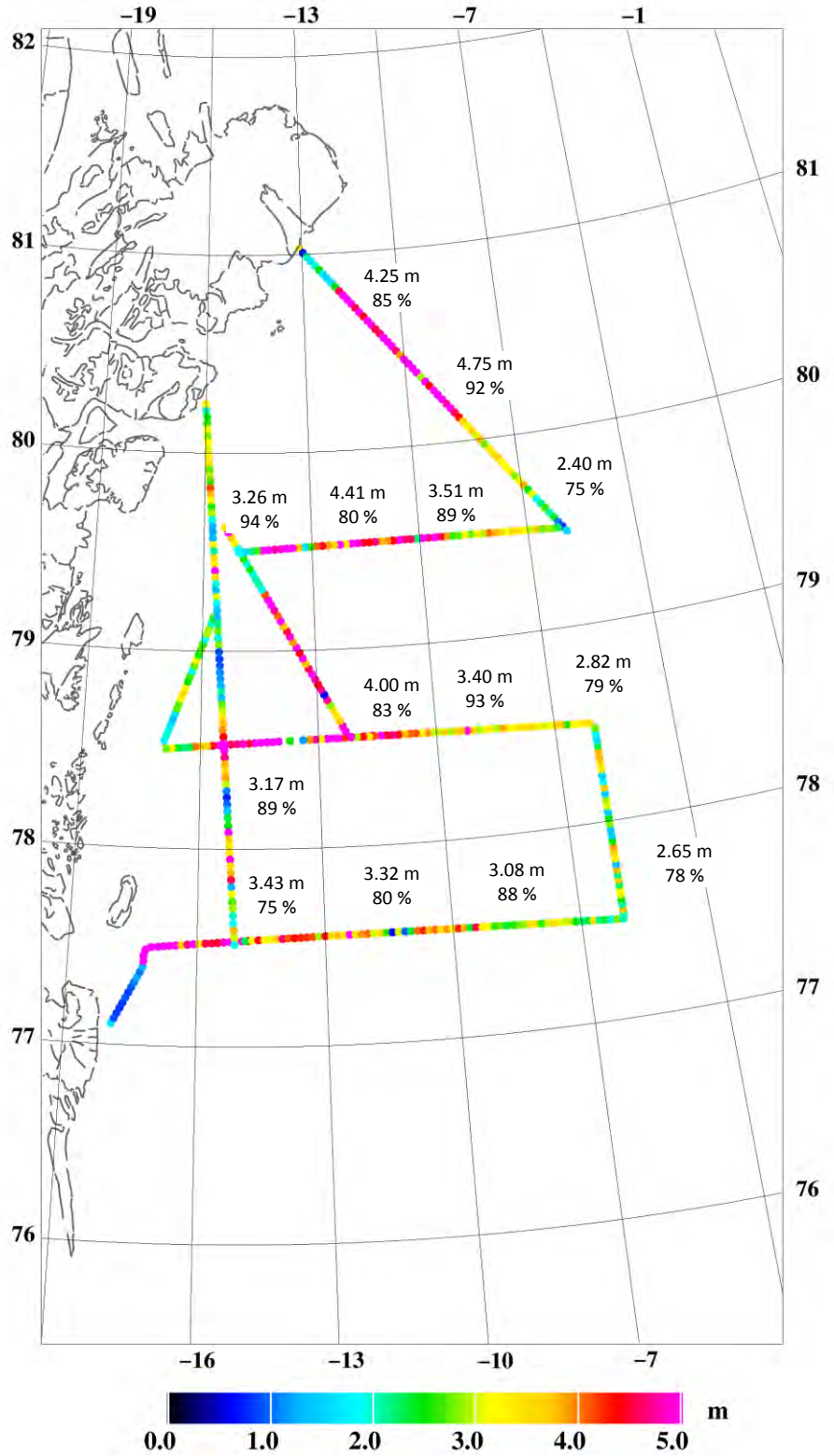

Figure 7.7: Ice thickness in the NE Greenland shelf area from 2011 lidar flights. Numbers show averages in 3 degree longitude x 1 degree latitude blocks, along with probability of ice thickness greater than 80 cm

7.2. Comparison of sea ice freeboard heights from satellite altimetry and airborne laser scanner measurements

The airborne data set from 2011 (presented **in chapter 7.1**) could, in principle, be compared to CryoSat-2 radar altimetry. However, the CryoSat-2 data are not ready for such comparison studies and is left for later analysis, see **chapter 4.2.**

The only overlapping data sets are freeboard heights from airborne laser scanner and ICESat measurements from 2008. The laser scanner freeboard heights are plotted on top of the ICEsat freeboard heights in **figure 7.8**. Direct comparison is questionable, as the airborne data set is from April 24, whereas the ICESat is from the period February 17 – March 21. However, the sea ice thickness is about its annual maximum in February-March, and except for the changes due to ice drift there is not expected much changes in the sea ice distribution north of 76^0 N before the beginning of May.

The sea ice freeboard distribution of all airborne laser scanner data from 2008 (**figure 7.8**), is plotted in **figure 7.9**, together with the freeboard distributions from all ICESat periods 2003-2008. The 2008 ICESat distribution, matches best the distribution of the airborne freeboard heights with FYI representing the major parts. The distribution of ICESat freeboard heights tend to underestimate the presence of thick ice and deformed ice, e.g. the ice represented by the tail of the distribution is not as pronounced as in the case of airborne laser measurements.

This is explained by direct comparison of sea ice freeboard heights from coincident tracks of ICESat and airborne laser scanner measurements. In Skourup and Forsberg (2006) it is shown, that the "lowest-level" filtering technique applied to ICESat data underestimates the sea ice freeboard heights by up to 37 cm in heavy ice conditions with only a few open leads. The bias is a result of the lower spatial sampling of ICESat and of the averaging of the freeboard across the footprint, whereas the high resolution airborne laser scanner data system picks up even the smallest leads and hence freeboard heights from these data should not be biased. This is consistent with results from a similar study made by Kurtz et al. (2008), who found a bias of less than 2 cm, between ICESat freeboard heights and airborne laser freeboard heights, in areas of relative flat ice with many open leads. In areas of thicker ice with fewer open leads they found that the ICESat freeboard heights were underestimated by up to 9 cm. Thus, the biases introduced from the "lowest-level" filtering technique are dependent on sea ice concentration and ice thickness, where thick ice and ice of high concentration are underestimated.

The freeboard distribution plots of the 2011 airborne flights are plotted together with the ICESat distribution plots in **figure 7.10**. All the data used is plotted in **figure 7.7 chapter 7.1**. The 2011 freeboard distribution is best represented by the ICESat distributions of 2005 and 2006.

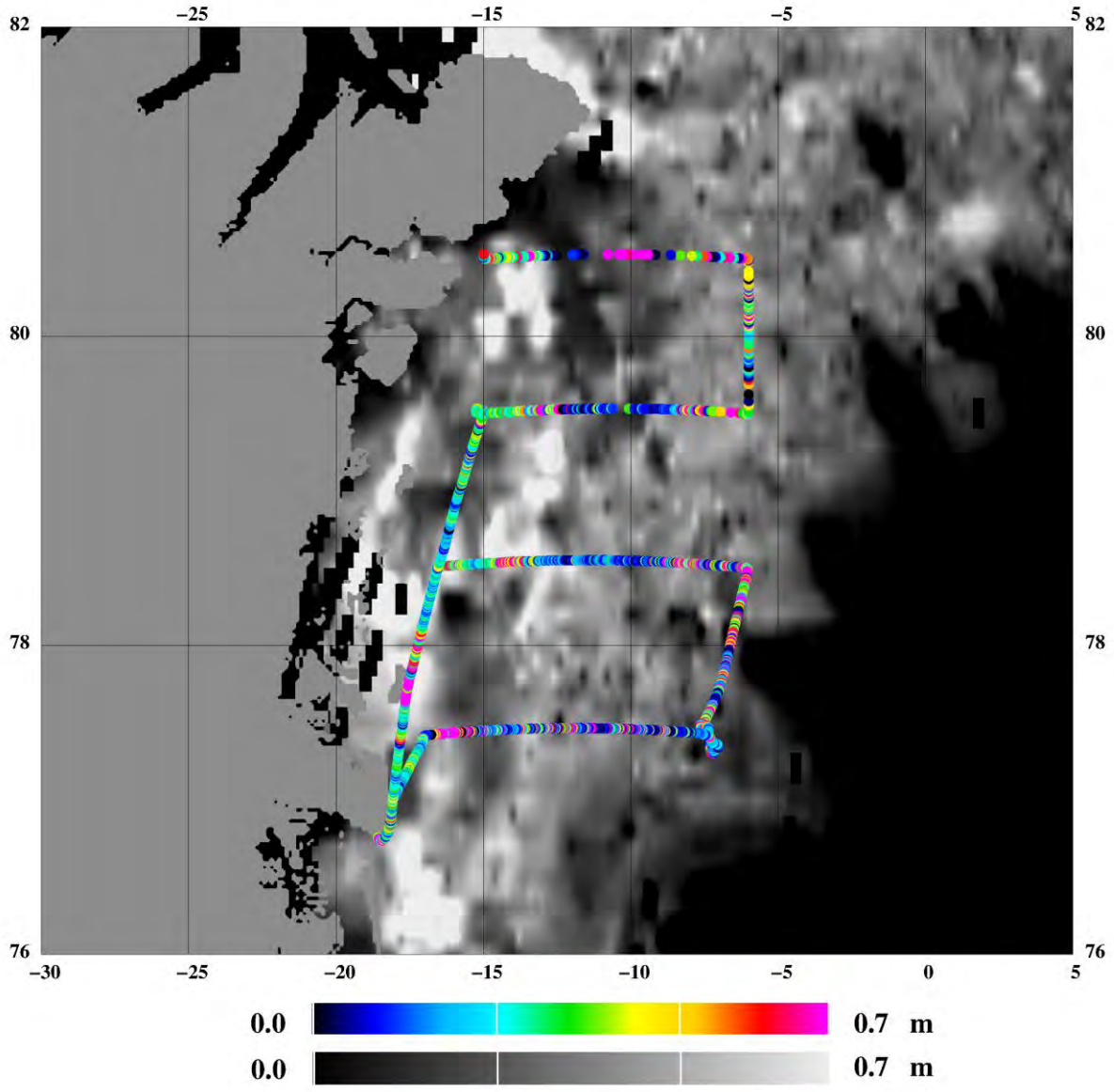

Figure 7.8: Freeboard heights from 2008 airborne laser scanner (April 24) overlaid ICESat freeboard heights (February 17 – March 21)

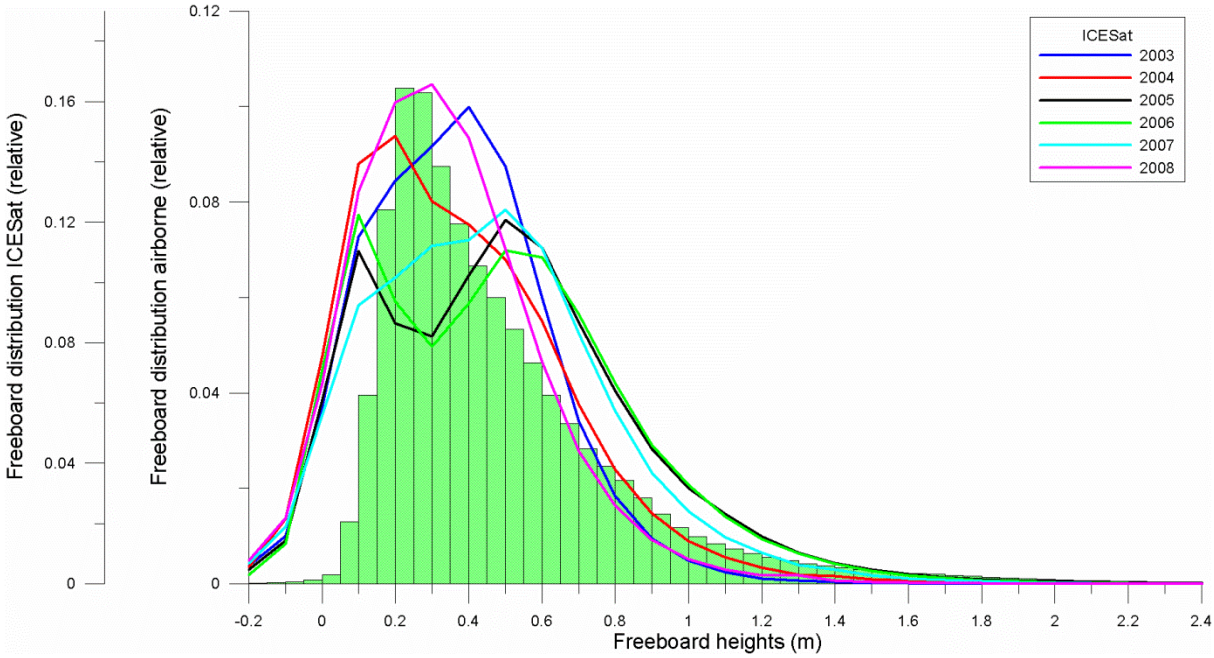

Figure 7.9: Freeboard distribution from 2008 airborne laser scanner (green histogram) and 2003-2008

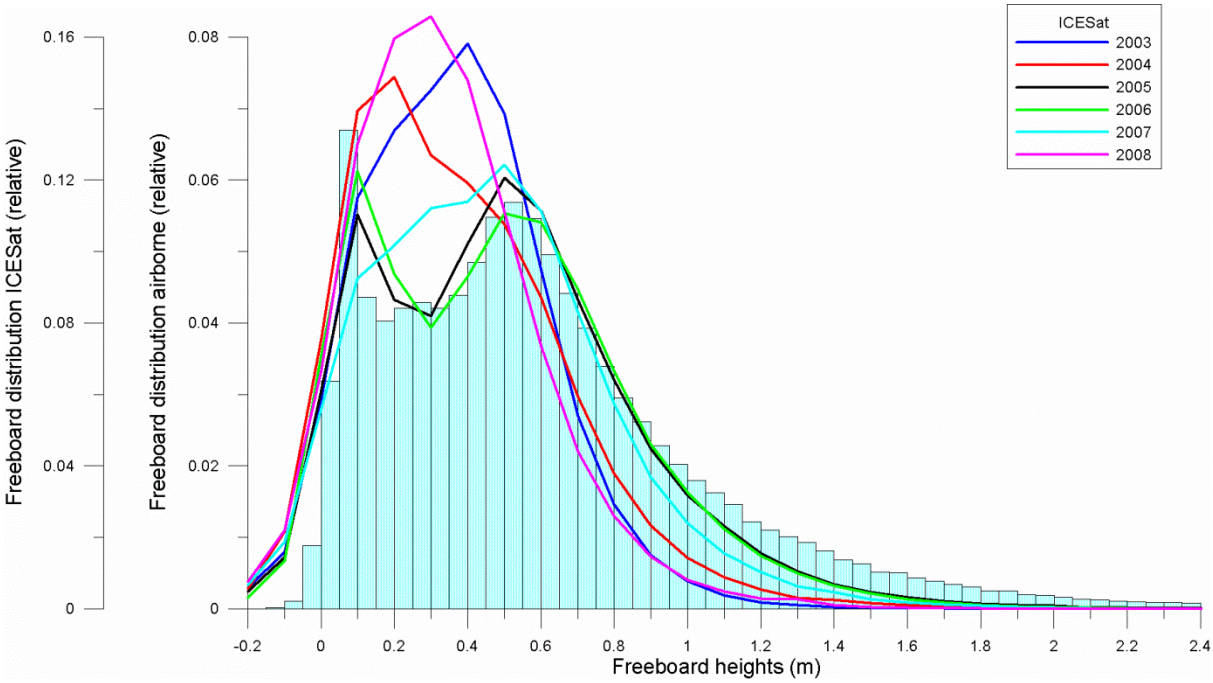

Figure 7.10: Freeboard distribution from 2011 airborne laser scanner (cyan histogram) and 2003-2008 ICESat (lines)

8. Detailed ice free days/periods etc

East Greenland 1979-2010 and 2001-2010

The table below shows the minimum, average and maximum number of days with ice cover (ice concentration) less than 30%, 40% and 60% respectively, for each of the regular lat/lon-boxes (given by bottom-right corner coordinates) shown on **figure 3.1 and 3.2**.

	1979-2010									2001-2010								
		<30%			<40%			<60%			<30%			<40%			<60%	
lat, lon	min	mean	max	min	mean	max	min	mean	max	min	mean	max	min	mean	max	min	mean	max
80, -13	0	16	70	0	42	115	0	86	125	0	14	58	0	29	115	0	66	123
80, -10	0	34	96	1	59	110	40	91	124	10	45	96	45	78	110	92	108	124
80, -7	0	26	80	0	39	100	11	67	116	1	38	76	16	55	100	53	86	116
80, -4	0	15	70	0	26	74	0	45	101	0	23	62	0	35	73	16	55	101
80, -1	0	9	58	0	15	65	0	33	95	0	14	58	0	22	65	1	41	95
80, 2	0	7	55	0	14	74	0	55	156	0	12	55	0	18	72	0	56	133
79, -13	0	6	49	0	13	61	0	46	110	0	11	49	0	17	61	0	31	110
79, -10	0	18	63	0	33	85	0	66	111	0	29	63	0	45	85	8	76	111
79, -7	0	24	87	0	40	106	2	69	124	0	43	87	2	62	106	49	88	124
79, -4	0	17	88	0	28	99	2	56	109	0	31	88	0	44	99	9	71	109
79, -1	0	14	66	0	28	98	5	74	150	0	21	66	0	34	98	19	78	149
79, 2	0	81	182	10	135	286	70	235	357	31	82	162	49	134	226	121	232	305
78, -16	0	4	60	0	5	70	0	13	98	0	10	60	0	13	70	0	22	98
78, -13	0	10	78	0	13	91	0	34	110	0	18	78	0	23	91	0	38	110
78, -10	0	15	81	0	25	95	1	58	113	0	29	81	0	44	95	31	75	113
78, -7	0	19	82	0	30	93	2	65	120	0	37	82	0	51	93	33	82	120
78, -4	0	20	82	0	35	98	17	84	156	0	37	82	2	52	98	63	99	156
78, -1	9	127	271	75	199	327	193	304	358	45	141	218	99	211	288	245	310	355
77, -16	0	13	86	0	22	99	0	42	118	0	29	86	0	38	99	0	52	118
77, -13	0	18	96	0	26	101	5	53	121	0	38	96	0	48	101	32	72	121
77, -10	0	20	96	0	30	107	16	67	126	0	43	96	14	58	107	49	88	126
77, -7	0	26	102	0	39	117	18	81	158	0	51	102	15	69	117	61	105	158
77, -4	0	50	170	8	83	202	85	184	266	17	76	170	41	109	202	136	199	260
77, -1	167	284	362	219	321	364	271	346	365	239	305	357	282	340	364	343	360	365
76, -16	0	19	88	0	31	102	0	55	123	0	33	88	0	44	102	0	66	123
76, -13	0	21	95	0	34	105	9	67	122	0	46	95	8	61	105	55	85	122
76, -10	0	31	105	0	46	114	37	86	157	20	62	105	31	73	114	70	108	157
76, -7	0	50	170	5	79	195	87	154	228	33	85	170	42	115	195	98	169	228
76, -4	45	189	306	109	247	339	203	320	365	166	224	291	208	274	331	259	339	365
75, -16	0	20	96	0	30	106	2	60	126	0	44	96	0	54	106	27	84	126
75, -13	0	33	103	0	47	108	39	80	134	32	63	103	42	73	108	68	98	134
75, -10	1	70	158	6	101	195	116	175	246	43	104	158	63	131	195	136	186	246
75, -7	92	238	321	122	278	356	198	319	365	209	266	317	225	309	348	265	343	365
74, -16	0	33	117	0	50	122	31	89	135	13	66	117	32	82	122	57	111	135
74, -13	1	63	129	16	89	162	108	150	234	45	91	128	60	119	162	116	167	234
74, -10	66	216	308	115	257	341	172	299	364	192	246	297	218	289	341	231	329	364

73, -19	0	53	124	4	76	139	83	142	205	25	87	124	68	107	139	128	159	205
73, -16	1	57	124	10	77	142	64	119	203	29	88	124	51	107	142	95	142	203
73, -13	25	155	261	96	192	286	132	248	333	122	187	261	182	220	286	211	271	318
73, -10	120	267	364	162	288	364	177	314	366	213	313	364	218	328	364	257	347	366
72, -19	0	52	133	0	66	135	11	96	150	19	92	133	58	104	135	88	127	150
72, -16	13	94	188	42	120	221	108	188	269	58	125	188	79	147	221	145	203	269
72, -13	76	221	330	118	245	350	172	282	364	186	259	323	199	282	350	228	316	364
72, -10	144	282	364	174	299	366	208	320	366	225	328	364	240	340	366	264	351	366
71, -19	0	61	132	4	78	144	64	118	168	43	100	132	65	113	144	110	139	168
71, -16	40	185	295	60	213	313	138	252	359	170	213	276	184	240	286	212	281	359
71, -13	138	278	366	185	292	366	193	314	366	230	322	366	239	334	366	258	348	366
70, -19	20	86	143	61	109	162	102	157	205	73	117	143	93	132	162	130	168	205
70, -16	98	224	336	138	247	354	175	289	364	166	252	310	186	279	342	241	330	363
69, -22	0	57	143	0	83	168	59	131	284	56	102	143	81	120	168	109	165	284
69, -19	64	135	211	98	170	243	149	237	335	114	160	211	135	187	243	181	257	312
68, -25	9	85	141	47	103	156	82	137	202	78	116	141	94	130	156	124	157	202
68, -22	60	122	211	82	152	236	140	217	326	109	154	211	131	179	236	175	241	326
68, -19	136	276	364	185	301	364	230	328	365	210	308	364	242	324	364	293	345	365

Table showing number of days with less than 30%, 40% and 60% ice respectively from the OSISAF satellite dataset. Left part is 1979-2010 data, and right part is 2001-10.

9. Detailed ice drift data

Details of ice drift statistics. All numbers are average drift velocity over 24 hours.
Tables consist of 3 parts.
Leftmost part (brownish) is number of datapoints in statistics (number of independently observed ice drift vectors)
Center part (bluish) shows average drift, rightmost part (greenish) shows maximum observed drift
Upper row shows longitude of grid point, eft column show latitude of grid point

JANUARY

	Number of independent datapoints												Average drift												Max drift											
	-24	-21	-18	-15	-12	-9	-6	-3	0,5	3,5	6,5	9,5	-24	-21	-18	-15	-12	-9	-6	-3	0,5	3,5	6,5	9,5	-24	-21	-18	-15	-12	-9	-6	-3	0,5	3,5	6,5	9,5
80	0	29	1521	5477	7083	5040	5186	3279	955	0	0	0	0	0,1	0	0	0,4	5,7	11,8	13,4	13,1	0	0	0	0	0,7	1,5	2,2	24,3	24,2	24,6	24,6	24,4	0	0	0
79	0	45	2404	12169	11798	10105	8304	3165	394	0	0	0	0	0,1	0	0	2,2	9,3	11,4	13,1	12,9	0	0	0	0	1,5	1,1	19,4	24,4	24,7	24,7	24,5	24,3	0	0	0
78	0	0	1381	7831	10879	10856	4896	118	0	0	0	0	0	0	0	3,4	9	9,9	10,2	16,4	0	0	0	0	0	0	2	24,7	24,6	24,6	24,5	24,5	0	0	0	0
77	0	0	1118	7504	8674	8472	2329	1	0	0	0	0	0	0	0,4	7,4	10,5	9	8,6	7,4	0	0	0	0	0	0	18,7	24,5	24,6	24,6	24,2	7,4	0	0	0	0
76	0	7	1180	4242	3255	1208	10	0	0	0	0	0	0	0,1	0,1	8,5	10,2	9,4	10,9	0	0	0	0	0	0	0,3	17,8	24,6	24,5	22,1	14,9	0	0	0	0	0
75	0	15	261	1998	307	5	0	0	0	0	0	0	0	0,1	11,3	11	13,2	19,8	0	0	0	0	0	0	0	0,3	26,9	27	24,3	20,2	0	0	0	0	0	0
74	0	58	1070	729	4	0	0	0	0	0	0	0	0	0,1	12,4	12,1	15	0	0	0	0	0	0	0	0	0,7	27,3	24,8	15,6	0	0	0	0	0	0	0
73	0	619	1048	110	0	0	0	0	0	0	0	0	0	2,7	13,9	18,5	0	0	0	0	0	0	0	0	0	26,7	27,4	24,2	0	0	0	0	0	0	0	0
72	0	526	312	17	0	0	0	0	0	0	0	0	0	9,1	16,5	19,7	0	0	0	0	0	0	0	0	0	27,2	27	23,1	0	0	0	0	0	0	0	0
71	130	115	29	0	0	0	0	0	0	0	0	0	0,1	15,1	18,3	0	0	0	0	0	0	0	0	0	0,7	26,9	25,1	0	0	0	0	0	0	0	0	0
70	0	292	10	0	0	0	0	0	0	0	0	0	0	9,2	16,6	0	0	0	0	0	0	0	0	0	0	22,6	19,3	0	0	0	0	0	0	0	0	0
69	16	26	0	0	0	0	0	0	0	0	0	0	5,6	8,6	0	0	0	0	0	0	0	0	0	0	22,9	21,9	0	0	0	0	0	0	0	0	0	0
68	0	0	0	0	0	0	0	0	0	0	0	0	0	0	0	0	0	0	0	0	0	0	0	0	0	0	0	0	0	0	0	0	0	0	0	0

FEBRUARY

	Number of independent datapoints												Average drift												Max drift											
	-23,5	-20,5	-17,5	-14,5	-11,5	-8,5	-5,5	-2,5	0,5	3,5	6,5	9,5	-23,5	-20,5	-17,5	-14,5	-11,5	-8,5	-5,5	-2,5	0,5	3,5	6,5	9,5	-23,5	-20,5	-17,5	-14,5	-11,5	-8,5	-5,5	-2,5	0,5	3,5	6,5	9,5
80	0	13	1132	4264	5202	4242	4137	3407	1151	0	0	0	0	0,1	0	0	0,7	3,2	6,6	9,3	8	0	0	0	0	0,7	4,4	4,6	24,4	24,3	24,3	24,4	24,4	0	0	0
79	0	32	1943	9021	9171	8473	5852	2430	410	0	0	0	0	0,3	0	0	1,8	6,2	8	9,1	7,9	0	0	0	0	1,1	4,7	15	24,4	24,6	24,5	24,4	21,8	0	0	0
78	0	0	1214	6251	8355	8566	3251	24	0	0	0	0	0	0	0	3,9	7,6	7,3	6,8	8,2	0	0	0	0	0	0	4,6	24	24,5	24,6	24,4	19,7	0	0	0	0
77	0	0	930	6319	7267	5545	1149	0	0	0	0	0	0	0	0,2	7,4	7,9	6,4	4,3	0	0	0	0	0	0	0	15,6	24,5	24,5	24,4	24,2	0	0	0	0	0	0
76	0	8	1101	4455	3097	852	16	0	0	0	0	0	0	0,3	0	8	9,7	7,2	10,7	0	0	0	0	0	0	1,1	4,4	26,3	27	24,3	14,6	0	0	0	0	0	0
75	0	8	303	2846	480	14	0	0	0	0	0	0	0	0,1	10,3	10,6	12,9	11,1	0	0	0	0	0	0	0	0,3	19,5	27,1	27,1	15,2	0	0	0	0	0	0	0
74	0	28	1355	1168	22	0	0	0	0	0	0	0	0	1	10,7	11	19,8	0	0	0	0	0	0	0	0	13,4	27,3	24	23,5	0	0	0	0	0	0	0	0
73	0	601	1395	278	0	0	0	0	0	0	0	0	0	4,7	12,3	13	0	0	0	0	0	0	0	0	0	22,6	27,4	21,8	0	0	0	0	0	0	0	0	0
72	0	711	780	42	0	0	0	0	0	0	0	0	0	10,9	14,3	13,9	0	0	0	0	0	0	0	0	0	27	27,1	18,2	0	0	0	0	0	0	0	0	0
71	260	278	370	0	0	0	0	0	0	0	0	0	0,2	14,8	15,5	0	0	0	0	0	0	0	0	0	1	27,3	27	0	0	0	0	0	0	0	0	0	0
70	0	343	91	0	0	0	0	0	0	0	0	0	0	16,7	16,2	0	0	0	0	0	0	0	0	0	0	26,8	26,1	0	0	0	0	0	0	0	0	0	0
69	91	122	0	0	0	0	0	0	0	0	0	0	16,9	16,7	0	0	0	0	0	0	0	0	0	0	27,2	27,6	0	0	0	0	0	0	0	0	0	0	0	0
68	0	0	0	0	0	0	0	0	0	0	0	0	0	0	0	0	0	0	0	0	0	0	0	0	0	0	0	0	0	0	0	0	0	0	0	0	0	0

MARCH

	-23,5	-20,5	-17,5	-14,5	-11,5	-8,5	-5,5	-2,5	0,5	3,5	6,5	9,5	-23,5	-20,5	-17,5	-14,5	-11,5	-8,5	-5,5	-2,5	0,5	3,5	6,5	9,5	-23,5	-20,5	-17,5	-14,5	-11,5	-8,5	-5,5	-2,5	0,5	3,5	6,5	9,5
80	0	10	720	2787	3768	2185	1566	1113	277	0	0	0	0	0	0	0	0,9	6,2	12,7	13,7	13,3	0	0	0	0	0,2	1,4	1,9	15,9	24,1	24,4	24,6	24,5	0	0	0
79	0	35	1129	6075	6606	4747	2548	751	38	0	0	0	0	0	0	0	1,7	10	13,2	15,3	16,3	0	0	0	0	0,8	0,7	7,5	24,3	24,5	24,5	24,3	23,8	0	0	0
78	0	0	584	3740	5354	4684	1530	23	0	0	0	0	0	0	0	3,8	9,4	10,4	12,7	16,1	0	0	0	0	0	0	1,4	24,5	24,5	24,5	24,5	24,1	0	0	0	0
77	0	0	398	3232	4473	3986	641	1	0	0	0	0	0	0	0,1	8,4	10,1	9,7	11,3	17,7	0	0	0	0	0	0	12,2	24,3	24,4	24,4	22,9	17,7	0	0	0	0
76	0	5	638	2075	2273	547	1	0	0	0	0	0	0	0,1	0	10,3	10,8	9,7	19,4	0	0	0	0	0	0	0,3	9	26,5	27	24,1	19,4	0	0	0	0	0
75	0	12	129	938	171	0	0	0	0	0	0	0	0	0	13,2	13,5	14	0	0	0	0	0	0	0	0	0,3	26	27,2	25,7	0	0	0	0	0	0	0
74	0	65	838	655	53	0	0	0	0	0	0	0	0	0,3	14,9	15,7	16,3	0	0	0	0	0	0	0	0	18,6	27,5	27,2	27,3	0	0	0	0	0	0	0
73	0	562	1268	558	19	0	0	0	0	0	0	0	0	6,1	16,4	16,9	15,6	0	0	0	0	0	0	0	0	27,5	27,4	27,3	22,1	0	0	0	0	0	0	0
72	0	474	789	96	0	0	0	0	0	0	0	0	0	13,1	16,4	17,4	0	0	0	0	0	0	0	0	0	27,4	27,3	25,3	0	0	0	0	0	0	0	0
71	120	192	433	0	0	0	0	0	0	0	0	0	0,1	17,1	15,1	0	0	0	0	0	0	0	0	0	1,6	26,5	26,8	0	0	0	0	0	0	0	0	0
70	8	215	59	0	0	0	0	0	0	0	0	0	0,3	14,8	14,4	0	0	0	0	0	0	0	0	0	0,5	27,2	26,6	0	0	0	0	0	0	0	0	0
69	20	48	0	0	0	0	0	0	0	0	0	0	8,1	19,2	0	0	0	0	0	0	0	0	0	0	22,1	27,1	0	0	0	0	0	0	0	0	0	0
68	0	0	0	0	0	0	0	0	0	0	0	0	0	0	0	0	0	0	0	0	0	0	0	0	0	0	0	0	0	0	0	0	0	0	0	0

APRIL

	-23,5	-20,5	-17,5	-14,5	-11,5	-8,5	-5,5	-2,5	0,5	3,5	6,5	9,5	-23,5	-20,5	-17,5	-14,5	-11,5	-8,5	-5,5	-2,5	0,5	3,5	6,5	9,5	-23,5	-20,5	-17,5	-14,5	-11,5	-8,5	-5,5	-2,5	0,5	3,5	6,5	9,5
80	0	32	1434	4901	5913	4252	4436	2808	1175	0	0	0	0	0,2	0,1	0	0,3	6,4	10,7	11,8	11,2	0	0	0	0	4,5	4,5	4,5	14,1	23,9	24,3	24,5	24,5	0	0	0
79	0	28	2383	10722	10957	9398	6387	2269	338	0	0	0	0	0,1	0	0	1,4	9	10,8	12,6	12,5	0	0	0	0	0,5	4,5	4,5	23	24,6	24,5	24,4	24,3	0	0	0
78	0	0	1395	6813	8661	8770	3331	67	0	0	0	0	0	0	0	2,1	8,2	9,3	9,4	13,9	0	0	0	0	0	0	4,4	24,4	24,6	24,6	24,2	24,2	0	0	0	0
77	0	0	834	5563	7334	6304	1236	2	0	0	0	0	0	0	0	7,2	9,1	8,4	8,2	15,7	0	0	0	0	0	0	3,1	24,5	24,5	24,6	24,6	15,7	0	0	0	0
76	0	3	923	4088	3706	1118	7	0	0	0	0	0	0	0,3	0	8,6	10,1	9,5	14,9	0	0	0	0	0	0	1	1,4	24,5	24,6	24,2	20,9	0	0	0	0	0
75	0	9	226	2515	376	2	0	0	0	0	0	0	0	0,3	10,4	10,7	11,5	11,6	0	0	0	0	0	0	0	1,2	23,1	23,8	23,1	11,9	0	0	0	0	0	0
74	0	24	896	1113	3	0	0	0	0	0	0	0	0	0,2	11,7	10,7	14,9	0	0	0	0	0	0	0	0	1,1	27,4	27,6	15,4	0	0	0	0	0	0	0
73	0	485	1111	279	0	0	0	0	0	0	0	0	0	4,3	13,2	11,7	0	0	0	0	0	0	0	0	0	27,3	27,4	26,6	0	0	0	0	0	0	0	0
72	0	668	556	4	0	0	0	0	0	0	0	0	0	12,4	14	8,6	0	0	0	0	0	0	0	0	0	27,4	27,3	14,3	0	0	0	0	0	0	0	0
71	245	252	178	0	0	0	0	0	0	0	0	0	0,1	16,9	15,5	0	0	0	0	0	0	0	0	0	0,9	27,5	27,4	0	0	0	0	0	0	0	0	0
70	0	171	74	0	0	0	0	0	0	0	0	0	0	13,7	11,2	0	0	0	0	0	0	0	0	0	0	25,4	25,5	0	0	0	0	0	0	0	0	0
69	70	124	0	0	0	0	0	0	0	0	0	0	8,4	12,8	0	0	0	0	0	0	0	0	0	0	27,2	27	0	0	0	0	0	0	0	0	0	0
68	0	0	0	0	0	0	0	0	0	0	0	0	0	0	0	0	0	0	0	0	0	0	0	0	0	0	0	0	0	0	0	0	0	0	0	0

MAY

	-23,5	-20,5	-17,5	-14,5	-11,5	-8,5	-5,5	-2,5	0,5	3,5	6,5	9,5	-23,5	-20,5	-17,5	-14,5	-11,5	-8,5	-5,5	-2,5	0,5	3,5	6,5	9,5	-23,5	-20,5	-17,5	-14,5	-11,5	-8,5	-5,5	-2,5	0,5	3,5	6,5	9,5
80	0	7	872	3983	4258	2208	1454	1373	490	0	0	0	0	0	0	0	0,3	3,4	7,8	8,2	6,8	0	0	0	0	0,2	1,5	1,5	10	24,3	24,1	24	23,4	0	0	0
79	0	27	1670	8365	8607	5444	2452	950	164	0	0	0	0	0,1	0	0	0,4	4,6	7,6	8,2	6,9	0	0	0	0	0,5	1,5	7,3	21,7	24,5	24	22,4	15,8	0	0	0
78	0	0	1010	5131	5764	5629	1274	59	0	0	0	0	0	0	0	0,4	4	4,7	6,2	10,8	0	0	0	0	0	0	1,5	18,7	23,3	24,2	24,4	16,8	0	0	0	0
77	0	0	595	4054	5225	3877	348	2	0	0	0	0	0	0	0	4	5,9	3,8	3,2	1,9	0	0	0	0	0	0	5,2	19,6	23,8	23,8	23,5	2,3	0	0	0	0
76	0	5	735	2658	2198	474	0	0	0	0	0	0	0	0,2	0	6,1	7,3	5,3	0	0	0	0	0	0	0	0,4	4,8	25,5	25	20,5	0	0	0	0	0	0
75	0	7	88	1399	111	0	0	0	0	0	0	0	0	0	4,3	6,8	12	0	0	0	0	0	0	0	0	0,3	15,2	24,7	25,8	0	0	0	0	0	0	0
74	0	18	484	347	0	0	0	0	0	0	0	0	0	0	6,8	6	0	0	0	0	0	0	0	0	0	0,8	19	18	0	0	0	0	0	0	0	0
73	0	337	701	81	0	0	0	0	0	0	0	0	0	1,4	7,4	7,5	0	0	0	0	0	0	0	0	0	13	19,9	13,4	0	0	0	0	0	0	0	0
72	0	168	278	0	0	0	0	0	0	0	0	0	0	5,8	10,5	0	0	0	0	0	0	0	0	0	0	16,3	18,6	0	0	0	0	0	0	0	0	0
71	105	29	170	0	0	0	0	0	0	0	0	0	0,3	12,8	11,4	0	0	0	0	0	0	0	0	0	0,9	20	19	0	0	0	0	0	0	0	0	0
70	0	93	43	0	0	0	0	0	0	0	0	0	0	8,8	7,1	0	0	0	0	0	0	0	0	0	0	20,6	13	0	0	0	0	0	0	0	0	0
69	20	65	0	0	0	0	0	0	0	0	0	0	15,9	11,1	0	0	0	0	0	0	0	0	0	0	24,2	25,3	0	0	0	0	0	0	0	0	0	0
68	0	0	0	0	0	0	0	0	0	0	0	0	0	0	0	0	0	0	0	0	0	0	0	0	0	0	0	0	0	0	0	0	0	0	0	0

JUNE

	-23,5	-20,5	-17,5	-14,5	-11,5	-8,5	-5,5	-2,5	0,5	3,5	6,5	9,5	-23,5	-20,5	-17,5	-14,5	-11,5	-8,5	-5,5	-2,5	0,5	3,5	6,5	9,5	-23,5	-20,5	-17,5	-14,5	-11,5	-8,5	-5,5	-2,5	0,5	3,5	6,5	9,5
80	0	3	334	2253	2291	447	20	373	579	0	0	0	0	0,1	0	0	0,2	1,9	7,7	8,1	7,1	0	0	0	0	0,1	3	3,3	10,7	23,9	25,8	20,1	23,1	0	0	0
79	0	19	696	5336	5019	812	195	248	223	0	0	0	0	0,2	0	0	0,2	2	5,3	6,9	6,3	0	0	0	0	1	3	4,1	14,6	15,4	21,6	17,2	15,4	0	0	0
78	0	0	516	3730	2881	936	35	13	0	0	0	0	0	0	0	0,1	1,4	3,3	7,8	16,4	0	0	0	0	0	0	3	13,5	12,6	11,7	18	19,4	0	0	0	0
77	0	0	353	2429	1447	491	0	0	0	0	0	0	0	0	0,2	0,3	3,5	2,6	0	0	0	0	0	0	0	0	4,9	12,2	14,9	14,4	0	0	0	0	0	0
76	0	3	317	1315	305	126	0	0	0	0	0	0	0	0,1	0,1	1,7	3,4	2,7	0	0	0	0	0	0	0	0,3	4,2	14,4	13,1	12,9	0	0	0	0	0	0
75	0	2	39	755	4	0	0	0	0	0	0	0	0	0,3	1,6	2,1	11,3	0	0	0	0	0	0	0	0	0,4	10,2	17,9	11,8	0	0	0	0	0	0	0
74	0	0	213	43	0	0	0	0	0	0	0	0	0	0	3,1	2,7	0	0	0	0	0	0	0	0	0	0	16,8	10,8	0	0	0	0	0	0	0	0
73	0	29	111	3	0	0	0	0	0	0	0	0	0	0,1	7	14,4	0	0	0	0	0	0	0	0	0	1,4	16,3	16	0	0	0	0	0	0	0	0
72	0	15	41	0	0	0	0	0	0	0	0	0	0	4,8	5,7	0	0	0	0	0	0	0	0	0	0	7,3	8,7	0	0	0	0	0	0	0	0	0
71	134	0	0	0	0	0	0	0	0	0	0	0	0,1	0	0	0	0	0	0	0	0	0	0	0	1,3	0	0	0	0	0	0	0	0	0	0	0	0
70	0	21	3	0	0	0	0	0	0	0	0	0	0	8,3	10,3	0	0	0	0	0	0	0	0	0	0	12,5	12,4	0	0	0	0	0	0	0	0	0
69	1	13	0	0	0	0	0	0	0	0	0	0	11,4	10,2	0	0	0	0	0	0	0	0	0	0	11,4	13,7	0	0	0	0	0	0	0	0	0	0
68	0	0	0	0	0	0	0	0	0	0	0	0	0	0	0	0	0	0	0	0	0	0	0	0	0	0	0	0	0	0	0	0	0	0	0	0

JULY

	-23,5	-20,5	-17,5	-14,5	-11,5	-8,5	-5,5	-2,5	0,5	3,5	6,5	9,5	-23,5	-20,5	-17,5	-14,5	-11,5	-8,5	-5,5	-2,5	0,5	3,5	6,5	9,5	-23,5	-20,5	-17,5	-14,5	-11,5	-8,5	-5,5	-2,5	0,5	3,5	6,5	9,5
80	0	19	857	3297	1477	330	81	838	750	0	0	0	0	0,1	0	0	0,9	2,6	2,5	7,1	5,3	0	0	0	0	1	1,9	6,9	12,1	13,4	15,9	24	23,2	0	0	0
79	0	28	1515	7761	4206	648	342	319	186	0	0	0	0	0,2	0	0	0,2	7,6	1,5	6,3	5,6	0	0	0	0	2	2,1	7,5	15,4	21,2	20,6	20,7	20	0	0	0
78	0	0	714	2868	1039	128	34	5	0	0	0	0	0	0	0	0,4	1,6	4,7	4	5	0	0	0	0	0	0	3,8	10,4	16,9	15,8	10,3	5,9	0	0	0	0
77	0	0	168	1168	429	73	0	0	0	0	0	0	0	0	0,1	1,1	0,4	4,5	0	0	0	0	0	0	0	0	3,9	10,2	14	14,2	0	0	0	0	0	0
76	0	2	259	810	101	4	0	0	0	0	0	0	0	0,1	0,1	0,9	1,8	2,3	0	0	0	0	0	0	0	0,3	4,7	11,8	12,6	2,7	0	0	0	0	0	0
75	0	2	44	203	3	0	0	0	0	0	0	0	0	0,1	2,1	3,1	5,7	0	0	0	0	0	0	0	0	0,2	5,2	13,1	6,6	0	0	0	0	0	0	0
74	0	0	15	2	0	0	0	0	0	0	0	0	0	0	3,3	4,1	0	0	0	0	0	0	0	0	0	0	7,2	4,5	0	0	0	0	0	0	0	0
73	0	10	3	0	0	0	0	0	0	0	0	0	0	0,2	9,3	0	0	0	0	0	0	0	0	0	0	1,2	10,2	0	0	0	0	0	0	0	0	0
72	0	0	0	0	0	0	0	0	0	0	0	0	0	0	0	0	0	0	0	0	0	0	0	0	0	0	0	0	0	0	0	0	0	0	0	0
71	64	0	0	0	0	0	0	0	0	0	0	0	0,3	0	0	0	0	0	0	0	0	0	0	0	2	0	0	0	0	0	0	0	0	0	0	0
70	0	0	0	0	0	0	0	0	0	0	0	0	0	0	0	0	0	0	0	0	0	0	0	0	0	0	0	0	0	0	0	0	0	0	0	0
69	0	0	0	0	0	0	0	0	0	0	0	0	0	0	0	0	0	0	0	0	0	0	0	0	0	0	0	0	0	0	0	0	0	0	0	0
68	0	0	0	0	0	0	0	0	0	0	0	0	0	0	0	0	0	0	0	0	0	0	0	0	0	0	0	0	0	0	0	0	0	0	0	0

AUGUST

	-23,5	-20,5	-17,5	-14,5	-11,5	-8,5	-5,5	-2,5	0,5	3,5	6,5	9,5	-23,5	-20,5	-17,5	-14,5	-11,5	-8,5	-5,5	-2,5	0,5	3,5	6,5	9,5	-23,5	-20,5	-17,5	-14,5	-11,5	-8,5	-5,5	-2,5	0,5	3,5	6,5	9,5
80	0	6	320	1388	285	20	1	874	830	0	0	0	0	0,1	0,1	0,2	1,3	3,2	3,7	4,8	3,2	0	0	0	0	0,2	1,8	7,6	9,5	12,4	3,7	18,4	17,8	0	0	0
79	0	55	910	4088	818	44	24	236	187	0	0	0	0	0,2	0	0	0,6	3,7	7,1	3,5	3,4	0	0	0	0	0,9	4,1	3,9	8,3	8,9	13,8	22,5	22,3	0	0	0
78	0	0	263	749	34	202	167	0	0	0	0	0	0	0	0	0,3	2,2	5,2	5,4	0	0	0	0	0	0	0	3,9	9,1	10,6	14,4	16,4	0	0	0	0	0
77	0	0	1	50	2	3	2	0	0	0	0	0	0	0	0,1	4,7	3,4	4,1	20,8	0	0	0	0	0	0	0	0,1	8	3,5	4,6	21,3	0	0	0	0	0
76	0	0	21	14	2	0	0	0	0	0	0	0	0	0	0,1	0,3	3,1	0	0	0	0	0	0	0	0	0	2,2	2,2	3,4	0	0	0	0	0	0	0
75	0	0	0	0	0	0	0	0	0	0	0	0	0	0	0	0	0	0	0	0	0	0	0	0	0	0	0	0	0	0	0	0	0	0	0	0
74	0	0	0	0	0	0	0	0	0	0	0	0	0	0	0	0	0	0	0	0	0	0	0	0	0	0	0	0	0	0	0	0	0	0	0	0
73	0	0	0	0	0	0	0	0	0	0	0	0	0	0	0	0	0	0	0	0	0	0	0	0	0	0	0	0	0	0	0	0	0	0	0	0
72	0	0	0	0	0	0	0	0	0	0	0	0	0	0	0	0	0	0	0	0	0	0	0	0	0	0	0	0	0	0	0	0	0	0	0	0
71	0	0	0	0	0	0	0	0	0	0	0	0	0	0	0	0	0	0	0	0	0	0	0	0	0	0	0	0	0	0	0	0	0	0	0	0
70	0	0	0	0	0	0	0	0	0	0	0	0	0	0	0	0	0	0	0	0	0	0	0	0	0	0	0	0	0	0	0	0	0	0	0	0
69	0	0	0	0	0	0	0	0	0	0	0	0	0	0	0	0	0	0	0	0	0	0	0	0	0	0	0	0	0	0	0	0	0	0	0	0
68	0	0	0	0	0	0	0	0	0	0	0	0	0	0	0	0	0	0	0	0	0	0	0	0	0	0	0	0	0	0	0	0	0	0	0	0

SEPTEMBER

	-23,5	-20,5	-17,5	-14,5	-11,5	-8,5	-5,5	-2,5	0,5	3,5	6,5	9,5	-23,5	-20,5	-17,5	-14,5	-11,5	-8,5	-5,5	-2,5	0,5	3,5	6,5	9,5	-23,5	-20,5	-17,5	-14,5	-11,5	-8,5	-5,5	-2,5	0,5	3,5	6,5	9,5
80	0	6	224	903	743	460	553	1009	714	0	0	0	0	0,1	0,1	0,2	0,9	3	8	6,5	3,7	0	0	0	0	0,4	3,7	5,3	24,1	15,5	23,2	24,2	22	0	0	0
79	0	16	581	2759	1292	432	332	528	151	0	0	0	0	0,3	0,1	0,1	1,2	3,2	7,7	4,8	2,8	0	0	0	0	1,1	5	10,6	23,7	22,6	24,4	24,3	20,4	0	0	0
78	0	0	174	998	936	232	110	10	0	0	0	0	0	0	0,1	2	4,6	5,1	6,9	3,1	0	0	0	0	0	0	5	20,4	24,7	24	19,1	4,6	0	0	0	0
77	0	0	6	530	311	89	12	0	0	0	0	0	0	0	5,4	6,7	7,6	7,9	7	0	0	0	0	0	0	0	12	21,7	22,3	15,2	15	0	0	0	0	0
76	0	0	1	50	6	0	0	0	0	0	0	0	0	0	8,5	11,9	6,9	0	0	0	0	0	0	0	0	0	8,5	22,3	11,4	0	0	0	0	0	0	0
75	0	0	0	0	0	0	0	0	0	0	0	0	0	0	0	0	0	0	0	0	0	0	0	0	0	0	0	0	0	0	0	0	0	0	0	0
74	0	0	0	0	0	0	0	0	0	0	0	0	0	0	0	0	0	0	0	0	0	0	0	0	0	0	0	0	0	0	0	0	0	0	0	0
73	0	0	0	0	0	0	0	0	0	0	0	0	0	0	0	0	0	0	0	0	0	0	0	0	0	0	0	0	0	0	0	0	0	0	0	0
72	0	0	0	0	0	0	0	0	0	0	0	0	0	0	0	0	0	0	0	0	0	0	0	0	0	0	0	0	0	0	0	0	0	0	0	0
71	0	0	0	0	0	0	0	0	0	0	0	0	0	0	0	0	0	0	0	0	0	0	0	0	0	0	0	0	0	0	0	0	0	0	0	0
70	0	0	0	0	0	0	0	0	0	0	0	0	0	0	0	0	0	0	0	0	0	0	0	0	0	0	0	0	0	0	0	0	0	0	0	0
69	0	0	0	0	0	0	0	0	0	0	0	0	0	0	0	0	0	0	0	0	0	0	0	0	0	0	0	0	0	0	0	0	0	0	0	0
68	0	0	0	0	0	0	0	0	0	0	0	0	0	0	0	0	0	0	0	0	0	0	0	0	0	0	0	0	0	0	0	0	0	0	0	0

OCTOBER

	-23,5	-20,5	-17,5	-14,5	-11,5	-8,5	-5,5	-2,5	0,5	3,5	6,5	9,5	-23,5	-20,5	-17,5	-14,5	-11,5	-8,5	-5,5	-2,5	0,5	3,5	6,5	9,5	-23,5	-20,5	-17,5	-14,5	-11,5	-8,5	-5,5	-2,5	0,5	3,5	6,5	9,5
80	0	5	371	1725	2379	2100	2186	1948	934	0	0	0	0	0,1	0	0	2,1	6,5	9,4	9,8	9,7	0	0	0	0	0,2	3,1	10,9	24,3	24,5	21,6	24,3	24,1	0	0	0
79	0	29	747	4044	4836	4602	3560	1896	500	0	0	0	0	0,2	0,1	0,1	3	7,6	10,1	10,3	7,8	0	0	0	0	1,1	6,2	15,2	24,4	24,5	24,3	24,4	23,9	0	0	0
78	0	0	426	3177	4560	4205	1890	78	0	0	0	0	0	0	0,4	3,2	6	8,7	11,6	17,1	0	0	0	0	0	0	15,3	24	24,3	24,6	24,3	24,4	0	0	0	0
77	0	0	212	2864	3487	2575	784	5	0	0	0	0	0	0	1,2	5,4	6,5	8,5	8,3	6,8	0	0	0	0	0	0	19	24,1	24,3	24,5	23,1	8	0	0	0	0
76	0	0	144	1804	1202	385	1	0	0	0	0	0	0	0	0,2	5,7	7	10,3	9,1	0	0	0	0	0	0	0	15,6	24,5	23,3	23,8	9,1	0	0	0	0	0
75	0	5	47	616	75	0	0	0	0	0	0	0	0	0,1	6,1	7,1	6,3	0	0	0	0	0	0	0	0	0,2	21,7	26,8	23,2	0	0	0	0	0	0	0
74	0	5	168	137	0	0	0	0	0	0	0	0	0	0,1	8,4	3,9	0	0	0	0	0	0	0	0	0	0,6	21	12,3	0	0	0	0	0	0	0	0
73	0	18	11	1	0	0	0	0	0	0	0	0	0	2,8	12,1	6,8	0	0	0	0	0	0	0	0	0	8,8	19,8	6,8	0	0	0	0	0	0	0	0
72	0	28	9	0	0	0	0	0	0	0	0	0	0	8,2	17,9	0	0	0	0	0	0	0	0	0	0	20,5	19,2	0	0	0	0	0	0	0	0	0
71	30	0	0	0	0	0	0	0	0	0	0	0	0,1	0	0	0	0	0	0	0	0	0	0	0	1,3	0	0	0	0	0	0	0	0	0	0	0	0
70	0	0	0	0	0	0	0	0	0	0	0	0	0	0	0	0	0	0	0	0	0	0	0	0	0	0	0	0	0	0	0	0	0	0	0	0	0
69	0	0	0	0	0	0	0	0	0	0	0	0	0	0	0	0	0	0	0	0	0	0	0	0	0	0	0	0	0	0	0	0	0	0	0	0	0
68	0	0	0	0	0	0	0	0	0	0	0	0	0	0	0	0	0	0	0	0	0	0	0	0	0	0	0	0	0	0	0	0	0	0	0	0	0

SEPTEMBER

	-23,5	-20,5	-17,5	-14,5	-11,5	-8,5	-5,5	-2,5	0,5	3,5	6,5	9,5	-23,5	-20,5	-17,5	-14,5	-11,5	-8,5	-5,5	-2,5	0,5	3,5	6,5	9,5	-23,5	-20,5	-17,5	-14,5	-11,5	-8,5	-5,5	-2,5	0,5	3,5	6,5	9,5
80	0	6	224	903	743	460	553	1009	714	0	0	0	0	0,1	0,1	0,2	0,9	3	8	6,5	3,7	0	0	0	0	0,4	3,7	5,3	24,1	15,5	23,2	24,2	22	0	0	0
79	0	16	581	2759	1292	432	332	528	151	0	0	0	0	0,3	0,1	0,1	1,2	3,2	7,7	4,8	2,8	0	0	0	0	1,1	5	10,6	23,7	22,6	24,4	24,3	20,4	0	0	0
78	0	0	174	998	936	232	110	10	0	0	0	0	0	0	0,1	2	4,6	5,1	6,9	3,1	0	0	0	0	0	0	5	20,4	24,7	24	19,1	4,6	0	0	0	0
77	0	0	6	530	311	89	12	0	0	0	0	0	0	0	5,4	6,7	7,6	7,9	7	0	0	0	0	0	0	0	12	21,7	22,3	15,2	15	0	0	0	0	0
76	0	0	1	50	6	0	0	0	0	0	0	0	0	0	8,5	11,9	6,9	0	0	0	0	0	0	0	0	0	8,5	22,3	11,4	0	0	0	0	0	0	0
75	0	0	0	0	0	0	0	0	0	0	0	0	0	0	0	0	0	0	0	0	0	0	0	0	0	0	0	0	0	0	0	0	0	0	0	0
74	0	0	0	0	0	0	0	0	0	0	0	0	0	0	0	0	0	0	0	0	0	0	0	0	0	0	0	0	0	0	0	0	0	0	0	0
73	0	0	0	0	0	0	0	0	0	0	0	0	0	0	0	0	0	0	0	0	0	0	0	0	0	0	0	0	0	0	0	0	0	0	0	0
72	0	0	0	0	0	0	0	0	0	0	0	0	0	0	0	0	0	0	0	0	0	0	0	0	0	0	0	0	0	0	0	0	0	0	0	0
71	0	0	0	0	0	0	0	0	0	0	0	0	0	0	0	0	0	0	0	0	0	0	0	0	0	0	0	0	0	0	0	0	0	0	0	0
70	0	0	0	0	0	0	0	0	0	0	0	0	0	0	0	0	0	0	0	0	0	0	0	0	0	0	0	0	0	0	0	0	0	0	0	0
69	0	0	0	0	0	0	0	0	0	0	0	0	0	0	0	0	0	0	0	0	0	0	0	0	0	0	0	0	0	0	0	0	0	0	0	0
68	0	0	0	0	0	0	0	0	0	0	0	0	0	0	0	0	0	0	0	0	0	0	0	0	0	0	0	0	0	0	0	0	0	0	0	0

OCTOBER

	-23,5	-20,5	-17,5	-14,5	-11,5	-8,5	-5,5	-2,5	0,5	3,5	6,5	9,5	-23,5	-20,5	-17,5	-14,5	-11,5	-8,5	-5,5	-2,5	0,5	3,5	6,5	9,5	-23,5	-20,5	-17,5	-14,5	-11,5	-8,5	-5,5	-2,5	0,5	3,5	6,5	9,5
80	0	5	371	1725	2379	2100	2186	1948	934	0	0	0	0	0,1	0	0	2,1	6,5	9,4	9,8	9,7	0	0	0	0	0,2	3,1	10,9	24,3	24,5	21,6	24,3	24,1	0	0	0
79	0	29	747	4044	4836	4602	3560	1896	500	0	0	0	0	0,2	0,1	0,1	3	7,6	10,1	10,3	7,8	0	0	0	0	1,1	6,2	15,2	24,4	24,5	24,3	24,4	23,9	0	0	0
78	0	0	426	3177	4560	4205	1890	78	0	0	0	0	0	0	0,4	3,2	6	8,7	11,6	17,1	0	0	0	0	0	0	15,3	24	24,3	24,6	24,3	24,4	0	0	0	0
77	0	0	212	2864	3487	2575	784	5	0	0	0	0	0	0	1,2	5,4	6,5	8,5	8,3	6,8	0	0	0	0	0	0	19	24,1	24,3	24,5	23,1	8	0	0	0	0
76	0	0	144	1804	1202	385	1	0	0	0	0	0	0	0	0,2	5,7	7	10,3	9,1	0	0	0	0	0	0	0	15,6	24,5	23,3	23,8	9,1	0	0	0	0	0
75	0	5	47	616	75	0	0	0	0	0	0	0	0	0,1	6,1	7,1	6,3	0	0	0	0	0	0	0	0	0,2	21,7	26,8	23,2	0	0	0	0	0	0	0
74	0	5	168	137	0	0	0	0	0	0	0	0	0	0,1	8,4	3,9	0	0	0	0	0	0	0	0	0	0,6	21	12,3	0	0	0	0	0	0	0	0
73	0	18	11	1	0	0	0	0	0	0	0	0	0	2,8	12,1	6,8	0	0	0	0	0	0	0	0	0	8,8	19,8	6,8	0	0	0	0	0	0	0	0
72	0	28	9	0	0	0	0	0	0	0	0	0	0	8,2	17,9	0	0	0	0	0	0	0	0	0	0	20,5	19,2	0	0	0	0	0	0	0	0	0
71	30	0	0	0	0	0	0	0	0	0	0	0	0,1	0	0	0	0	0	0	0	0	0	0	0	1,3	0	0	0	0	0	0	0	0	0	0	0	0
70	0	0	0	0	0	0	0	0	0	0	0	0	0	0	0	0	0	0	0	0	0	0	0	0	0	0	0	0	0	0	0	0	0	0	0	0	0
69	0	0	0	0	0	0	0	0	0	0	0	0	0	0	0	0	0	0	0	0	0	0	0	0	0	0	0	0	0	0	0	0	0	0	0	0	0
68	0	0	0	0	0	0	0	0	0	0	0	0	0	0	0	0	0	0	0	0	0	0	0	0	0	0	0	0	0	0	0	0	0	0	0	0	0

NOVEMBER

	-23,5	-20,5	-17,5	-14,5	-11,5	-8,5	-5,5	-2,5	0,5	3,5	6,5	9,5	-23,5	-20,5	-17,5	-14,5	-11,5	-8,5	-5,5	-2,5	0,5	3,5	6,5	9,5	-23,5	-20,5	-17,5	-14,5	-11,5	-8,5	-5,5	-2,5	0,5	3,5	6,5	9,5
80	0	3	400	1518	1856	1561	1951	2025	920	0	0	0	0	0,1	0	0	1,5	6,8	8,9	8,7	8	0	0	0	0	0,1	2,5	5,7	20,9	24	21,1	22,5	23,4	0	0	0
79	0	11	754	3385	3670	3822	3663	1859	423	0	0	0	0	0,1	0	0,1	2,6	7,6	9,4	10,5	9,1	0	0	0	0	0,8	7,2	10,8	24,2	24,1	23,1	22,9	24,1	0	0	0
78	0	0	558	3480	4334	4305	2498	109	0	0	0	0	0	0	0,1	2,8	6,6	8,7	9,1	12,7	0	0	0	0	0	0	9,9	24,2	24,4	24,4	22,4	21,6	0	0	0	0
77	0	0	408	3452	3234	3041	1837	3	0	0	0	0	0	0	0,7	4,3	8,1	9,2	8,2	12	0	0	0	0	0	0	20,7	24,3	24,4	24,4	24,3	15	0	0	0	0
76	0	5	500	2212	1540	799	43	0	0	0	0	0	0	0,2	0,2	4,8	8,2	9,1	10,1	0	0	0	0	0	0	0,7	15	22,2	24	26,7	24,3	0	0	0	0	0
75	0	1	177	1343	156	0	0	0	0	0	0	0	0	0,2	8,7	8,1	10,9	0	0	0	0	0	0	0	0	0,2	14,5	24,1	24,2	0	0	0	0	0	0	0
74	0	18	835	482	1	0	0	0	0	0	0	0	0	1,1	9,7	9,8	12,6	0	0	0	0	0	0	0	0	7,7	18,9	16,6	12,6	0	0	0	0	0	0	0
73	0	202	712	12	0	0	0	0	0	0	0	0	0	5,3	11,3	12,4	0	0	0	0	0	0	0	0	0	22	26,5	15,6	0	0	0	0	0	0	0	0
72	0	299	194	0	0	0	0	0	0	0	0	0	0	11,7	16,2	0	0	0	0	0	0	0	0	0	0	24,7	26,8	0	0	0	0	0	0	0	0	0
71	62	14	1	0	0	0	0	0	0	0	0	0	0,1	21,6	15,2	0	0	0	0	0	0	0	0	0	0,6	24,8	15,2	0	0	0	0	0	0	0	0	0	0
70	0	2	0	0	0	0	0	0	0	0	0	0	0	2,2	0	0	0	0	0	0	0	0	0	0	0	2,3	0	0	0	0	0	0	0	0	0	0
69	5	0	0	0	0	0	0	0	0	0	0	0	5,7	0	0	0	0	0	0	0	0	0	0	0	8,5	0	0	0	0	0	0	0	0	0	0	0	0
68	0	0	0	0	0	0	0	0	0	0	0	0	0	0	0	0	0	0	0	0	0	0	0	0	0	0	0	0	0	0	0	0	0	0	0	0	0

DECEMBER

	-23,5	-20,5	-17,5	-14,5	-11,5	-8,5	-5,5	-2,5	0,5	3,5	6,5	9,5	-23,5	-20,5	-17,5	-14,5	-11,5	-8,5	-5,5	-2,5	0,5	3,5	6,5	9,5	-23,5	-20,5	-17,5	-14,5	-11,5	-8,5	-5,5	-2,5	0,5	3,5	6,5	9,5
80	0	9	552	2445	3620	2244	2116	1655	357	0	0	0	0	0,1	0	0	1,1	6,9	11,9	12	11,2	0	0	0	0	0,6	4	4,3	20,8	24,5	24,6	24,6	24,4	0	0	0
79	0	43	1135	5717	5387	4871	4018	1415	62	0	0	0	0	0,1	0	0,1	2,8	10,8	11,9	12	11,8	0	0	0	0	1	3,7	16,1	24,6	24,7	24,7	24,7	24,3	0	0	0
78	0	0	643	4287	5376	4541	2199	46	0	0	0	0	0	0	0	4,3	9,8	10,7	10	9,7	0	0	0	0	0	0	2,9	23,6	24,7	24,6	24,6	16,6	0	0	0	0
77	0	0	466	3483	3819	2111	362	0	0	0	0	0	0	0	0,5	6,8	10	9,9	8,2	0	0	0	0	0	0	0	13,7	24,3	24,4	24,6	24,5	0	0	0	0	0
76	0	6	550	2284	1254	251	4	0	0	0	0	0	0	0,1	0,1	8,2	11,6	10	11,9	0	0	0	0	0	0	0,2	9,2	25,3	24,6	21,1	13,2	0	0	0	0	0
75	0	8	119	1209	64	0	0	0	0	0	0	0	0	0,1	9,6	10,3	12,1	0	0	0	0	0	0	0	0	0,2	15,1	26,9	20	0	0	0	0	0	0	0
74	0	15	477	241	0	0	0	0	0	0	0	0	0	0,3	11,4	11,7	0	0	0	0	0	0	0	0	0	2,8	21,3	25,6	0	0	0	0	0	0	0	0
73	0	278	639	9	0	0	0	0	0	0	0	0	0	8	12,1	16,1	0	0	0	0	0	0	0	0	0	25,6	25,4	18	0	0	0	0	0	0	0	0
72	0	347	426	10	0	0	0	0	0	0	0	0	0	11,7	15,6	18,5	0	0	0	0	0	0	0	0	0	27	27,4	25,4	0	0	0	0	0	0	0	0
71	102	85	137	0	0	0	0	0	0	0	0	0	0,2	14,5	18	0	0	0	0	0	0	0	0	0	1,3	27,3	27,4	0	0	0	0	0	0	0	0	0
70	0	196	10	0	0	0	0	0	0	0	0	0	0	12,6	13,4	0	0	0	0	0	0	0	0	0	0	25,8	16,5	0	0	0	0	0	0	0	0	0
69	23	48	0	0	0	0	0	0	0	0	0	0	13,2	15,8	0	0	0	0	0	0	0	0	0	0	20,4	26,6	0	0	0	0	0	0	0	0	0	0
68	0	0	0	0	0	0	0	0	0	0	0	0	0	0	0	0	0	0	0	0	0	0	0	0	0	0	0	0	0	0	0	0	0	0	0	0

10. References

Aagaard, K. & E. C. Carmack (1989). The role of sea ice and other fresh water in the arctic circulation. *Journal of Geophysical Research 94*(C10), 14485-14498.

Andersen, S., Tonboe, R., Kern, S., Schyberg, H., 2006, Improved retrieval of sea ice total concentration from spaceborn passive microwave observations using numerical weather prediction model fields: An intercomparison of nine algorithms. Remote sensing of Environment 104 (4)

Barry, R. G. & R. J. Chorley (1992). *Atmosphere, weather & climate*. Sixth edition. Routledge, London & New York.

Björg, G., & J. Söderkvist (2002). Dependence of the Arctic Ocean ice thickness distribution on the poleward energy flux in the atmosphere. *Journal of Geophysical Research 107*(C10), 3173, doi:10.1029/2000JC000723.

Broecker, W. S. (1997). Thermohaline circulation, the Achilles heel of our climate system: will man-made CO_2 upset the current balance. *Science 278*, 1582-1588.

Cappelen, J., B. V. Jørgensen, E. V. Laursen, L. S. Stannius, & R. S. Thomsen (2001). The observed climate of Greenland, 1958-99 – with climatological standard normals, 1961-90. Danish Meteorological Institute - Technical Report 00-18, p. 136. Copenhagen.

Deser, C., J. E. Walsh, & M. S. Timlin (2000). Arctic sea ice variability in the context of recent atmospheric circulation trends. *Journal of Climate 13*, 617-633.

Dickson, B. (1999). All change in the Arctic. *Nature 397*, 389-391.

Doble, M. J., Skourup, H., Wadhams, P., and Geiger, C.: The relation between sea ice surface elevation and draft: Results from high-resolution mapping by co-incident AUV sonar and airborne scanning laser. JGR Oceans, 2011JC007076, 2011, in press

Eastwood, S., Larsen, K. R., Lavergne, T., Nielsen, E., Tonboe, R., April 2010, Global Sea Ice Concentration Reprocessing - Product User Manual, Product OSI-409, Vers. 1.1. Ocean and Sea Ice SAF, URL http://saf.met.no/docs/

EUMETSAT/OSISAF, 2010, Global sea ice concentration reprocessing dataset 1978-2009, vers. 1, (Digital media), Norwegian and Danish Meteorological Institutes, URL http://osisaf.met.no

EUMETSAT/OSISAF, 2011, Global sea ice concentration operational dataset 2009-2010, (Digital media), Norwegian and Danish Meteorological Institutes, URL http://osisaf.met.no

Ezraty, R., Cavanié, A., 1999, Intercomparison of backscatter maps over Arctic sea ice from NSCAT and the ERS scatterometer, Journal of Geophysical Research, Vol. 104, No. C5

Ezraty, R., Piollé, J., August 2001. Convection Rep. No. 5: SeaWinds on QuikSCAT Polar Sea Ice Grids - User Manual. Ifremer/CERSAT.

Farrell, S. L., S. W. Laxon, D. C. McAdoo, D. Yi, and H. J. Zwally: Five years of Arctic sea ice freeboard measurements from the Ice, Cloud and land Elevation Satellite, *J. Geophys. Res.*, 114, C04008, doi:10.1029/2008JC005074, 2009

Forsberg, R. and Skourup, H. : Arctic Ocean gravity, geoid and sea ice freeboard heights from ICESat and GRACE. Geophysical Research Letters, 32(L21502), 2005

Giles, K. A., S. W. Laxon, and A. L. Ridout: Circumpolar thinning of Arctic sea ice following the 2007 record ice extent minimum, *Geophys. Res. Lett.*, 35, L22502, doi:10.1029/2008GL035710, 2008

Girard-Ardhuin, F., Ezraty, R., Croizé-Fillon, D., 2009, Ascat/Metop Scatterometer data: First results for sea ice study, Technical report, Ifremer, LOS/CERSAT

Haarpaintner, J., J. O'Dwyer, J.-C. Gascard, P. M. Haugan, U. Schauer, & S. Østerhus (2001a). Seasonal Transformation of Water Masses, Circulation and Brine Formation Observed in Storfjorden, Svalbard. *Annals of Glaciology 33*, 437-443.

Haarpaintner, J., J.-C. Gascard, & P. M. Haugan (2001b). Ice production and brine formation in Storfjorden, Svalbard. *Journal of Geophysical Research 106*(C7), 14001-14013.

Hibler, W. D. (1979). A dynamic thermodynamic sea ice model. *Journal of Physical Oceanography 9*, 815-846.

Hurrell, J. W. (1995). Decadal trends in the North Atlantic oscillation: regional temperatures and precipitation. *Science 269*, 676-679.

Hurrell, J. W., Y. Kushnir, G. Ottersen, & M. Visbeck (2003). An overview of the North Atlantic Oscillation. In: J. W. Hurrell, Y. Kushnir, G. Ottersen, & M. Visbeck (Eds.) *The North Atlantic Oscillation climatic significance and environmental impact. Geophysical Monograph 134*, (pp. 1-35). American Geophysical Union.

Hvidegaard, S. M., R. Forsberg, S. Hanson, H. Skourup, and L. T. Pedersen: Sea ice conditions off NW and NE Greenland from satellite measurements, airborne and in-situ data. Contract report for Greenland Bureau of Minerals and Petroleum, October 2008

Hvidegaard, S.M, R. Forsberg, and H. Skourup. Sea ice thickness estimates from airborne laser scanning. In P. Wadhams and G. Amanatidis, editors, Arctic Sea Ice Thickness: Past, Present and Future. Climate Change and Natural Hazards Series, Brussels, 2006

Hvidegaard, S. M. and Forsberg, R. 2002: Sea-ice thickness from airborne laser altimetry over the Arctic Ocean north of Greenland. Geophysical Research Letters, 29(20):1952, 2002

Ifremer/CERSAT, 2003, SeaWinds on QuikSCAT Level 3 Sea-Ice Maps on 25km Polar Grid (Digital media). Ifremer/CERSAT, URL http://www.ifremer.fr/cersat/en/data/download/gridded/psiqscat.htm

Ifremer/CERSAT, 2011, ASCAT Sea-Ice Maps on 12.5km Polar Grid (Digital media), Ifremer/CERSAT.

Krabill, W. B., R. H. Thomas, C. F. Martin, R. N. Swift, and E. B. Frederick. Accuracy of airborne laser altimetry over the Greenland icesheet. Int. J. Remote Sensing, 16(7):1211–1222, 1995

Kurtz, N. T., Markus, T. M., Cavalieri, D. J., Krabill,W., Sonntag, J. G., and Miller, J.: Comparison of ICESat data with airborne laser altimeter measurements over Arctic sea ice. IEEE Transaction on Geoscience and Remote Sensing, 46(7):1913–1924, 2008

Kwok, R., & D. A. Rothrock (1999). Variability of Fram Strait ice flux and North Atlantic Oscillation. *Journal of Geophysical Research 104*(C3), 5177-5189.

Kwok, R., Zwally, H. J., and Yi, D: ICESat observations of Arctic sea ice: A first look. Geophysical Research Letters, 31(L16401), 2004

Kwok, R. , 2005, Variability of Nares Strait ice flux, Geophysical Research Letters, Vol. 32, L24502, doi:10.1029/2005GL024768

Kwok, R., Cunningham, G. F., Zwally, H. J., and Yi, D.: ICESat over Arctic sea ice: Interpretation of altimetric and reflectivity profiles. Journal of Geophysical Research, 111(C06006), 2006

Kwok, R., Cunningham, G. F., Zwally, H. J., and Yi, D.: Ice, Cloud, and land Elevation Satellite (ICESat) over Arctic sea ice: Retrieval of freeboard. Journal of Geophysical Research, 112(C12013), 2007

Laxon, S., Peacock, N., and Smith, D.: High interannual variability of sea ice thickness in the Arctic region. Nature, 425:947–950, 2003

Lubin, D., Massom, R., 2006. Polar Remote Sensing, Vol. 1: Atmosphere and Oceans. Springer-Praxis

Maslanik, J. A., M C. Serreze, & R. G. Barry (1996). Recent decreases in Arctic summer ice cover and linkages to atmospheric circulation anomalies. *Geophysical Research Letters* 23, 1677-1680.

Maslowski, W., D. C. Marble, W. Walczowski, & A. J. Semtner (2001). On large scale shifts in the Arctic Ocean and sea-ice conditions during 1979-98. *Annals of Glaciology 33*, 545-550.

Maykut, G. A. (1986). The surface heat and mass balance. In: N. Untersteiner (Ed.) *The Geophysics of Sea Ice*. NATO ASI series, series B: Physics Vol. 146. New York & London: Plenum Press.

Overland, J. E. (1998). Arctic meteorology and air/ice coupling. In M. Leppäranta (ed.): *The physics of ice-covered seas* (pp. 775-786). Helsinki University Printing House, Helsinki.

Parkinson, C. L. & D. J. Cavalieri (1989). Arctic sea ice 1973-1987: seasonal, regional, and interannual variability. *Journal of Geophysical Research 94*(C10), 14499-14523.

Peacock, N. R. and Laxon, S. W.: Sea surface height determination in the Arctic Ocean from ERS altimetry. Journal of Geophysical Research, 109, 2004

Poulsen, S. K., L. Stenseng, H. Skourup, L. T. Pedersen, R. Forsberg, and L. S. Sørensen: Initial results of CryoSat-2 data from the Arctic. In proceedings CryoSat Validation Workshop, Frascati, Italy, February 1-3, 2011

Rudels, B. (1998). Aspects of Arctic oceanography. In M. Leppäranta (ed.): *The physics of ice-covered seas* (pp. 517-568). Helsinki University Printing House, Helsinki.

Serreze, M. C., & R. G. Barry (1988). Synoptic activity in the Arctic Basin, 1979-85. *Journal of Climate 1*, 1276-1295.

Skourup, H.: A study of Arctic sea ice freeboard heights, gravity anomalies and dynamic topography from ICESat measurements. PhD Thesis, University of Copenhagen, 2010

Skourup, H. and R. Forsberg: Sea ice freeboards from ICESat – A comparison to airborne lidar measurements. Arctic Sea Ice Thickness: Past, present and future, edited by P. Wadhams and G. Amanaditis. Climate Change and Natural Hazards Series, Brussels, 2006

Thompson, D. W. J., & J. M. Wallace (1998). The Arctic Oscillation in the wintertime geopotential height and temperature fields. *Geophysical Research Letters 25*(9), 1297-1300.

Thorndike, A. S. (1992). A toy model linking atmospheric thermal radiation and sea ice growth. *Journal of Geophysical Research 97*, 9401-9410.

Thorndike, A. S., & R. Colony (1982). Sea ice motion response to geostrophic winds. *Journal of Geophysical Research 87*(C8), 5845-5852.

Tonboe, R. T. (2001). Detailed wind speed information from Radarsat ScanSAR wide. Danish Meteorological Institute technical report 01-04, p. 17, Copenhagen.

Tonboe, R., Haarpaintner, J., 2003. Implementation of QuikScat SeaWinds Data in the EUMETSAT Ocean and Sea Ice Product (Technical Report 03-13). Danish Meteorological Institute, Copenhagen. URL http://www.dmi.dk/dmi/index/viden/dmi-publikationer/Tekniskerapporter

Vinje, T. (2001). Anomalities and trends of sea-ice extent and atmospheric circulation in the Nordic Seas during the period 1864-1998. *Journal of Climate 14*, 255-267.

Vinje, T., N. Nordlund, & Å. Kvambekk (1998). Monitoring ice thickness in Fram Strait. *Journal of Geophysical Research 103*(C5), 10437-10449.

Wadhams, P. (1981). The ice cover in the Greenland and Norwegian Seas. *Reviews of Geophysics and Space Physics 19*(3), 345-393.

Wadhams, P. (1986). The seasonal ice zone. In: N. Untersteiner (Ed.) *The Geophysics of Sea Ice*. (pp. 825-992) NATO ASI series, series B: Physics Vol. 146. New York & London: Plenum Press.

Wadhams, P. (2000). *Ice in the Ocean.* Gordon & Breach Science Publishers.

Wang, J., L. A. Mysak, R. G. Ingram (1994). Sea-ice cover in Hudson Bay, Baffin Bay and the Labrador Sea. *Atmosphere – Ocean 32*(2), 421-447.